

# **Discovery of novel competitive dihydropteridine reductase inhibitors via high throughput screening and their effect on metabolic pterin balance of fibroblast**

THÈSE N° 8371 (2018)

PRÉSENTÉE LE 26 JANVIER 2018

À LA FACULTÉ DES SCIENCES DE BASE

LABORATOIRE D'INGÉNIERIE DES PROTÉINES

PROGRAMME DOCTORAL EN CHIMIE ET GÉNIE CHIMIQUE

ÉCOLE POLYTECHNIQUE FÉDÉRALE DE LAUSANNE

POUR L'OBTENTION DU GRADE DE DOCTEUR ÈS SCIENCES

PAR

**Yann Mathieu PIERSON**

acceptée sur proposition du jury:

Prof. K. Severin, président du jury  
Prof. K. Johnsson, Prof. V. Hatzimanikatis, directeurs de thèse  
Prof. N. Winssinger, rapporteur  
Prof. M. Lochner, rapporteur  
Dr M. Chambon, rapporteur



ÉCOLE POLYTECHNIQUE  
FÉDÉRALE DE LAUSANNE

Suisse  
2018



## ***Acknowledgements***

Curiosity has always been a strong driving force in my life. Curiosity, especially when it comes to risky endeavors, is thrilling but can be dangerous. Boundaries and thoughtful supervision over the exploration of curiosity were always given by my dad. Under his watchful eye, I was able to perform my first experiments, be it with electricity or with chemicals, allowing me to quickly develop a taste for science. I thank him first and foremost to have triggered, since my youngest age, my creativity, critical judgment and a “do it my way” autonomy. Later, as a mediocre teenager schoolboy, teachers often told me I would not succeed at studying. I thank these people. Proving them wrong was a challenge that drove me where I am now.

“*A PhD requires stamina*” those were some of the first words my supervisor, Kai Johnson, told me before I started as a grad student. As correct as this sentence is I believe this marathon could have lasted a decade longer. Additionally, Kai seems to have a keen eye when it comes to hiring clever people with great technical and social skills. Research topics, collaboration and leisure times were all on point! A sentence he happens to say is “*I have the best job in the world*”. It would be a lie if I did not think sometimes it is my case too. I thank him for these almost four years were I could specialize in probably the greatest work environments.

Furthermore, I thank Dr. Julien Hiblot and Dr. Rudolf Griss as they taught me the niftiest tricks in the field of biology as soon as I arrived. I thank Dr. Johannes Broichhagen and Dr. Luc Reymond for their excellent counsels and discussions around the topic of chemical synthesis. I thank Nicolas Goeldel and Dr. Ruud Hovius for their sense of criticism and their wisdom when it came to “put things back in perspective”. Finally I’d like to thanks all the remaining members of the LIP group which made this period unforgettable.

## ***Abstract***

The development of tool compounds for the study of the tetrahydrobiopterin (BH4) metabolic network perturbation is of interest especially in the case of oxidative and nitrosative stress genesis. A semisynthetic FRET sensor was engineered in order to study competitive dihydropteridine reductase (DHPR) inhibition. A high-throughput screen, using the designed sensor, was performed on the Prestwick library to discover thirteen new competitively interacting small molecules. Triamterene (TRI), ebselen (EBS), adrenosterone (ADR) and deoxycorticosterone (DCS) were found to be the most potent inhibitors of this set. Their inhibition potency were assayed *in-vitro* on four of the members of the BH4 metabolic pathway, GTP cyclohydrolase I (GCH1), sepiapterin reductase (SPR), dihydrofolate reductase (DHFR) and DHPR. TRI was discovered to be the most active DHPR inhibitor and confirmed to be a potent DHFR binder. EBS showed potency in altering GCH1 and SPR catalytic activity probably by covalently modifying some of the catalytic cysteine residues. Finally, the drug candidates were assayed on adult human dermal fibroblast for their potency to influence the concentration ratios of BH4 and 7,8-dihydrobiopterin (BH2). Here, TRI showed to be the best candidate by reducing the basal BH4/BH2 ratio of ~15 to unity. This effect is more pronounced than that generated by other previously described DHPR inhibitors such as aminopterin. Finally, the observed pterin metabolic imbalance generated by TRI makes it a useful compound to investigate the relevance of BH4/BH2 imbalance.

Keywords: FRET, semisynthetic sensor, dihydropteridine reductase, tetrahydrobiopterin, drug screening, triamterene, ebselen, sterone.

## ***Résumé***

Le développement de composés « outils » pour l'étude de la perturbation du réseau métabolique de la tetrahydrobioptérine (BH4) est d'intérêt, particulièrement dans le cas de la génération du stress oxydatif ou nitrosatif. Un senseur semi-synthétique basé sur l'effet FRET a été créé afin d'étudier l'inhibition compétitive de l'enzyme dihydroptéridine réductase (DHPR). Treize nouveaux inhibiteurs compétitifs ont été découverts lors d'un criblage à haut débit ayant été effectué sur la librairie chimique Prestwick en utilisant le senseur mentionné. Triamtérène (TRI), ebsélène (EBS), adrenostérone (ADR) et déoxycorticostérone (DCS) sont les inhibiteurs possédant le plus haut potentiel inhibitif du set découvert. Leur potentiel inhibitif a été étudié sur quatre des enzymes du réseau métabolique de la tetrahydrobioptérine (BH4) : la guanosine triphosphate cyclohydrolase I (GCH1), la sépiaptérine réductase (SPR), la dihydrofolate réductase (DHFR) et DHPR. Il a été découvert que TRI est le meilleur inhibiteur de la DHPR et confirmé qu'il était aussi un inhibiteur performant de la DHFR. Altération de la capacité enzymatique de la SPR et de la GCH1 par EBS, probablement due à une modification covalente des cystéines catalytiques ou adjacentes aux sites actifs, a été démontrée. Finalement, les molécules candidates ont été testées pour leur potentiel à altérer la balance métabolique entre BH4 et 7,8-dihydrobioptérine (BH2) dans les cellules mammifères de type fibroblaste cutané adulte. La balance métabolique BH4/BH2 basale de quinze a été altérée pour une valeur finale de un par TRI. Cet effet est plus prononcé que celui effectuée par des molécules inhibitrices de la DHPR, précédemment décrites, comme l'aminoptérine. En conclusion, le déséquilibre générée par TRI sur le métabolisme des ptérines dans le model fibroblaste peut être d'intérêt afin d'étudier la pertinence du ratio BH4/BH2.

Mots clés : FRET, senseur semi-synthétique, dihydroptéridine réductase, tetrahydrobioptérine, criblage à haut débit, triamtérène, ebsélène, stérone.

## List of Figures

Fig 1 Tetrahydrobiopterin metabolic network.....	- 5 -
Fig 2 Nomenclature of pterins.....	- 7 -
Fig 3 Electrochemical oxidation scheme of tetrahydrobiopterin.....	- 10 -
Fig 4 DHPR structure.....	- 11 -
Fig 5 Structure of various DHPR substrates. ....	- 12 -
Fig 6 GCH1 & GFRP structure and catalytic mechanism .....	- 16 -
Fig 7 Structure and catalytic mechanism of PTPS. ....	- 19 -
Fig 8 Structure and catalytic mechanism of SPR .....	- 21 -
Fig 9 Structure of DHFR.....	- 24 -
Fig 10 hDHFR catalytic cycles with FH4.....	- 26 -
Fig 11 Structure and catalytic mechanism of PCD.....	- 28 -
Fig 12 Structure and catalytic mechanism of PAH .....	- 30 -
Fig 13 Global structural features of NOSs.....	- 34 -
Fig 14 AGMO catalytic mechanism and schematic structure .....	- 39 -
Fig 15 Typical Snifit scaffold .....	- 43 -
Fig 16 Scheme for the development of semisynthetic FRET sensors. ....	- 45 -
Fig 17 DHPR assay and $K_M$ determination.....	- 47 -
Fig 18 Inhibition assay of DHPR with APT and MTX. ....	- 48 -
Fig 19 Inhibitor derivatives and fluorescent linkers. ....	- 49 -
Fig 20 Inhibition assay of DHPR with derivatives of APT and MTX.....	- 50 -
Fig 21 Comparison between DHPR, labeled and unlabeled minimal scaffolds.....	- 51 -
Fig 22 Fluorescence intensity assay of labeled minimal constructs. ....	- 52 -
Fig 23 Fluorescence polarization, tethered ligand unbinding by APT .....	- 53 -
Fig 24 Models of qBH2 and MTX docking in DHPR.....	- 56 -
Fig 25 Enzymatic assay with DHPR-p30-SNAP.....	- 57 -

Fig 26 Labeled DHPR-Halo-P30-SNAP titration with NADH. ....	- 58 -
Fig 27 Sensor TMR assay and opening.....	- 59 -
Fig 28 cpDHPR constructs ratio change. ....	- 62 -
Fig 29 Sensors optimization based on scaffold rigidification.....	- 63 -
Fig 30 Four DHPR candidates and their IC50 curve. ....	- 67 -
Fig 31 Inhibition potential assessment of the four drug candidates on DHPR and SPR. ....	- 68 -
Fig 32 DHFR inhibition assay with the drug candidates.....	- 68 -
Fig 33 GCH1 enzymatic assay and inhibition.....	- 70 -
Fig 34 Total intracellular pterin concentration. ....	- 71 -
Fig 35 Influence of drugs on pterin intracellular concentrations in FIB.....	- 73 -
Fig 36 Conversion from number of cells per ml to protein concentration. ....	- 75 -
Fig 37 Influence of drugs candidates on pterin intracellular concentrations in FIB.....	- 77 -
Fig 38 EBS catalytic mechanism .....	- 79 -
Fig 39 Pterin quantification method based on HPLC coupled to fluorescence and electrochemical detection.....	- 93 -

## ***List of Tables***

Table 1 Half-life of degradation of different pterins at 25 °C. ....	- 8 -
Table 2 Spectroscopic characteristics of certain pterins. ....	- 9 -
Table 3 Summary of DHPR substrates and inhibitors.....	- 13 -
Table 4 GCH1 regulation by cytokines and compounds. ....	- 17 -
Table 5 Summary of known SPR inhibitors. ....	- 23 -
Table 6 Summary of the drugs discovered via the HTS campaign. ....	- 65 -
Table 7 <i>In-vitro</i> inhibition potentials of the drug candidates towards enzymes members of the BH4 metabolic pathway.....	- 69 -
Table 8 Conversion table from cells to protein content in FIB and neuroblastoma.....	- 96 -



## ***List of Abbreviations***

1'-oxo-PH4	1'-oxo-2'-hydroxypropyl-tetrahydropterin
2'-oxo-PH4	1'-hydroxy-2'-oxopropyl-tetrahydropterin
5HT	5-hydroxy-L-tryptophamine
5HW	5-hydroxy-L-tryptophane
6,7MPH2	6,7-dimethyldihydropterin
6,7MPH4	6,7-dimethyltetrahydropterin
6,7MqPH4	6,7-dimethylquinoidhydropterin
6MPH2	6-methyl-dihydropterin
6MPH4	6-methyltetrahydropterin
6MqPH4	6-methylquinoidhydropterin
ACN	Acetonitrile
ADR	Adrenosterone
AGMO	Alkylglycerol monoxygenase
AMP	Ampicilin
APT	Aminopterin
AR	Aldose reductase
BCA	Bicinchoninic acid
BCN-lysine	(2S)-2-Amino-6-({[(1R,8S)-bicyclo[6.1.0]non-4-yn-9-ylmethoxy]carbonyl}amino)hexanoic acid
BH2	7,8-dihydrobiopterin
BH4	Tetrahydrobiopterin
BSA	Bovine serum albumin
CMP	Chloramphenicol
CNS	Central nervous system
cpDHPR	Circular permutated DHPR
CR	Carbonyl reductase
DAHP	2,4-diamino-6-hydroxypyrimidine

DCS	Deoxycorticosterone
DHFR	Dihydrofolate reductase
DHPR	Dihydropteridine reductase
EB	Estradiol benzoate
EBS	Ebselen
EC50	Half maximal efficient concentration
EDTA	Ethylenediaminetetraacetic acid
EG	Ethyleneglycol
eNOS	Endothelial NOS
FH2	Dihydrofolate
FH4	Tetrahydrofolate
FIB	Fibroblast
FICC	Ferricytochrome-c
FMOC	Fluorenylmethyloxycarbonyl chloride
FOCC	Ferrocycytochrome-c
FP	Fluorescence Polarization
FRET	Förster resonance energy transfer
GABA	$\gamma$ -aminobutyric acid
GCH1	GTP cyclohydrolase 1
GFRP	GCH1 feedback regulatory protein
GSH Px	Glutathione peroxidase
GTP	Guanosine triphosphate
H2NTP	7,8-dihydroneopterin triphosphate
HPLC	High pressure liquid chromatography
HUVECS	Human umbilical vascular endothelial cells
IC50	Half maximal inhibitory concentration
IL-1 $\beta$	Interleukin-1 $\beta$
INF- $\gamma$	Interferon- $\gamma$

iNOS	Induced NOS
K <sub>i</sub>	Inhibition constant
K <sub>m</sub>	Michaelis-Menten constant
L-DOPA	L-dihydroxyphenylalanine
LPS	Lipopolysaccharides
MTX	Methotrexate
NADH	Nicotinamide adenine dinucleotide
NADPH	Nicotinamide adenine dinucleotide phosphate
NAS	N-acetyl serotonin
Neop	Neopterin
NGF	Nerve growth factor
nNOS	Neuronal NOS
NO	Nitric oxide
NOS	Nitric oxide synthase
P30	Proline 30-mer
PAH	Phenylalanine hydroxylase
PCD	Pterin-4 $\alpha$ -carbinolamine dehydratase
PEG	Polyethyleneglycol
PKU	Phenylketonuria
PPH4	6-pyruvoyl-tetrahydropterin
PTPS	6-pyruvoyltetrahydropterin synthase
qBH2	Quinoid-dihydrobioterin
R <sub>max</sub>	Maximal ratio of acceptor over donor fluorescence intensities
ROS	Reactive oxygen species
Sepia	Sepiapterin
SiR	Silicon rhodamine
SMZ	Sulfametazine
SPR	Sepiapterin reductase

SPY	Sulfapyridine
STZ	Sulfathiazole
TCA	Trichloroacetic acid
TMP	Trimetoprim
TMR	Tetramethylrhodamine
TNF- $\alpha$	Tumor necrosis factor- $\alpha$
TPH	Tryptophan hydroxylase
TRI	Triamterene
TYH	Tyrosine hydroxylase
V0	Initial reaction rate
Xantho	Xanthopterin

## ***Table of Contents***

Acknowledgements .....	iii
Abstract.....	iv
Résumé .....	v
List of Figures .....	vi
List of Tables.....	viii
List of Abbreviations.....	ix
Chapter 1. Introduction.....	- 1 -
1.1 The Tetrahydrobiopterin Metabolic Network.....	- 1 -
1.2 Properties of Pterins .....	- 6 -
1.2.1 Nomenclature.....	- 6 -
1.2.2 Physicochemical Properties.....	- 7 -
1.3 Enzymes of the BH4 Metabolic Network .....	- 10 -
1.3.1 Dihydropteridine reductase (DHPR) .....	- 10 -
1.3.2 GTP Cyclohydrolase 1 (GCH1) and GCH1 Feedback Regulatory Protein (GFRP).....	- 14 -
1.3.3 6-pyruvoyltetrahydropterin synthase (PTPS) .....	- 18 -
1.3.4 Sepiapterin Reductase (SPR) .....	- 20 -
1.3.5 Dihydrofolate Reductase (DHFR) .....	- 23 -
1.3.6 Pterin-4 $\alpha$ -carbinolamine dehydratase (PCD) .....	- 27 -
1.4 Biological Relevance of Pterins.....	- 29 -
1.4.1 Amino Acid Hydroxylases .....	- 29 -
1.4.2 Nitric Oxide Synthesis.....	- 32 -
1.4.3 Phenylketonuria.....	- 35 -
1.4.4 Dopamine-Responsive Dystonia .....	- 36 -
1.4.5 Neuropathic Pain .....	- 37 -
1.4.6 Alkylglycerol Monooxygenase .....	- 38 -
1.4.7 Vitiligo .....	- 39 -
1.5 In Vivo Pterin Quantification .....	- 40 -
1.5.1 Chemical Oxidation .....	- 40 -
1.5.2 Electrochemical Detection .....	- 41 -
1.5.3 Liquid Chromatography Mass Spectrometry.....	- 41 -
1.6 Semi-Synthetic Sensors.....	- 41 -
Chapter 2. Results .....	- 45 -

2.1	A Sensor for DHPR Inhibitors.....	- 45 -
2.1.1	Sensor Development Strategy .....	- 45 -
2.1.2	DHPR Assay.....	- 47 -
2.1.3	Drug Derivatization and Linker Synthesis.....	- 49 -
2.1.4	Anisotropy Study of the Binding .....	- 52 -
2.1.5	In-Silico Modeling for Rational Sensor Design.....	- 54 -
2.1.6	Scaffold Spacing .....	- 56 -
2.1.7	First Sensor Iteration.....	- 58 -
2.1.8	Sensor Optimization.....	- 61 -
2.2	Prestwick Library Screen .....	- 65 -
2.2.1	Library Selection .....	- 65 -
2.2.2	New DHPR Inhibitors.....	- 65 -
2.3	Further Candidate Characterization .....	- 67 -
2.3.1	In-Vitro Characterization .....	- 67 -
2.3.2	In-Vivo Characterization .....	- 71 -
2.4	Discussion on the Discovered Compounds .....	- 78 -
2.4.1	On Triamterene.....	- 78 -
2.4.2	On Ebselen.....	- 79 -
2.4.3	On Adrenosterone and Deoxycorticosterone.....	- 82 -
Chapter 3.	Conclusion .....	- 85 -
3.1	Achievements.....	- 85 -
3.2	Future Development.....	- 86 -
Chapter 4.	Material and Methods .....	- 87 -
4.1	General Methods.....	- 87 -
4.1.1	Cloning.....	- 87 -
4.1.2	Protein Expression .....	- 87 -
4.1.3	Protein Labeling .....	- 87 -
4.2	Enzymatic Assays .....	- 88 -
4.2.1	DHPR Cytochrome-c Based Assay .....	- 88 -
4.2.2	DHFR Assay .....	- 89 -
4.2.3	SPR Assay.....	- 89 -
4.2.4	GCH1 Assay.....	- 89 -
4.3	Fluorescence Polarization .....	- 90 -
4.4	High Throughput Screen .....	- 90 -

4.5	Cell Culture .....	- 91 -
4.6	HPLC Fluorescence and Electrochemical Detection .....	- 91 -
4.7	Pterin Quantification .....	- 92 -
4.8	In-Silico Docking .....	- 94 -
4.9	Unnatural Amino Acids Incorporation .....	- 94 -
4.10	Protein content per Cell .....	- 95 -
4.11	Chemical Synthesis .....	- 96 -
4.11.1	General Procedures .....	- 97 -
4.11.2	MTX and APT Derivatives .....	- 98 -
4.11.3	Linkers and Control Linkers .....	- 100 -
	References .....	- 105 -
	Appendix: Amino Acid Sequences .....	- 120 -
	Appendix: protein gels and yields .....	- 123 -
	Appendix: Structures of the Hits .....	- 126 -
	Curriculum Vitae.....	- 128 -





## **Chapter 1. Introduction**

This thesis focused on a characterization of the tetrahydrobiopterin metabolic network, and most importantly on the role of dihydropteridine reductase, one of its enzymes. We focused on this enzyme as tool compounds for its selective inhibition were lacking, yet it plays an important role in recycling oxidized cofactor. Furthermore, screening for inhibitors based on FDA approved drugs was of interest in order to see if side effects of certain administered drugs could be linked to unwanted interactions with the tetrahydrobiopterin network. Consequently, development of a system allowing one to characterize the interactions of small molecules with our enzyme of interest was undertaken.

### **1.1 The Tetrahydrobiopterin Metabolic Network**

The word pterin comes from the Greek word wing: “*pteron*”. The pterin family was first described in the late 1800s when F. G. Hopkins purified the compound xanthopterin from the English brimstone butterfly. Several other pterin derivatives were isolated later on from butterflies and excreted substances. Currently, pterins are mostly studied for their biological relevance as metabolites.

Tetrahydrobiopterin (BH<sub>4</sub>), a reduced form of pterin, is the key compound of what will be named here the tetrahydrobiopterin metabolic network. Synthesized *de novo* from GTP by the successive action of three enzymes – GTP cyclohydrolase 1 (GCH1), 6-pyruvoyltetrahydropterin synthase (PTPS) and sepiapterin reductase (SPR) – the metabolism of BH<sub>4</sub> is complex (Fig. 1). The committing step is realized at the level of GCH1 where pathway regulation takes place. Although SPR-mediated BH<sub>4</sub> biosynthesis is favored, there is an alternative BH<sub>4</sub> synthesis pathway from 6-pyruvoyl-tetrahydropterin (PPH<sub>4</sub>) involving aldose reductase (AR) B1 and C3, and carbonyl reductase (CR). Double reduction of PPH<sub>4</sub> by AR-B1, yields in first instance 1'-hydroxy-2'-oxopropyl-tetrahydropterin (2'-oxo-PH<sub>4</sub>), and then BH<sub>4</sub> in a nicotinamide adenine dinucleotide phosphate (NADPH) dependent fashion. Furthermore, reduction of

PPH4 can, as well, via the action of CR or AR-C3 yield 1'-oxo-2'-hydroxypropyl-tetrahydropterin (1'-oxo-PH4), from which BH4 can be then accessed by enzymatic conversion through SPR.

BH4 is a cofactor for the hydroxylases phenylalanine hydroxylase (PAH), tyrosine hydroxylase (TYH) and tryptophan hydroxylase (TPH). It acts as an electron donor and feedback regulator for the biosynthesis of tyrosine, L-dihydroxyphenylalanine (L-DOPA) and 5-hydroxy-L-tryptophan (5HT) the precursor of the neurotransmitter serotonin (Fig1, blue rectangle). During these reactions BH4 is oxidized to 4 $\alpha$ -hydroxy-tetrahydropterin (4HTP), which enters the recycling pathway. 4HTP can dehydrate in a non-enzymatic fashion or via enzymatic catalysis by pterin-4 $\alpha$ -carbinolamine dehydratase (PCD) to yield 6,7-dihydrobiopterin, commonly called quinoid-dihydrobiopterin (qBH2). 4HTP can in some conditions non-enzymatically isomerize to C7 derivatized analogues.

Oxidized BH4 can be reformed via 2 routes. In the recycling pathway, dihydropteridine reductase (DHPR) reduces qBH2 to BH4 via nicotinamide adenine dinucleotide (NADH)-mediated catalysis, closing the recycling pathway loop (Fig 1, green rectangle). Secondly, the salvage pathway is accessed via two non-enzymatic oxidations. qBH2, from the recycling pathway, can isomerize to 7,8-dihydrobiopterin (BH2). In a similar fashion, 1'-oxo-PH4 can be oxidized to sepiapterin, which is converted in an NADPH-dependent fashion via SPR or CR to BH2. Dihydrofolate-reductase (DHFR) reduces, in an NADPH-mediated catalysis, BH2 to BH4 closing the salvage pathway loop (Fig 1, yellow rectangle).

BH4 biosynthesis is regulated via GCH1 where the enzyme usually resides attached to its feedback regulatory protein (GFRP). In this context BH4 acts as a feedback regulator, reducing GCH1 catalytic activity while phenylalanine acts as a feedforward modulator. Furthermore, the expression levels of the GCH1 is modulated by numbers of compounds such as cytokines. Each part of this pathway and the enzymes involved (except AR and CR) are described in greater detail in the following.

BH4 is involved in the regulation of the three nitric oxide synthase (NOS) isoforms. Endothelial NOS (eNOS), induced NOS (iNOS) and neuronal NOS (nNOS) all tightly bind BH4 as activator in order to promote the production of nitric oxide (NO). In addition, BH4 acts as an electron donor in the production of glycerol and aliphatic aldehydes in a reaction involving the enzyme alkylglycerol monooxygenase (AGMO). Finally, it has been recently discovered that BH4 is a regulator in the process of monoamine neurotransmitter sulfonation.

Therapeutically, defects in enzymes involved in the BH4 metabolic network can potentially lead to disastrous effects. Segawa's disease, also called DOPA responsive dystonia, is caused by mutations in the *gch1* gene and often translates in phenotypes such as postural disorders. More common, and involving most of the pathway's enzymes, is the disease phenylketonuria (PKU, further detailed later). PKU is caused by an increase of serum phenylalanine and low levels of serotonin, epinephrine and norepinephrine. Consequently, patients experience cognitive impairments, dystonia and tremors. Furthermore, BH4 availability, particularly increased levels, was shown to influence many sensory neurones. Often caused by lesions in the somatosensory system, GCH1 and nNOS upregulation is the optimal condition for NO overproduction. It triggers sensitizing nociceptors leading to pathological hypersensitivity. Finally, evidence also shows that BH4 has implications in the depigmentation disorder vitiligo. PCD deficiency leads to formation of 7-substituted pterins reported as inhibitors in the biosynthesis of melanin pigments.

# Tetrahydrobiopterin metabolic network: A recapitulative infographic

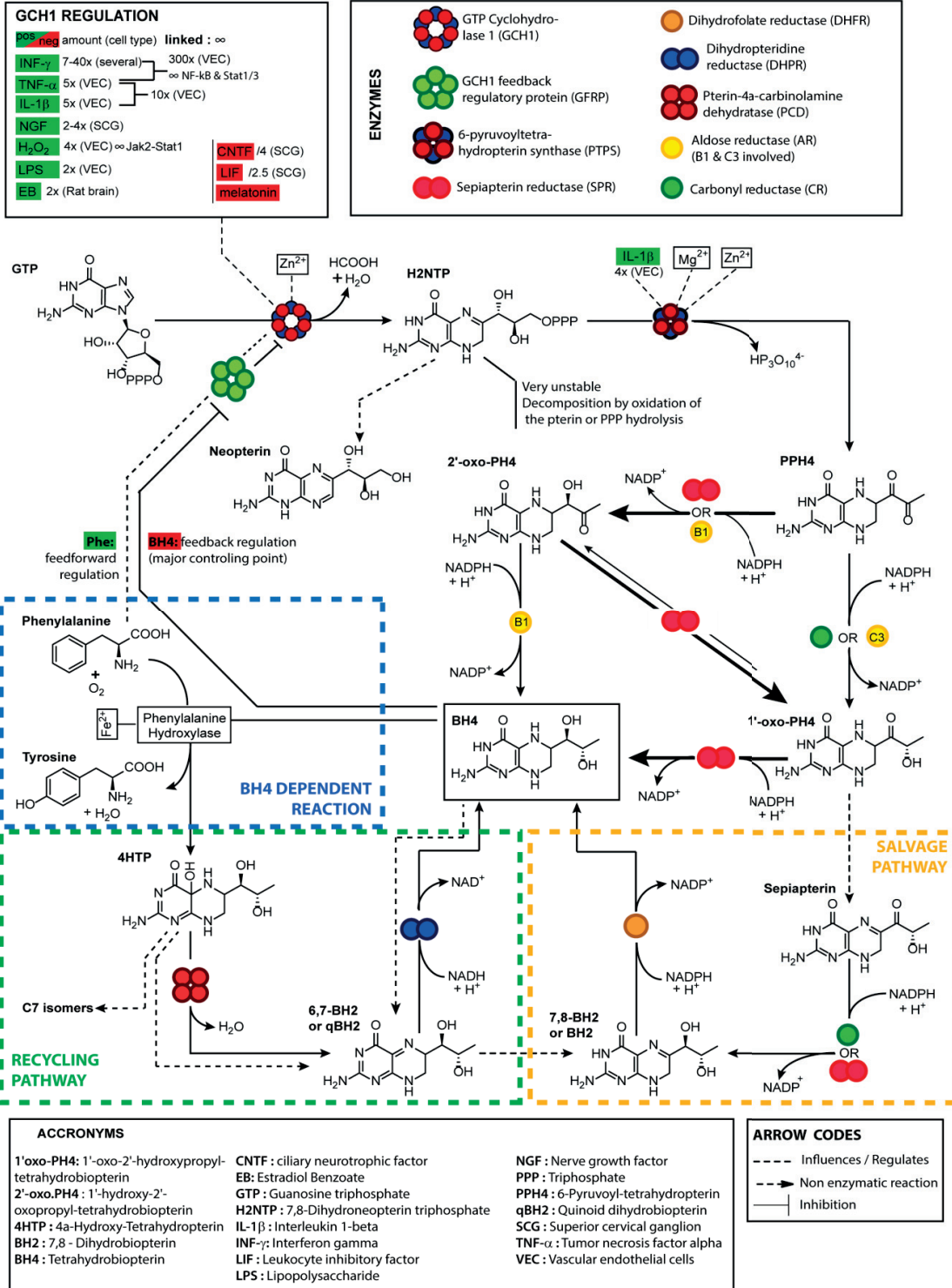


**Fig 1 Tetrahydrobiopterin metabolic network.** The network is composed of three main pathways. The *de novo* BH4 biosynthesis (not framed) is accomplished by principally GCH1, PTPS and SPR. GCH1 catalysis of GTP is the rate limiting step. It is regulated by feedback and feedforward mechanisms, mediated by GFRP, via the action of respectively BH4 and Phe. On the transcriptional level GCH1 activity is modulated via several biological molecule but markedly cytokines. BH4 is a cofactor for, but not exclusively, the hydroxylase family (blue frame) acting as an e<sup>-</sup> donor. The recycling pathway (green frame) regenerates the oxidized cofactor 4HTP via the action of PCD and DHPR. Water elimination from 4HTP is principally catalyzed by PCD but also occurs non-enzymatically. 4HTP can as well isomerize to C7 pterin isomers. qBH2, the product of dehydration by PCD, isomerizes to BH2 entering the salvage pathway (yellow frame). The salvage pathway can be accessed from sepiapterin, in case of SPR deficiency. A combination of AR-B1 and AR-C3, as well as CR can compensate for SPR deficiency. Compounds from the salvage pathway are reduced back to BH4 by DHFR.

## **1.2 Properties of Pterins**

### **1.2.1 Nomenclature**

The pteridine bicyclic system is composed of fused pyrazine and pyrimidine rings which are commonly numbered as detailed in Fig 2. The molecule 2-amino-4-hydroxy-pteridine is commonly called *pterin* and is found in all the naturally occurring derivatives of this compound. The pterins are divided in two subclasses: the conjugated and unconjugated pterins. The folic acid family is part of the conjugated pterin subclass since it bears on its C6 a p-aminobenzoylglutamic acid residue (Fig 2 seen in red). All other pterins are part of the unconjugated subclass even though most of the naturally-occurring pterins carry a side chain on the C6. Indication of the C6 carbon derivatization, as seen for neopterin, xanthopterin and sepiapterin, precedes "pterin". The redox state of atoms 5 to 8 is described by prefixing the degree of hydrogenation (Fig 2 seen in blue). The group of biosynthetically obtained pterins is called biopterins and often carries as structural feature a hydroxy- or keto-substituted propyl chain<sup>1</sup>. Pterins part of the BH4 metabolic network are only a fraction of naturally occurring forms of the pterin family. Nature derivatizes the C6 and C7 positions in myriads of ways<sup>2,3</sup> and by forming pterin dimers, like drosopterin and pterorhodin, created vast arrays of pigments present mostly in insects<sup>4</sup>

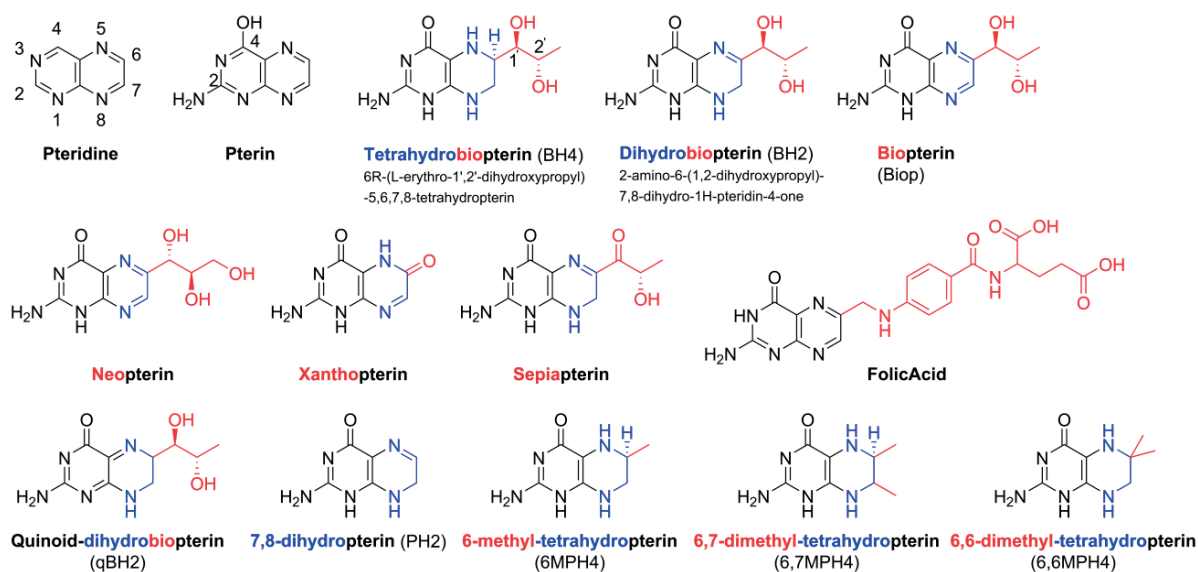


**Fig 2 Nomenclature of pterins.** The pteridine ring system is composed of fused pyrazine and pyrimidine rings. The figure shows the commonly used atoms numbering. Bearing on the C2 and C4 positions an amino and a carboxy group respectively is the pterin system. Prefixes are arranged to describe the C6 derivatization (red) and the redox state of N5 to N8 (blue).

### 1.2.2 Physicochemical Properties

Tetrahydrobiopterin is unstable in aqueous buffers and degrades due to aerobic oxidation to qBH2 and rearranges to BH2<sup>5</sup>. Auto-oxidation proceeds faster at higher pH and oppositely in acidic conditions. In certain conditions, complete loss of the 1,2-dihydropropyl moiety takes place<sup>6</sup>. Experimentally, this instability is problematic for quantification of the compound, study of enzymatic processes and study of protein-molecule interactions. Other synthetic analogues such as 6-methyl-tetrahydropterin (6MPH4) and 6,7-dimethyl-tetrahydropterin (6,7MPH4) have shown better stability in neutral aqueous solutions<sup>7,8</sup>. 6MPH4 is roughly two times more stable in aqueous buffer than 6,7MPH4<sup>9</sup>. These compounds are usually suitable substitutes for the study of pterin related *in vitro* experiments.

Generally, reducing agents such as dithiothreitol (DTT, 1% w/w) or ascorbic acid are used to prevent BH4 oxidation. It was shown that BH4 stability in 200 mM trichloro acetic acid (TCA) and 6.5 mM DTT is quantitative over 48 h<sup>10</sup>. Similar solutions are often used to precipitate proteins in cellular experiments. Chelating agents such as EDTA or DTPA have also shown to prevent transition metal driven oxidation<sup>8</sup>.

Compound rate of degradation at 25°C			
[BH4], half-life	Condition	[BH2], half-life	Condition
20 nM, $t_{1/2} > 48$ h	300 mM TCA, 6.5 mM DTE <sup>11</sup>	20 nM, $t_{1/2} = 3.3$ h	300 mM TCA, pH: 0.89 <sup>11</sup>
20 nM, 0.25 nM/h	50 mM phosphate, 6.5 mM DTE, pH: 7.4 <sup>11</sup>	20 nM, $t_{1/2} = 4.73$ h	300 mM TCA + 6.5 mM DTE, pH: 0.89 <sup>11</sup>
30 $\mu$ M, $t_{1/2} = 10$ min	100 mM phosphate, pH: 6.8 <sup>5</sup>	20 nM, $t_{1/2} = 79.7$ h	50 mM phosphate, pH: 7.4 <sup>11</sup>
30 $\mu$ M, $t_{1/2} = 6.5$ min	100 mM phosphate, pH: 8.2 <sup>5</sup>	20 nM, $t_{1/2} = 113$ h	50 mM citrate, pH: 6 <sup>11</sup>
30 $\mu$ M, $t_{1/2} = 38.5$ min	50 mM triethanolamine/HCl, pH: 7 <sup>12</sup>	20 nM, $t_{1/2} = 6.6$ h	50 mM citrate, pH: 3 <sup>11</sup>
100 $\mu$ M, $t_{1/2} \sim 30$ min	100 mM phosphate, 0.4 mM DTPA, pH 7.4 <sup>10</sup>		
[qBH2], half-life	Condition	[6,7MePH4], half-life	Condition
30 $\mu$ M, $t_{1/2} \sim 1.3$ min	100 mM phosphate, pH: 6.8 <sup>5</sup>	1 mM, $t_{1/2} = 120$ min	Chloroacetic acid, pH: 3 <sup>8</sup>
		1 mM, $t_{1/2} = 25$ min	HEPES, pH: 8 <sup>8</sup>
		1 mM, $t_{1/2} = 2$ min	NaOH, pH: 13 <sup>8</sup>
[6MqPH2], half-life	Condition	[6,7MqPH2], half-life	Condition
10 $\mu$ M, $t_{1/2} \sim 1.7$ min	100 mM phosphate, pH: 6.8 <sup>13</sup>	100 $\mu$ M, $t_{1/2} \sim 45$ s	100 mM phosphate, pH: 6.8 <sup>9</sup>
10 $\mu$ M, $t_{1/2} \sim 27.7$ min	100 mM Tris, pH: 6.8 <sup>13</sup>	100 $\mu$ M, $t_{1/2} \sim 14$ min	100 mM Tris, pH: 6.8 <sup>9</sup>

**Table 1 Half-life of degradation of different pterins at 25 °C.** The rate of endogenous and synthetic pterins is presented has half-life ( $t_{1/2}$ ) for first order reactions and with their respective units for zero order reaction. Concentration and conditions are indicated as they influence the degradation rate.

BH2 and other dihydro-analogues have a greater aqueous stability but will still degrade or oxidize relatively slowly in acidic conditions. Biopterin is the main degradation product of BH2, in aqueous buffers, regardless of the pH. It has been shown that both BH4 and BH2 stability, independent of the conditions, is concentration dependent as well. In acidic conditions, traditionally used for protein precipitation prior analysis, BH2 half-life was determined to be greater than 2.5 h<sup>11</sup>. The degradation half-life of several pterins is reported in Table 1.

Oxidized pterin rings have three characteristic UV absorbance bands around 230, 280 and 330nm<sup>5,14</sup>. BH4 is non-fluorescent, while BH2 is about half as brightly fluorescent as biopterin. Pterin also possesses very strong fluorescence. All of the fluorescent pterins can be excited around 350nm and emit around 450nm. A summary of the absorbance and fluorescence properties is given in Table 2.

Relevant to the method used later for the quantification of pterins are their electrochemical properties. BH4 was shown to possess an oxidation potential of  $E = 270$  to  $300$  mV vs NHE, a potential sufficient to reduce several biologically relevant molecules<sup>15</sup> and ferric iron<sup>8</sup>. Notably, BH4 reduces rapidly cytochrome-c ( $E_{(Fe+3)/Fe+2} = 260$  mV,  $k = 4.4E3 M^{-1}\cdot s^{-1}$ ) and cytochrome-b5 ( $E_{(Fe+3)/Fe+2} = 0$  mV,  $k = 0.2$



$M^{-1}\cdot s^{-1}$ ) potentially impacting mitochondrial functions<sup>16</sup>. The potential needed to oxidize BH2 was reported to be 820mV vs NHE.

Spectroscopic characteristics of certain pterins		
Name	Absorbance UV ext. coef. [ $M^{-1} cm^{-1}$ ] @ wl. [nm]; buffer	Fluorescence (quant. yield;ext[nm];em[nm];cond)
BH4	14300 @ 265; 0.1 M HCl <sup>17</sup> 5500 @ 295; 0.1 M HCl <sup>17</sup>	N.D.
BH2	26120 @ 230; 0.1 M phosphate, pH: 6.8 <sup>5</sup> 11330 @ 279; 0.1 M phosphate, pH: 6.8 <sup>5</sup> 6820 @ 330; 0.1 M phosphate, pH: 6.8 <sup>5</sup> 13510 @ 257; 0.1 M HCl <sup>5</sup> 4850 @ 367; 0.1 M HCl <sup>5</sup>	5.3e-2;350;450;- <sup>14</sup>
Biop	11000 @ 247; 0.1 M HCl <sup>18</sup> 5200 @ 350, 0.1	0.1, 350;450;- <sup>14</sup> 0.16, 360;450;pH: 3
PH2	10850 @ 275; 0.1 M phosphate, pH: 6.8 <sup>5</sup> 5400 @ 325; 0.1 M phosphate, pH: 6.8 <sup>5</sup> 13670 @ 259; 0.1 M HCl <sup>5</sup> 2180 @ 321; 0.1 M HCl <sup>5</sup> 1890 @ 370; 0.1 M HCl <sup>5</sup>	-
Pterin	11200 @ 235; AcOH, pH: 5 <sup>19</sup> 12300 @ 270; AcOH, pH: 5 <sup>19</sup> 6000 @ 338; AcOH, pH: 5 <sup>19</sup> 2683 @ 324; phosphate, pH: 6.8 <sup>20</sup>	0.33; 360; 450; acidic
XH2	1911 @ 324; phosphate, pH: 6.8 <sup>20</sup>	-
Neopterin		0.16, 360;450;pH: 3

**Table 2 Spectroscopic characteristics of certain pterins.** Various pterins absorbances at specific wavelength and conditions as well as quantum yields are given. N.D.: not detectable. Some conditions are not specified and are replaced by a dash.

Two electrochemical oxidation mechanisms, dependent on the experimental setup (pH variation, glassy carbon electrode vs polished carbon surface) were proposed. Reports diverge on the mechanism of electro-oxidation of BH4 to biopterin via qBH2 and BH2. Some authors argue that each oxidation step is a two electron process<sup>21,22</sup> while others present a single electron transfer forming a cation radical followed by a rapid chemical rearrangement<sup>15</sup> (Fig 3). All agree though that the qBH2 to BH2 isomerization cannot be forced by applying electrical potential and proceeds with a half-life of roughly 87 s.

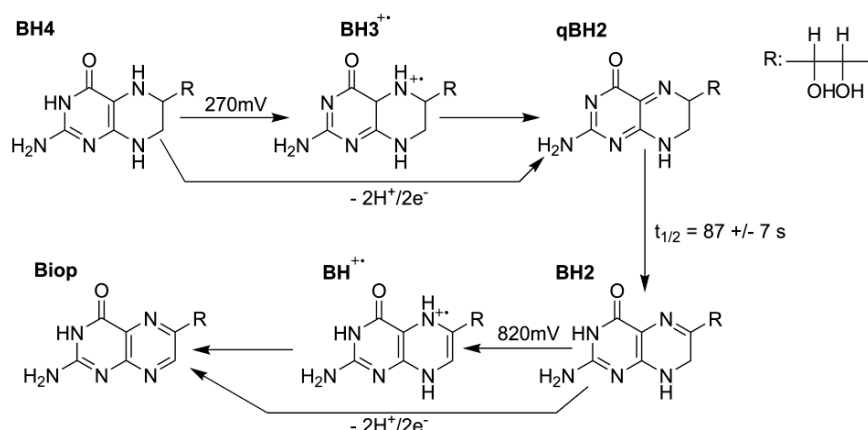


**Fig 3 Electrochemical oxidation scheme of tetrahydrobiopterin.** Two oxidation mechanisms have been proposed. One proceeds in a single step two-electron fashion, whereas the other proceeds in a two-step single-electron way. The latter mechanism is believed to form transient cationic radicals rapidly rearranging to form the oxidized analogue. qBH2 cannot be forced to isomerize to BH2.

### 1.3 Enzymes of the BH4 Metabolic Network

#### 1.3.1 Dihydropteridine reductase (DHPR)

##### 1.3.1.1 History of Discovery

S. Kaufman, in 1957, was studying the conversion of phenylalanine to tyrosine<sup>23</sup> and discovered that this reaction required two enzymes purified from liver, NADPH and oxygen to take place. In the same year, he suggested that an unknown cofactor might be implied in this conversion<sup>24</sup>. Following, he stipulated correctly, that this previously suggested cofactor, if missing, would lead to phenylketonuria<sup>25</sup>. The system was further described and in 1958 he was able to show that one of the two enzymes was a reductase. This enzyme promotes an interaction between the cofactor and NADPH and would not require oxygen<sup>26</sup>. It was noted that the cofactor could belong to the pteridine family based on the observation that it possessed high nitrogen content and on the activity of tetrahydrofolate in the assay<sup>27</sup>. Relying on this information, Kaufman tested 6,7-dimethyltetrahydropterin (6,7MBH4), and 6-methyltetrahydropterin (6MBH4) as cofactors in the system showing that the later was the most efficient<sup>7</sup>. In 1959, the roles of two enzymes were attributed showing that the second enzyme was an hydroxylase that had no interaction with NADPH and converted phenylalanine to tyrosine only in the

presence of BH4. It was also confirmed that the reductase keeps, in the presence of NADPH, the BH4 in its active form<sup>28,29</sup>. Between 1963 and 1966, Kaufman described the reductase cofactor further and, by observing high activity of the compounds sepiapterin and reduced biopterin concluded that the reductase enzyme cofactor is a dihydropteridine in its quinoid form<sup>30,31,32</sup>. He also discarded the possibility that DHFR might act as the reducing enzyme through the inhibition of both DHFR and DHPR enzymes by aminopterin (APT)<sup>33</sup>. The reductase enzyme was named DHPR in a later paper<sup>34</sup> and it was discovered by Nielsen et. al. in 1969 to have a much higher affinity for NADH<sup>13</sup>. These results marked the first milestone in the understanding of the BH4 recycling pathway.

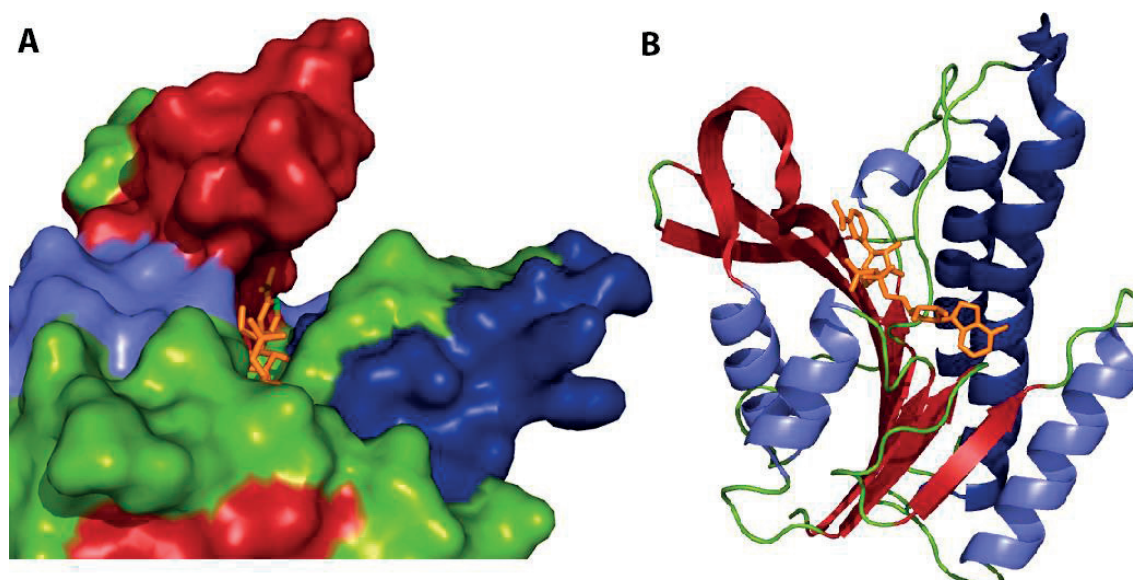


**Fig 4 DHPR structure:** (A) Surface representation of the active site. NADH is represented in orange and its C4, colored in light green. Points towards the active site cleft (red and green). (B) Cartoon representation of DHPR.  $\beta$ -sheets are represented in red and form the backbone of the enzyme. The  $\alpha$ -helices are colored in blue with, in dark blue, the helices responsible for the DHPR homodimer formation. Pdb reference : 1DIR

### 1.3.1.2 DHPR Structure

Isolated from rat liver, a first DHPR crystal structure with its natural cofactor NADH was proposed in 1992 by Varughese et. al.<sup>35</sup>. Obtainment of this structure was preceded by crystallization attempts<sup>36</sup> and primary structure studies on several homologues<sup>37</sup>. A year later the human DHPR structure along with its

full characterization was published<sup>38</sup>. Later on several homologues were crystalized but so far no structure has been reported with BH2 or with the natural cofactor qBH2<sup>39,40</sup> due to the instability of the cofactor.

DHPR is a member of the short chain dehydrogenase/reductase family<sup>41</sup>, a family presenting a common conserved Rossmann-type dinucleotide fold. As seen in Fig 4, the DHPR core is predominantly composed of  $\beta$ -sheets (red) whereas  $\alpha$ -helices (blue) flank the core to compose the outer shell. This protein fold is common in enzymes such as alcohol<sup>42</sup>, malate<sup>43</sup> and lactate dehydrogenase<sup>44</sup> where the dinucleotide binding domain, composed of 150 to 200 amino acids, is conserved and a second, substrate specific, binding domain has evolved to fulfill its catalytic function. The naturally occurring enzyme structure consists of a homodimer bound to two NADH molecules<sup>35,38</sup>. The dimeric structure is stabilized by a 4  $\alpha$ -helix cluster (Fig 4 dark blue), a common structural motif in these proteins<sup>45,46</sup>.

The DHPR active site is a U-shaped surface channel where qBH2 docks. The molecule qBH2 is reduced by the transfer of the pro-S hydrogen of NADH to its N5<sup>47</sup> (Fig 4A). A sequential substrate binding mechanism was reported<sup>48</sup> where first NADH binds to DHPR followed by qBH2. BH4 is then released first followed by NAD<sup>+</sup>. This mechanism is corroborated by the observation that DHPR was not able to bind to APT-agarose columns in the absence of NADH<sup>49</sup> and was further confirmed in our experiments. Further details on how qBH2 might bind are given in the results section.

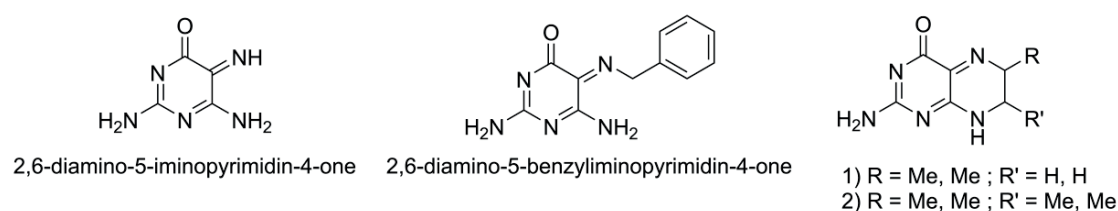


**Fig 5 Structure of various DHPR substrates.** DHPR has a weaker affinity for the two pyrimidino derivatives compared to pterin derivatives showing the importance of the closed pyrazine ring.

### 1.3.1.3 Substrates and Inhibitors

As previously described, the natural substrate qBH2 and cofactors NADH of DHPR are characterized with the respective  $K_d \approx 20 \text{ nM}^{50}$  and  $K_M = 0.15 \text{ }\mu\text{M}^{38}$ . The  $K_d$  of NADH is roughly 55-fold and 2000-fold lower than that of NADPH ( $K_d = 2.02 \text{ }\mu\text{M}$ ) and  $\text{NAD}^+$  ( $K_d \approx 0.1 \text{ mM}^{38}$ ), respectively. Furthermore, it is expected for the enzyme to be bound, in the cytosol, to NADH as the respective concentration is 5000 folds above the  $K_d$ . It is of importance when later designing a sensor which will be bound to NADH as to keep relevance with respect to the cellular conditions. Several synthetic derivatives of pterin are substrate analogues, see Table 3. As previously discussed, derivatization on both C6 and C7 are to a certain extent accepted by the enzyme. It was shown that methyl groups can saturate C6 & C7 of the pterin. Furthermore, the pyrazine ring does not need to be closed for a compound to be a substrate. As seen in Fig 5, several synthetic compounds were shown to be reduced even when the substrate lacked C6 and C7 or the C7-N8 bond<sup>51</sup>. It was reported that the  $K_M$  value for 2,6-diamino-5-iminopyrimidin-4-one is an order of magnitude higher than the  $K_M$  value for quinoid 6,6,7,7-tetrahydropterin supporting the notion that a conserved pyrazine ring improves binding<sup>51</sup>.

Substrates		
Name	$K_d / K_M$ [ $\mu\text{M}$ ]	[Cytoplasm] [ $\mu\text{M}$ ]
NADH	$K_d = 0.02$	$99 \pm 37$ <sup>52</sup>
$\text{NAD}^+$	$K_d \approx 100$	$230 \pm 111$ <sup>53</sup>
NADPH	$K_d = 2.02$	$100 \pm 50$ <sup>54</sup>
qBH2	$K_M = 0.15$	
BH4	$K_d = 30$	
6,7-dimethyl- quinoid-dihydropterin	$K_M = 13.4$ <sup>55</sup>	
6-methyl-quinoid-dihydropterin	$K_M = 19.4$ <sup>13</sup>	
Inhibitors		
Name	$K_i$ [ $\mu\text{M}$ ]	
Amethopterin (Methotrexate - MTX)	38	
Aminopterin (APT)	20	
2,4-Diaminopteroic acid	29.5	
2,4-Diaminopteroic-7,8-dihydropteroylglutamic acid	23	
Quinoid 2,4-Diaminopteroic-7,8-dihydropteroylglutamic acid	22	

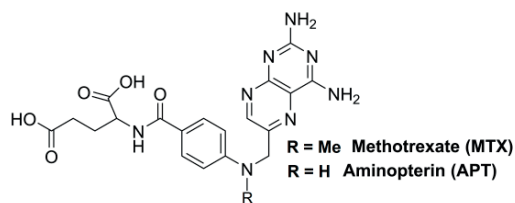


**Table 3 Summary of DHPR substrates and inhibitors.** Relevant DHPR substrate  $K_M$  and  $K_d$  as well as known competitive inhibitors are given. If not stated values come from the reference<sup>56</sup>. The structure of the inhibitors MTX and APT is given.

As previously discussed, quinoid forms of pterin are oxidized non-enzymatically to their 7,8 dihydropteridin forms becoming a DHFR substrate. Several DHFR competitive inhibitors were reported and are summarized in Table 3. The  $K_i$  values reported for these inhibitors were obtained on liver extracts (rat and sheep). Additionally, a large amount of studies have been made to determine the thermodynamic and kinetic values for the interaction of DHFR and its substrates. Reported values vary a lot due to the nature of the experiment used and the purification from tissues of different species. Several non-competitive or uncompetitive inhibitors were reported<sup>57,58,59</sup> but will not be further described here.

### ***1.3.2 GTP Cyclohydrolase 1 (GCH1) and GCH1 Feedback Regulatory Protein (GFRP)***

#### ***1.3.2.1 History of GCH1 & GFRP Discovery***

GCH1 was first purified in 1968 from *E.coli* cultures when A. W. Burg and G. M. Brown realized that an enzyme incorporated GTP in the pteridine moiety of folic acid and was releasing formic acid in the process<sup>60</sup>. It was hypothesized correctly that GCH1 was solely responsible, for the complex, multistep, catalysis of 7,8-dihydroneopterin triphosphate (H2NTP). A year later, G. M. Brown found evidence of the Amadori rearrangement taking place in the GTP ribose prior to pterin ring closure<sup>61</sup>. Mechanistic details, particularly on the hydrogen transfer, were later solved by Bracher et al.<sup>62</sup>. But it was only in 1995 when the first GCH1 crystal structure was presented by Nar that the role of some of the amino acids could be established<sup>63,64</sup>. In the meantime Harada pointed out correctly that GCH1 feedback inhibition by BH4 was due to another element. The p53 peptide, called now GFRP, was isolated and characterized<sup>65</sup>. Value disagreement during an experiment comparing GCH1 rates isolated from rat liver or purified from *E. coli* – lacking the BH4 metabolic pathway – in the presence of allosteric modulators shed light on the

regulatory peptide presence<sup>66</sup>. Finally, Maita reported in 2002 and 2004 crystal structures of GFRP bound to GCH1, setting a milestone in the research on GCH1-GFRP interaction and mechanism<sup>67,68</sup>.

### **1.3.2.2 Structure and Mechanism**

GCH1 is a 260 kDa torus-shaped homodimer of homopentamers. Each pentamer is formed via a 20 residues antiparallel  $\beta$ -sheet association combining face-to-face to form the homodecamer (Fig 6 A,C). GCH1 possesses 10 independent active sites each located at the interface of 3 monomers and bound to a zinc ion (Fig 6 D). Binding of GTP is highly specific and no other nucleotides were reported as suitable substrates. A  $K_M$  of 75  $\mu$ M for GTP was reported independent of GFRP binding<sup>69</sup>. His179 initiates the GTP conversion reaction by interacting with the guanidine N7 while His112 would H-bond to the ribose oxygen (Fig 6 E). Ring opening and formic acid elimination is mediated by the zinc ion coordinated by Cys110 and Cys181<sup>70</sup>. Finally, proton exchange and ketone formation, allowing ring closing via Schiff's base dehydration, is mediated by Ser135 to yield H2NTP<sup>63</sup>.

GFRP is a homopentamer of 50 kDa and part of the  $\beta$ -propeller family, where each subunit is composed of 83 amino acids<sup>71</sup>. Two GFRP units interact with one GCH1 homodecamer, binding at the top and bottom of the torus yielding a 360 kDa complex (Fig 6 B, C). A  $K_d$  of 8 to 15 nM has been reported for this interaction independent of the presence of substrates<sup>72,73</sup>. Three loops from one GFRP subunit interact with two GCH1 subunits creating an accessible cleft for phenylalanine and BH4 to bind.

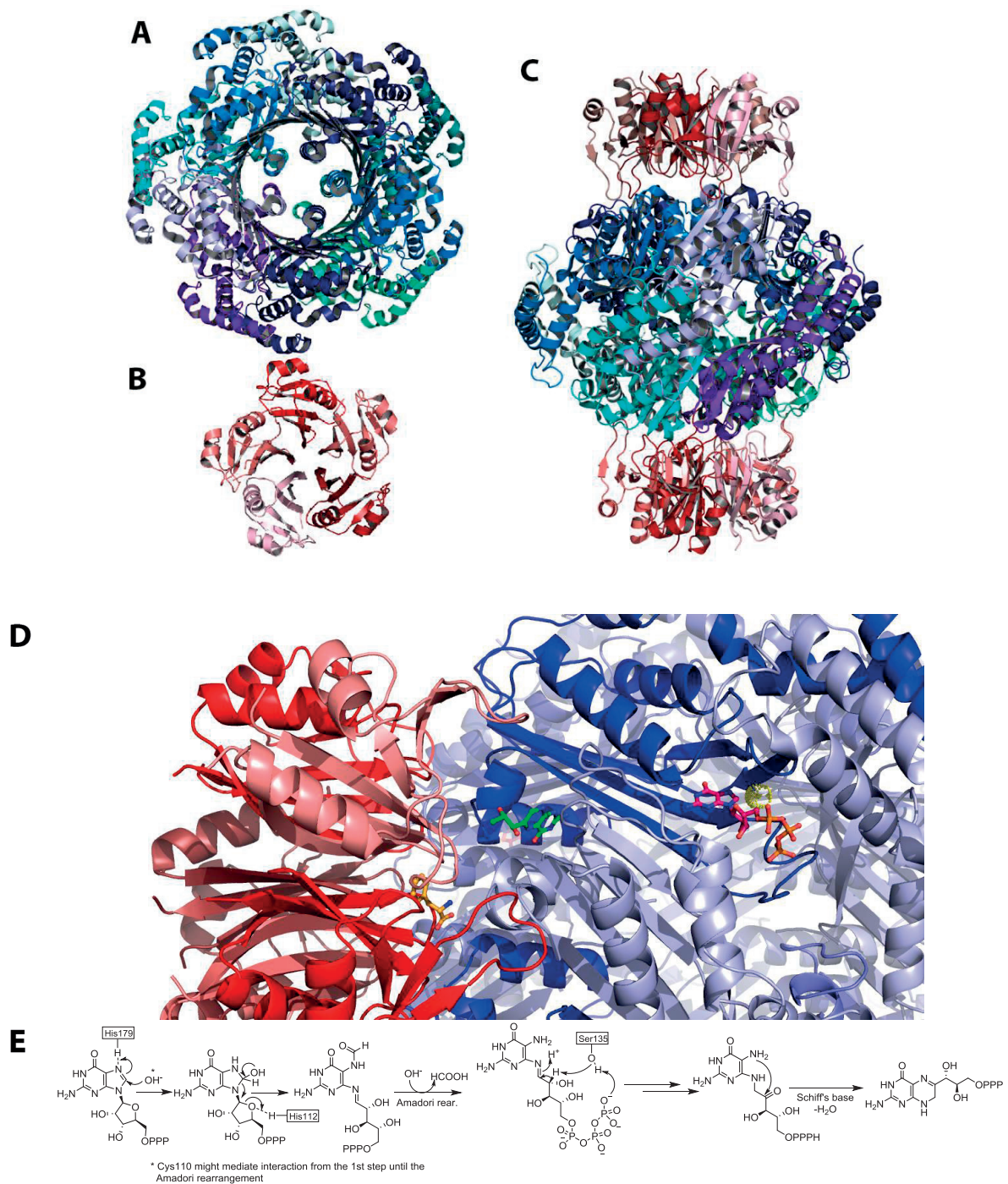


**Fig 6 GCH1 & GFRP structure and catalytic mechanism.** (A) Top view of the GCH1 homodecamer. (B) Top view of one GFRP homopentamer. (C) Side view of the GCH1-GFRP complex. GCH1 subunits are shown in cold colors. GFRP subunits are shown in warm colors. (D) Zoom on the binding sites of GTP, BH4 and Phe. GTP (pink, right) is bound between 3 subunits close to the Zn ion (yellow dotted). BH4 (green, center) and Phe (orange, left) are bound at the interface of GFRP and GCH1. The model is made by the alignment of three structures: Phe containing structure: 1IS7; GTP containing mutant: 1A8R; BH4 containing structure: 1WPL. (E) Catalytic mechanism for the transformation of GTP to H2NTP.



### 1.3.2.3 Regulation

GCH1 being involved in both the BH4 metabolic network and the folate synthesis is a strategic point for regulation. At the transcriptional level, strong up-regulation has been observed in the case of inflammatory response by cytokines<sup>74</sup> or by administration of lipopolysaccharides or estradiol. In different combinations, interferon- $\gamma$  (INF- $\gamma$ )<sup>75,76</sup>, tumor necrosis factor- $\alpha$  (TNF- $\alpha$ )<sup>77</sup>, interleukin-1 $\beta$  (IL-1 $\beta$ )<sup>78</sup>, nerve growth factor (NGF)<sup>79</sup>, lipopolysaccharides (LPS)<sup>80,81</sup>, estradiol benzoate<sup>82</sup> (EB) and H<sub>2</sub>O<sub>2</sub><sup>83</sup> have all shown to possess some influence on GCH1 transcription levels. GCH1 and BH4 levels were decreased in sympathetic neurons (SPN) by leukemia inhibition factor (LIF) and ciliary neurotrophic factor (CNTF)<sup>84</sup>. At the protein level, phenylalanine, BH4 and guanoside are able, via interaction with GFRP, to modulate the enzyme's kinetic properties. However, effect of single cytokines in the modulation of GCH1 activity seems case dependent as reports differ with respect to tissues, species and culture methods<sup>78</sup>. Table 4 summarizes the magnitude of GCH1 regulation by several cytokines.

Experimentally, TNF- $\alpha$  in combination with INF- $\gamma$  have been used to generate high pterin yielding cellular models. Such an activation method is commonly used and convenient when studying the effects of drugs on metabolites. At high GCH1 expression level, the enzyme is not the bottle-neck anymore, leading to excretion of overflowing H<sub>2</sub>NTP and neopterin from cells<sup>85,86</sup>.

<b>Combination</b>	INF- $\gamma$	TNF- $\alpha$	IL-1 $\beta$	NGF	2-4x	LIF (SPN)	~0.1x
INF- $\gamma$	7-40x (VEC)	300x (VEC)	-	LPS	2-3x (rat)	CNTF (SPN)	~0.2x
	TNF- $\alpha$	5x (VEC)	10x (VEC)	EB	2x (rat brain)		
	IL-1 $\beta$	5x(VEC)		H <sub>2</sub> O <sub>2</sub>	4x		

**Table 4 GCH1 regulation by cytokines and compounds.** The table presents the rates of activation of GCH1 alone or in different combinations. The values are case dependent and vary with respect to tissues and organisms.

The GCH1-GFRP complex is also subject to allosteric regulation. As described before, phenylalanine is able to bind, with a K<sub>d</sub> of ~100  $\mu$ M, at the GFRP-GCH1 interface and stimulates GTP conversion 2-fold<sup>87</sup>. It was also shown to increase the affinity of GFRP for GCH1<sup>72</sup>. Oppositely, bound BH4 will act as an inhibitor, lowering the V<sub>max</sub> for the formation of H<sub>2</sub>NTP but leaving the affinity for GTP unchanged<sup>65</sup>. The K<sub>d</sub> for BH4 was reported to be 4  $\mu$ M with maximal inhibition at 7  $\mu$ M. The binding of both BH4 and

phenylalanine are known to be pH sensitive and are given here at physiological pH. Furthermore, phenylalanine is able to overcome the inhibitory effect of BH4 by restoring the GCH1-GFRP complex in an active form<sup>65</sup>. GCH1 activity was shown to be modulated by post-translational modification. Phosphorylation on residues Ser-167 (in the rat sequence, conserved with human)<sup>88</sup> by protein kinase C was reported to elevate BH4 levels concomitant with an increased GCH1 activity. Furthermore, GCH1 activity as well as GCH1-GFRP complex formation are believed to be influenced by its N-terminus. Cleavage on the first 11 residues can be performed but as for now no solid evidence points towards a regulatory feature<sup>72,89</sup>.

Few inhibitors have been developed and only the weak 2,4-diamino-6-hydroxypyrimidine (DAHP, IC50 = 0.3 mM) compound has been reported to selectively inhibit GCH1 in a GFRP dependent fashion<sup>90,69</sup>.

### ***1.3.3 6-pyruvoyltetrahydropterin synthase (PTPS)***

#### ***1.3.3.1 History of the Discovery***

First mentions of PTPS appeared around 1980 as a Mg<sup>2+</sup>-dependent “phosphate-eliminating enzyme” known to convert H2NTP<sup>91</sup>. The first human homologue purification and characterization took place in 1986<sup>92</sup> incorrectly describing the enzyme as a homotetramer of 83 kDa. However, the authors stated correctly that phosphate elimination and dual hydroxyl oxidation proceeded in an NAD(P)H-independent fashion. Several purification attempts, on now recombinant proteins, successfully led to the amino acid sequence and subunit size identification<sup>93</sup> as well as description of the homodimer of homotrimer organization<sup>94</sup>. In the same year, the PTPS crystal structure was obtained describing a yet unusual type of subunit association and active site<sup>95</sup>. Complete mechanistic description and involvement of H2NTP proximal Cys, Glu and Zn was then described by Ploom et al.<sup>96</sup>.

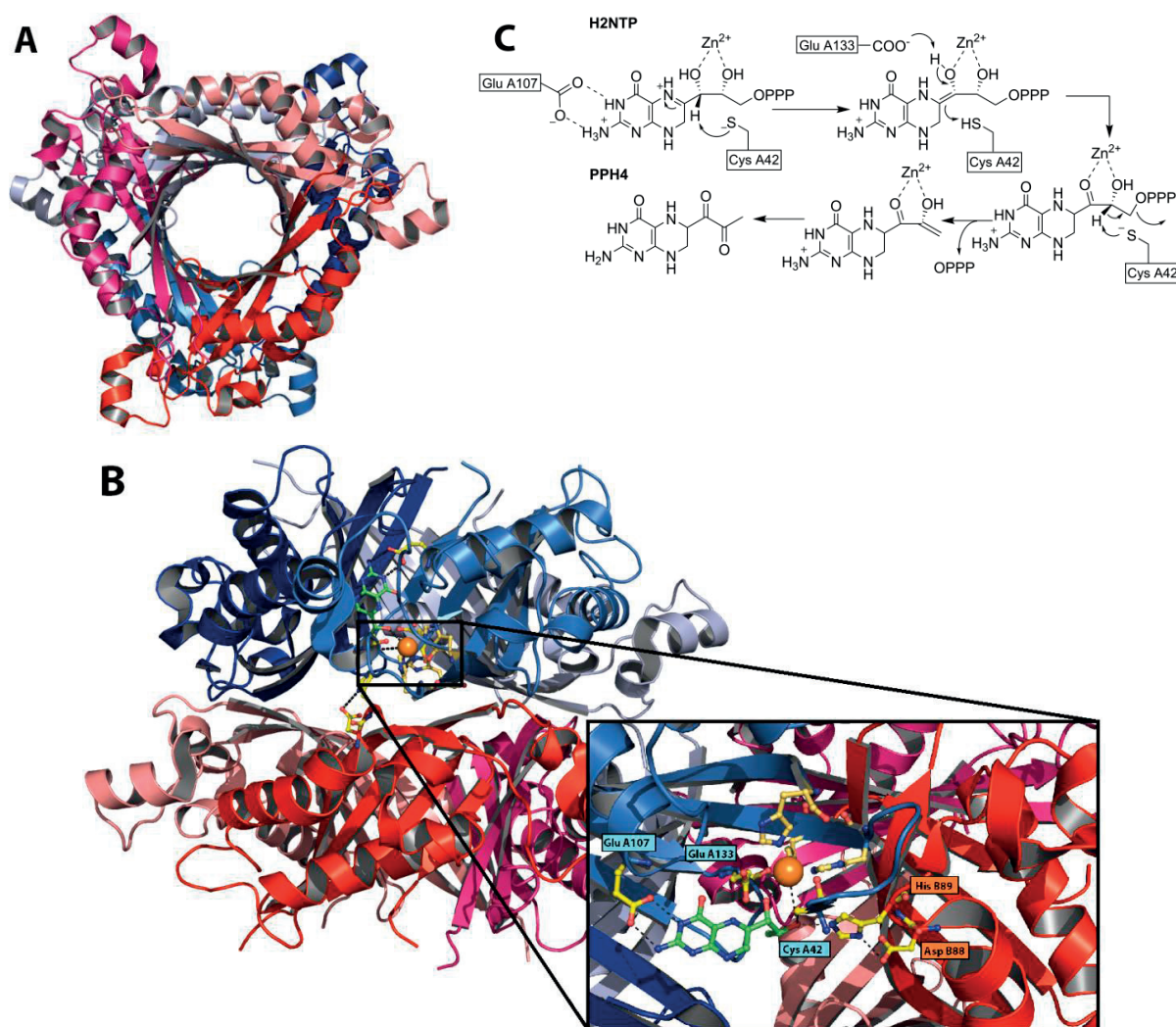


**Fig 7 Structure and catalytic mechanism of PTPS.** (A) Top view of the homo-hexamer. (B) Side view and zoom on the active site. In the zoom, subunit A is shown in blue while subunit B is shown in red. Pdb references : 1B66 (BH4 bound subunit) and 3I2B (Homo-hexamer). (C) Catalytic mechanism of the formation of PPH4 from H2NTP.

### 1.3.3.2 Structure and Mechanism

PTPS is a homohexamer of 93 kDa, structured as a homodimer of homotrimer. Each trimer is, in its center, organized as a 12-stranded antiparallel  $\beta$ -barrel while  $\alpha$ -helices form the outer rim. Three subunits, 2 from one trimer and 1 from the other (A, A' & B), form the active site, yielding 6 active sites per enzyme (Fig 7 A,B). Interestingly, this type of quaternary structure had been observed for GCH1 and already been described<sup>64</sup>. Mechanistically, GluA107, as pterin-anchor, will facilitate H2NTP binding to the active site via hydrogen binding with N2 and N3 of H2NTP (Fig 7 B, zoom). The first step, mediated by

CysA42, is the abstraction of the C1' proton<sup>97</sup>. This residue is activated by His B89 and Asp B88 forming a catalytic triad. The zinc ion coordinates the hydroxyl moieties of C1' and C2' from H2NTP in a *cis*-conformation increasing acidity of the C1' and C2' hydroxy protons<sup>96</sup>. Ketone formation and triphosphate elimination is performed via the action of Glu A133 and Cys A42 to yield PPH4 (Fig 7, C). Wild-type PTPS  $K_M$  for H2NTP was reported to be 8  $\mu$ M. In the endothelial model, IL-1 $\beta$  – and to a lesser extend TNF- $\alpha$  – mediated PTPS upregulation has been demonstrated. Roughly three fold increase of PTPS activity was reported, decreasing neopterin leakage in this cellular model<sup>98</sup>.

### **1.3.4 Sepiapterin Reductase (SPR)**

#### **1.3.4.1 History of the Discovery**

Matsubara et al. first described SPR in the early 60-ties<sup>99</sup>. They realized that sepiapterin was being converted to BH2 via the action of NADPH. Katoh, later on pointed out the capacity of SPR to slowly oxidize in the presence of NADP<sup>+</sup> some L-erythro and L-threo-dihydroneopterin, but not the D- isomers, as well as BH2. These observations shed light on the importance of the stereochemistry of the C1' functional groups<sup>100</sup>. In 1982, Sueoka described the molecular properties of the enzyme, a homodimer of molecular weight of ~55 kDa<sup>101</sup>. Two years later the same group, along with observations related to H2NTP conversion to PPH4<sup>102</sup>, proposed the implication of SPR in the biosynthesis of BH4<sup>103</sup>. These findings were refined later by Smith and Katoh correctly describing the conversion from PPH4 to BH4 via 1' and 2'-oxo-PH4 and non-enzymatic oxidation of 1'-oxo-PH4<sup>104,105</sup>. In the 90s the amino acid sequence and roles in catalysis as well as the crystal structure were reported, concluding the main description of SPR<sup>106,107,108</sup>.

#### **1.3.4.2 Structure and Mechanism**

SPR is a Rossmann fold containing enzyme structured as a 56kDa homodimer of 261 residues each. It is part of the short chain dehydrogenase/reductase family<sup>107</sup>. The dimer is stabilized by the formation of

four helix bundle maintained by hydrogen bonds, and interacting charges (Fig 8A, shown in darker colors). The assembled dimer possesses an antiparallel conformation. Similar to DHPR and to enzymes possessing a Rossmann fold, the nicotinamide ring is positioned at the C-terminal end of the  $\beta$ -strands (Fig 8B). SPR pterin substrates are anchored in the active site with their guanidino moiety oriented towards Asp258 and Gly200. In such conformation the C1'-carbonyl is oriented in close proximity to NADP C4'N and Tyr171 OH. Similarly to the hydride transfer mediated by Tyr151 on the qBH2 N5 in the case of DHPR, Tyr171 plays a role of mediator in the C1' ketone reduction. Sepsiapterin C1' carbonyl atom has been reported to be placed at 3.2 Å from the nicotinamide C4.

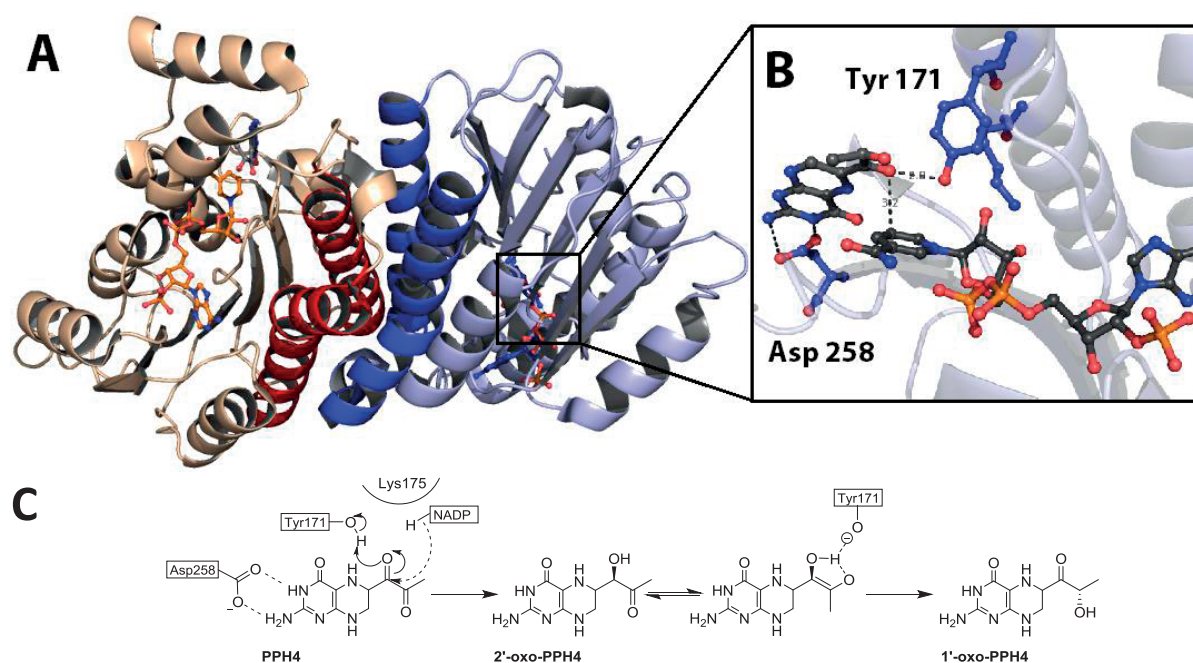


**Fig 8 Structure and catalytic mechanism of SPR:** (A) Mouse SPR dimer structure. Helices stabilizing the homodimer are shown in dark. NADPH is shown in orange and sepiapterin in grey. (B) Active site zoom. The pdb references were 1SEP and 1OAA. (C) Catalytic mechanism for the conversion of PPH4 to 1'-oxo-PPH4.

SPR has been shown to be a promiscuous enzyme able to reduce, in a NADPH dependent fashion, various carbonyl and aldehyde functions<sup>103,109</sup>. However, in the case of BH4 biosynthesis, it catalyzes the PPH4 C1' ketone reduction first, taking on the role of reductase. The reduction is stereospecific with the hydride transfer taking place on the C1' carbon followed by the abstraction of the Tyr171 proton (Fig 8C).

Lys175 is believed to orient the nicotinamide ring. SPR then takes on the role of an isomerase and catalyzes the formation of the C2' hydroxy group. This reaction is pursued in a NADPH independent way, through the formation of an enediol intermediate stabilized by the tyrosinate residue<sup>110</sup>. The newly formed C1' ketone is finally reduced to yield BH4. As previously explained, BH2 formation from sepiapterin is catalyzed by SRP in the salvage pathway. Two cysteine residues (Cys160 and Cys172) are believed to act as additional proton sources and isomerization mediators.

In pathological cases of SPR deficiency, *de novo* production of BH4 can be performed via AR and CR through the salvage pathway<sup>111,112</sup>. Homeostasis can be maintained via this pathway as it is believed that the recycling pathway is dominant over the *de novo*<sup>113</sup>. Generally, PKU symptoms, in newborns with SPR deficiency, are not observed.

#### **1.3.4.3 Substrates and Inhibitors**

As previously mentioned SPR possesses several substrates. Sepiapterin's  $K_M$  was measured to be between 15 and 41  $\mu\text{M}$ <sup>99b, 100, 114, 101</sup>. SPR most active dinucleotide, NADPH, has a  $K_M$  between 1 and 14  $\mu\text{M}$ <sup>100, 114, 101</sup> while  $K_M$  for NADH is roughly a quarter to a half of the natural cofactor<sup>99b</sup>. Affinity for NADH was measured in house to be  $K_d = 1 \mu\text{M}$ . Furthermore PPH4, 1' and 2'-oxo-PH4 were found to have  $K_M$  of respectively 2, 8, and 7  $\mu\text{M}$ <sup>104</sup>.

N-acetyl serotonin (NAS) has been shown to be a competitive SPR inhibitor<sup>118</sup>. It was the first reported potent drug and has often been used as molecular benchmark. Melatonin, serotonin and L-norepinephrine also act as weak binders. A derivative of NAS, termed SPRi3 was developed by structure-activity relationship and presented a 25-fold increased SPR inhibitory potential vs NAS.<sup>115</sup> More recently, xanthurenic acid, part of the kynurenine pathway was reported as being as well an SPR inhibitor<sup>117</sup>. Furthermore, a yeast-three-hybrid study revealed that sulfa drugs were off-target SPR inhibitor. Several

sulfa drugs have shown in-vitro and in-vivo potency<sup>116,119</sup>. All the inhibitory values are reported in Table

5.

Compound	In-vitro		In-vivo
	IC50	Ki	IC50
NAS	1.9 $\mu$ M, <sup>115</sup> 3.1 $\mu$ M <sup>116</sup> , 3.8 $\mu$ M <sup>117</sup>	0.2 $\mu$ M <sup>118</sup>	54 $\mu$ M <sup>a,115</sup>
Melatonin		30 $\mu$ M <sup>118</sup>	
Serotonin		2.3 mM <sup>118</sup>	
L-norepinephrine		3.4 mM <sup>118</sup>	
SPRi3	74 nM <sup>115</sup>		5.2 $\mu$ M <sup>a,115</sup>
Sulfasalazine	23 nM <sup>116</sup> , 7 nM <sup>119</sup>		Non permeable <sup>a,119</sup>
N-acetyl sulfapyridine	290 nM <sup>116</sup>		
Sulfapyridine	480 nM <sup>116</sup> , 82 nM <sup>119</sup>		201 $\mu$ M <sup>a,119</sup>
Mesalamine	370 $\mu$ M <sup>116</sup>		
Sulfathiazole	14 nM <sup>119</sup>		23 $\mu$ M <sup>a,119</sup>
Sulfamethoxazole	19 nM <sup>119</sup>		59 $\mu$ M <sup>119</sup>
Sulfamethizole	19 nM <sup>119</sup>		
Phthalylsulfathiazole	24 nM <sup>119</sup>		
Chlorpropamide	36 nM <sup>119</sup>		
Sulfadiazine	43 nM <sup>119</sup>		
Glibenclamide	82 nM <sup>119</sup>		
Tolbutamide	92 nM <sup>119</sup>		
Sulfamethazine	16 $\mu$ M <sup>119</sup>		Non permeable <sup>a,119</sup>
Xanthurenic acid	150 nM <sup>117</sup>		

<sup>a</sup>: IC50 in-vivo measured by total BH4 biosynthesis

**Table 5 Summary of known SPR inhibitors.** Some values for drugs inhibition potential is given for both in vitro and in vivo experiments

### 1.3.5 Dihydrofolate Reductase (DHFR)

#### 1.3.5.1 History of the Discovery

DHFR has mostly been studied for its involvement in the folic acid metabolism. Starting in the late 50-ies, the research on DHFR was closely linked to discoveries of PAH and DHPR<sup>30</sup>. Early research showed that extracts of horse liver lysates were able to convert folic acid to tetrahydrofolate (FH4)<sup>120</sup>. It was discovered in 1956 that a dinucleotide was needed to perform this conversion<sup>121</sup>. In the two following years the terms “folic acid reductase” and “dihydrofolic reductase” were mentioned, and it was demonstrated that the reaction using an enzyme partially purified from chicken liver extract, could be inhibited by APT and MTX<sup>122,123,124,125</sup>. Detailed stoichiometry and efficient cofactor activity of NADPH were also described. In 1963, Morales et al. established that 6MPH2 was a cofactor of relatively low

activity compared to FH2 and correctly postulated, based on S. Kaufmann's work, that BH2 could be a cofactor<sup>126,127</sup>. DHFR due to its small size and stability was relatively quickly crystalized<sup>128</sup> and in 1988, Oefner et al. reported the human recombinant crystal structure of DHFR (hDHFR) in complex with dihydrofolate (FH2)<sup>129</sup>. Mctigue et. al. later proposed that only the vertebrae structure bound to a pterin cofactor<sup>130</sup>. Finally, the notable interspecies differences of the catalytic mechanism were described in the 90s<sup>131,132</sup>.

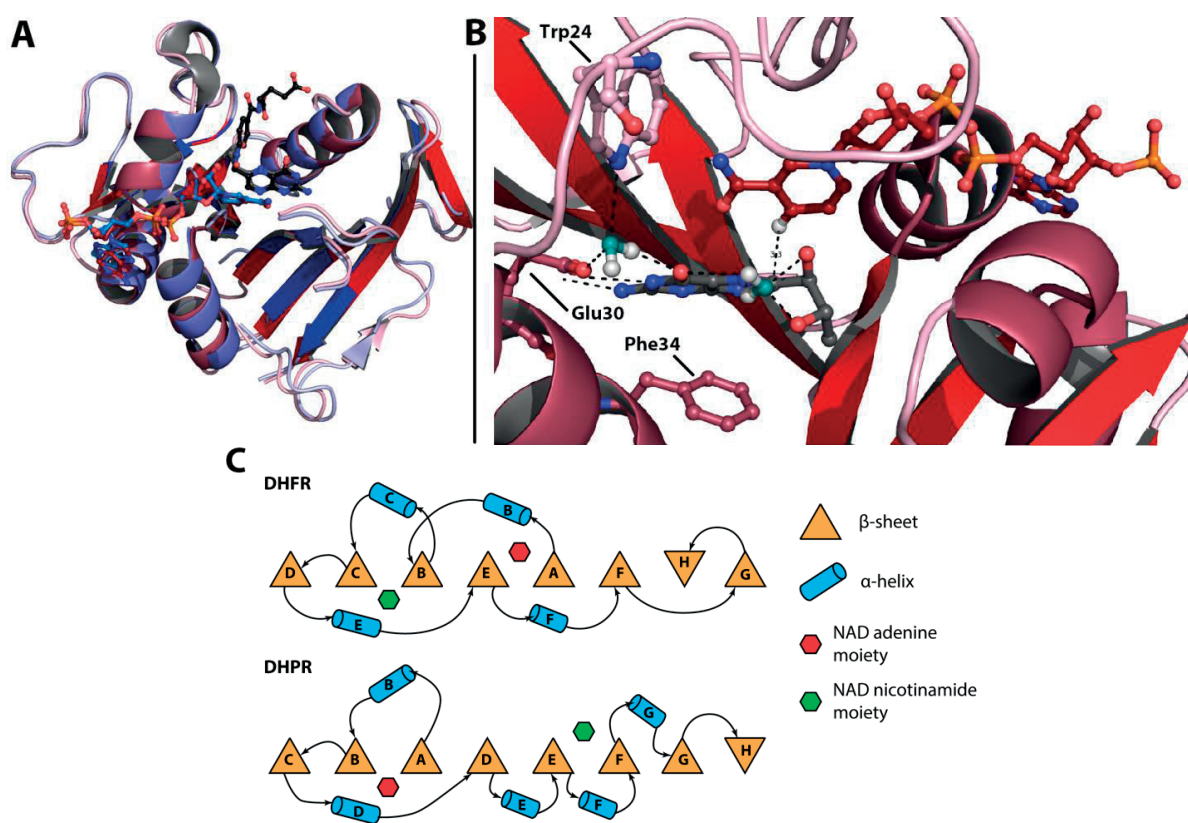


**Fig 9 Structure of DHFR.** (A) Superimposed structures of hDHFR (blue) in complex with NADP<sup>+</sup> and folate, and cDHFR (red) with biopterin and NADP<sup>+</sup>. Loops are shown in pale tints,  $\alpha$ -helices in mid tints and  $\beta$ -sheets in dark. Folate is shown in black and biopterin in grey. Reference structures are hDHFR = 4M6K, cDHFR = 1DR1. (B) Focus on the biopterin binding pocket in cDHFR. Biopterin is anchored by Glu30 and stabilized by a two water H-bonding lattice with Glu30 and Trp24. Phe34 stabilizes the biopterin orientation by  $\pi$ - $\pi$  stacking. Biopterin C6 is in close proximity to NADP<sup>+</sup> for optimal hydride transfer. (C) Overall comparison of the organization of  $\alpha$ -helices and  $\beta$ -sheets of DHFR and DHPR.



## ***Structure and Mechanism***

A large percentage of research on DHFR structure and mechanism has been performed on the *E.coli* homologue (eDHFR)<sup>133</sup>. Furthermore, no structure of hDHFR exists in complex with a pterin molecule. Therefore, a chicken liver DHFR (cDHFR) structure<sup>130</sup> complexed with biopterin and NADP<sup>+</sup> is used in comparison to hDHFR complexed with folate and NADP<sup>+</sup> to describe the enzyme structure<sup>134</sup>. DHFR is a 18 kDa monomer possessing an  $\alpha/\beta$  structure. Eight  $\beta$ -sheets are flanked by 4  $\alpha$ -helices with a backbone similar to DHRP due to their respective NAD-dependency<sup>135</sup>. The connectivity of the  $\alpha$ -helices with respect to the  $\beta$ -sheets diverges in DHFR in comparison to the traditional Rossmann-fold<sup>35</sup> (Fig 9,C). Nevertheless, as seen in Fig 9,A the crystal structures are very similar. As a general observation, biopterin (shown in grey) and FH2 (shown in black) pterin rings overlap while their side chains orientations differ. NADP<sup>+</sup> adenine moieties are slightly tilted while the two nicotinamide moieties are aligned in close proximity to the substrates. Similarly to PTPS and SPR, Glu30 anchors biopterin by H-bonding with N2 and N3 (Fig 9,B). Phe34 stabilizes the biopterin conformation via  $\pi$ - $\pi$  stacking. Furthermore, a water molecule present in other DHFR crystal structures plays a role in extending the H-interaction lattice formed by Trp24 and Glu30. Additionally, another water molecule orients the side chain away from the NADPH nicotinamide ring. NADPH hydride donor C4 is in 3.3 Å proximity with BH2 C6 a similar value to what is observed in dinucleotide dependent reductases. The same interactions were reported for hDHFR complexed with folate<sup>136</sup>. Furthermore, it has been shown that eDHFR and hDHFR possess a Met20 loop (Fig 9,B loop in the first plane containing Trp24)<sup>134</sup>. This loop adopts in hDHFR a single locked conformation allowing the enzyme to access to two mechanistic catalytic pathways<sup>131</sup>. However, in eDHFR the loop adopts both a closed (eDHFR:NADPH) and occluded (eDHFR:NADP<sup>+</sup>:Folate) conformation. To our knowledge, no detailed kinetic studies have been made on the pterin catalytic cycle in hDHFR. It can be assumed that the overall kinetic cycle for the folate catalysis is conserved but the kinetic values change. The hDHFR:NADP<sup>+</sup>:FH4 complex is a branch point in the FH4 catalytic cycle as either NADP<sup>+</sup> or

FH4 can dissociate leading to two different catalytic pathways (Fig 10)<sup>132</sup>. Generally the rate limiting steps are the substrates dissociation as conversion from FH2 to FH4 has been shown to be fast and fairly unidirectional. The cycle starting by NADP<sup>+</sup> dissociation has been reported to account for roughly 65% of the total reaction turnover.

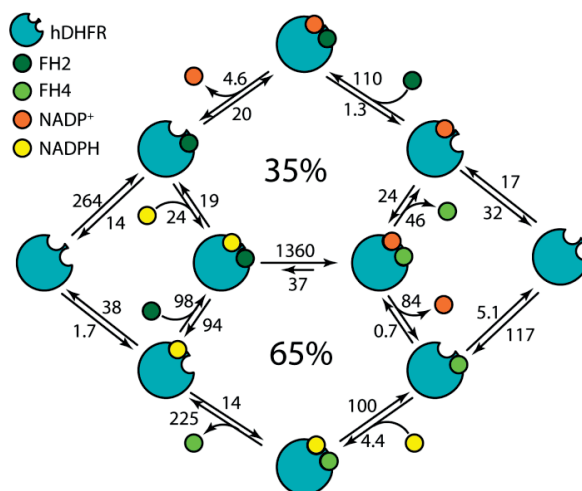


**Fig 10 hDHFR catalytic cycles with FH4.** hDHFR possesses two catalytic cycles, branching at the substrates dissociation in the hDHFR:NADP<sup>+</sup>:FH4 complex. The upper cycle, not present in eDHFR, exchanges 35% of the cofactors. The bottom cycle, present as well in eDHFR, exchanges 65% of the cofactors. Values are for hDHFR only with unimolecular rates given in s<sup>-1</sup> and bimolecular rates given in M<sup>-1</sup>.s<sup>-1</sup>.

Interspecies DHFR homologues possess significant sequence differences. Indeed, it has been reported that a homology of 75% exists between human and chicken DHFR. This difference is notable when it comes to substrates affinity and mostly to inhibitor potential. Additionally, in the biopterin model, N5 and N8 seem to be of importance for orienting the molecule. An eDHFR model in complex with 6-methyl-5,6,7,8-tetrahydroquinazoline-2,4-diamine shows a cofactor coplanar with biopterin but tilted by roughly 45 degrees<sup>137</sup>.

### 1.3.5.2 Substrates and Inhibitors

DHFR promotes the conversion of folate to FH2 and to a larger extend FH2 to FH4 in a NADPH-dependent fashion ( $K_M(FH_2) = 2.7 \mu M$ ,  $K_M(NADPH) = 4 \mu M$ ). FH4 is an essential component of the DNA synthesis pathway therefore its biosynthetic pathway is targeted for the development of antibiotics. The

enzyme, in the context of the BH4 metabolic network converts BH2 to BH4 (1-50% of the FH2 to FH4 conversion rate depending on the species<sup>130</sup>). Here, focus is brought to structural and mechanistic information related to BH2. As said previously, DHFR being a target of predilection in the treatment of several pathologies, and particularly in cancer treatment and as anti-bacterial target, a vast amount of small molecule inhibitors have been developed<sup>138</sup>. Here, only the most potent and widely used tool compounds will be described. Very early in the description of the folate metabolism, it was discovered that 4-amino substituted folic acid derivatives were potent inhibitors. MTX and APT (Structure on Table 3) were described as low pM range DHFR inhibitors and widely used as tool compounds and as treatment in oncology. Trimetoprim (TMP) is a potent drug against eDHFR as it binds 10<sup>5</sup> times stronger to bacterial than to mammalian DHFR. Several sulfa drugs such as sulfamethoxazole, sulfadiazine and sulfisoxazole present inhibitory potential towards eDHFR. TMP is commonly used in combination with sulfamethoxazole as antibacterial agent due to their synergistic effect against folate metabolism<sup>133</sup>.

### ***1.3.6 Pterin-4 $\alpha$ -carbinolamine dehydratase (PCD)***

#### ***1.3.6.1 History of the Discovery***

PCD was first observed as a contaminant during the purification of glucose dehydrogenase in the 50-ies<sup>139</sup>, and later on found as a protein that stimulates PAH<sup>140</sup>. The enzyme was, two years later, correctly described as a homotetramer related to the pterin metabolism<sup>141,142</sup>. Its role as enzyme catalyzing the dehydration of 4HTP to qBH2 was established 10 years later by Lazarus et al.<sup>143</sup>. Later, PCD implication in the prevention of 7-substituted pterin non-enzymatic formation was established<sup>144</sup>. Curiously, it was realized that PCD had already been described as dimerization cofactor of hepatocyte nuclear factor  $\alpha$  (DCoH), possessing the same amino acid sequence<sup>145,146</sup>. The crystal structures of human and rat homologues were later solved, concluding the main description of PCD<sup>147</sup>.

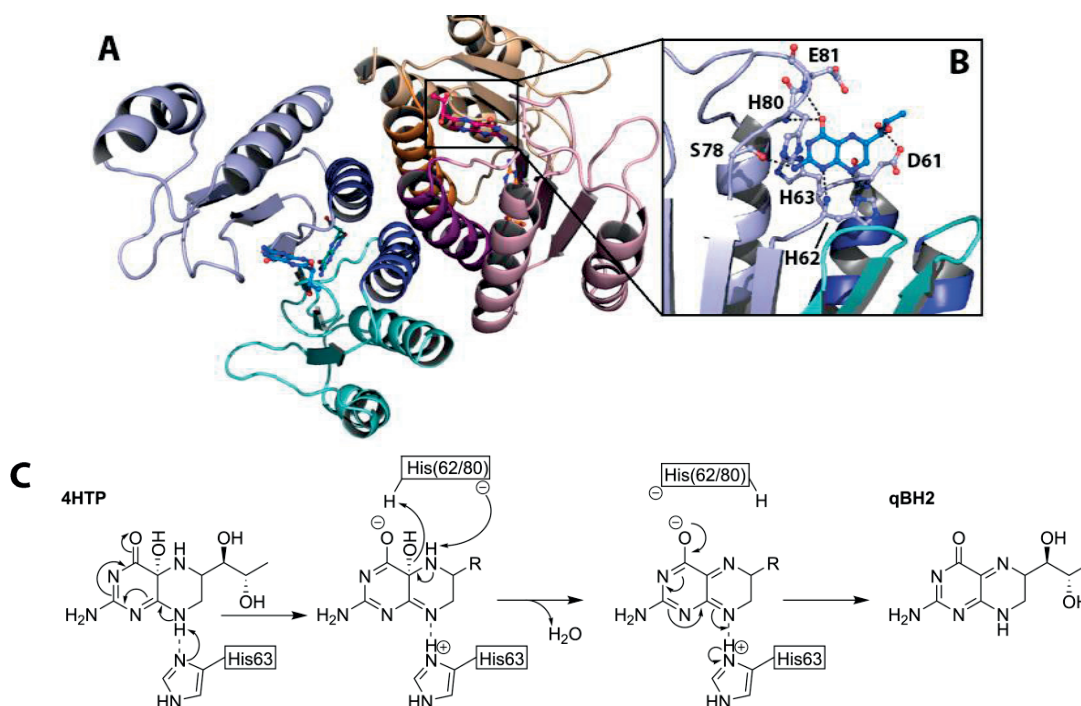


**Fig 11 Structure and catalytic mechanism of PCD.** (A) Structure of the homotetramer. Helices responsible for the tetramerization are shown in dark. BH2 is shown as a blue “ball and stick” model. (B) Zoom on the active site and highlight of important amino acids. (C) Catalytic mechanism of the conversion of 4HTP to qBH2. Pdb reference : 1DCP

### 1.3.6.2 Structure and Mechanism

PCD is a 48 kDa homotetramer of  $D_2$  symmetry, composed of 103 amino acids per subunit being part of the open-faced  $\alpha$ - $\beta$  sandwich structure family (Fig 11 A). The global enzyme arrangement can be described as a dimer of dimer. In each subunit, all the helices are aligned on one side in parallel with the anti-parallel  $\beta$ -sheet structure. By sharing an  $\alpha$ -helix, each monomer contributes to the tetramer stability by forming a four helix bundle at the center. The enzyme possesses in total 4 active sites for 4HTP to bind with no apparent residues shared between subunits to perform the catalytic activity<sup>147b</sup>. Only a BH2 bound structure of PCD was crystallized as basis for determination of the different residues involvement in 4HTP dehydration. It is expected that Ser78, Glu61, His63, His80N and Asp81N anchor 4HTP in the active pocket via both hydrogen bonding and charge stabilization while His62 is believed to orient the cofactor upon binding (Fig 11 B). The dehydration processes through general acid/base catalysis with the first step being His63 mediated deprotonation from N8 (Fig 11 C). The formed anionic oxygen is

consecutively stabilized by His80N and Asp81N facilitating the 4a-hydroxyl lability. The latter is eliminated via an acid/base exchange mediated by either His62, His80 or water. Finally, as the amide reforms, qBH2 is liberated. The uncatalyzed reaction has been reported to be roughly 2000 folds slower.

## ***1.4 Biological Relevance of Pterins***

### ***1.4.1 Amino Acid Hydroxylases***

The three hydroxylases (PAH, TYH and TPH) are part of the small family of monooxygenases all catalytically proceeding in a BH<sub>4</sub> and molecular oxygen dependent fashion. Structurally, crystal structure studies revealed that the enzymes possess an N-terminal regulatory domain, a central catalytic domain and a C-terminal oligomerization domain (Fig 12, A). Very similar catalytic domains (52% to 60% residue homology), all specific towards BH<sub>4</sub>, bind in their active site a molecular divalent iron via two His and a Glu. Being homotetrameric, they possess a C-terminal region stabilizing the protein complex via a long  $\alpha$ -helix (~40 residue, D<sub>2</sub> symmetry). Finally, the N-terminal regulatory domains, composed of 100 to 160 residues, possess a very low level of identity ( ~14 % )<sup>148</sup> and is structured as an ACT domain ( $\beta\alpha\beta\alpha\beta$  topology). The three enzymes possess to some extent a way to regulate their activity either by post-translational modification or allosteric binding. PAH is the only enzyme in this family shown to possess a homotropic ligand<sup>149</sup>. As the catalytic domain within the three enzymes is conserved, it is generally accepted that the hydroxylation mechanism is similar. The reaction can be described as a two-step process with (i) the formation of the hydroxylating intermediate, involving BH<sub>4</sub>, and (ii) the oxygen transfer to the substrate<sup>148</sup>. As seen on the mechanistic scheme described in Fig 12C the reaction yields 4HTP. Due to the hydroxylases similarity only the crystal structure of PAH will be presented and described.

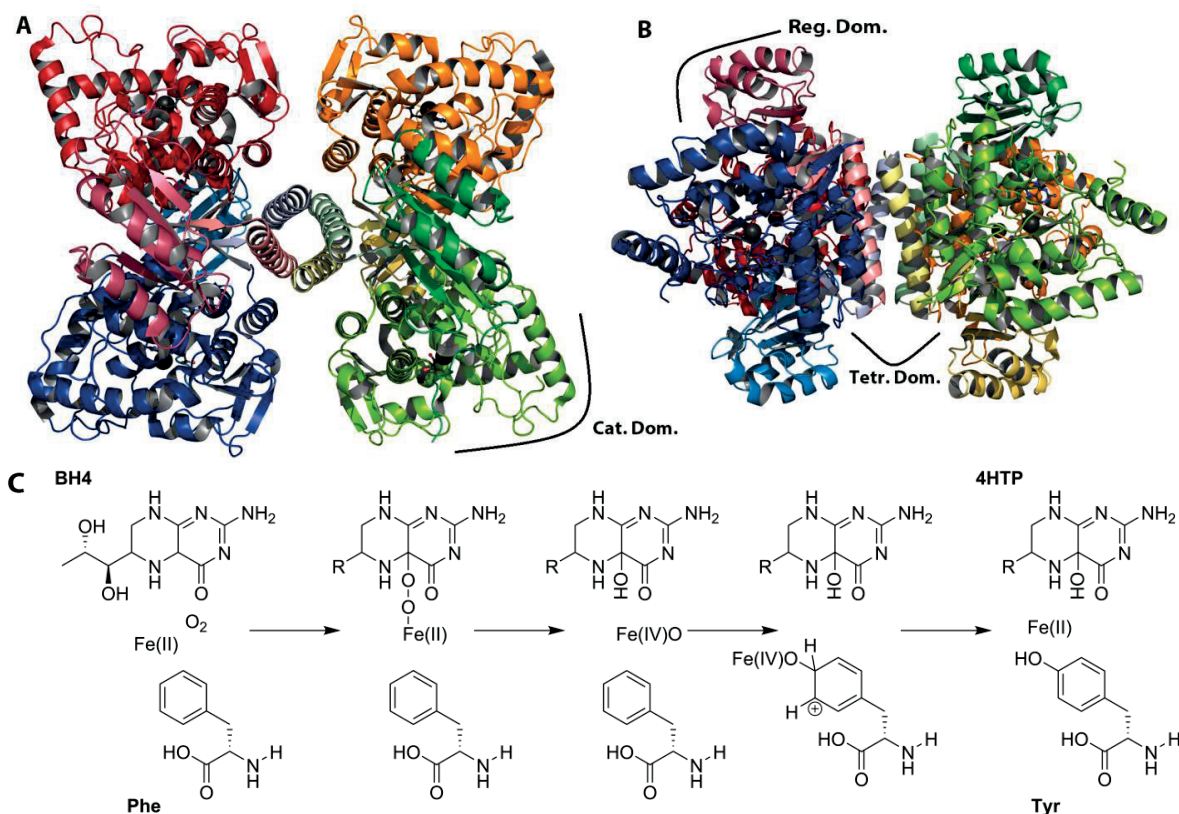


**Fig 12 Structure and catalytic mechanism of PAH.** (A) Top view of PAH. Each subunit is marked by a color and its subdomains by a shade of it. (B) Side view of PAH. Regulatory domains are at the extreme top and bottoms while the tetramerisation domain is in the center. The catalytic domain resides in the middle. (C) Catalytic mechanism for the conversion of Phe to Tyr. Pdb reference :5FGJ

### 1.4.1.1 Phenylalanine Hydroxylase

PAH catalyzes the conversion of phenylalanine to tyrosine in a BH<sub>4</sub>-dependent fashion. In order to avoid accumulation of phenylalanine but to leave it sufficient for protein synthesis, the enzyme activity must be tightly controlled. PAH is composed of an N-terminal 117 residues long regulatory domain. A 33 amino acid long flexible peptide spans over the active pocket acting, in the inactivated state, as a steric blocker for substrate binding<sup>150</sup>. The Phe driven enzyme activation mechanism is still debated nowadays. Two main mechanisms have been described, proposing (i) a large regulatory rotation and dimerization<sup>151</sup> and (ii) local change driven by Phe binding at the active or N-term adjacent site<sup>152</sup>. Furthermore, the geometry of the regulatory domain (ACT domain) is similar to the PCD subunit geometry. These geometries are known to be dimeric to tetrameric in essence, emphasizing on enzyme

activation by dimerization. A recent report presented an activated PAH crystal structure in which an allosteric binding pocket, at two regulatory-domain interfaces, exists for two Phe to bind<sup>153</sup>. A large conformational twist liberates the active site in order for the reaction to take place. Additionally, BH4 also acts as allosteric inhibitor presenting chaperone like characteristics. The allosteric substrate binding seems to induce a conformational change that keeps the enzyme in a low activity and low Phe affinity state<sup>154</sup>. Another mode of activation, involving phosphorylation of Ser16 was reported. This post-translational modification disrupts the binding of the N-termini peptide inside the catalytic binding pocket and facilitates the enzyme activation. Close to the binding site is a disordered region containing Tyr138, a residue which is believed to act as hinge for water bridging BH4 potentially acting as regulator. This feature is not detailed in the presented crystal structure. Mechanistically, sequential binding in the catalytic pocket of PAH has been reported. BH4 binds first ( $K_d = 65 \mu\text{M}$ ) followed by Phe ( $K_d = 130 \mu\text{M}$ )<sup>155</sup>. Interestingly, BH4 seems to have a 200 folds higher affinity than BH2. PAH can either be allosterically inhibited by BH4 or activated by Phe. Once activated, the enzyme can efficiently perform its catalytic task ( $K_M = 15 \mu\text{M}$ ). The last 43 residues compose the C-terminal homotetramerization domain.

#### **1.4.1.2 Tyrosine Hydroxylase**

TYH catalyzes the formation of 3,4-dihydroxyphenylalanine via BH4-mediated hydroxylation of Tyr. 3,4-dihydroxyphenylalanine is the precursor of the catecholamines dopamine, norepinephrine and epinephrine. As to now, no full TYH crystal structure has been reported. All models are based on computationally assembled truncated versions or NMR studies. Similarly to PAH, the regulatory domain possesses a disordered N-terminal peptide (AA 1-71) and a structured ACT domain C-terminal section (AA 72-159)<sup>156</sup>. The unfolded peptide is believed, also in the case of TYH, to hinder substrate binding by covering the active site. In solution, the regulatory domain is a homodimer which, adversely to PAH, does not appear to bear an allosteric binding site. Comparatively, the binding mode in the dimerization of both activated PAH and TYH regulatory domain is similar. Furthermore, TYH is activated by Phe and by

phosphorylation of the Ser19, Ser31 and Ser40 residues all located on the disordered N-terminal tail<sup>157</sup>. Additionally, catecholamines are known to inhibit the enzyme by competing with BH4<sup>158</sup>. Ser phosphorylation apparently decreases the inhibition by catecholamines<sup>159</sup>. The catalytic domain is composed of residue 160-456 and complexes its iron via His331, His36 and Glu376<sup>160</sup>. Interestingly, there seems to be no flexible loop, comparable to PAH Tyr 138, present in TYH. Finally, the long  $\alpha$ -helical C-terminal tetramerization domain spans over the last 42 residues.

### ***1.4.1.3 Tryptophan Hydroxylase***

Two isoforms, TPH1 and TPH2, exist in mammalian multicellular organism with respectively mostly peripheral and central nervous system distribution<sup>161</sup>. TPH catalyzes the rate limiting formation of 5-hydroxytryptophan, the precursor of serotonin (5-hydroxytryptamine, 5-HT) via BH4-dependent hydroxylation of Trp<sup>162</sup>. TPH is believed to be a main actor in occurrences of major depressive disorders. Structurally, the two TPH possess 71% of sequence identity mostly differing in their N-term region. Several Ser can be phosphorylated but no obvious consequence has been observed for all of these locations<sup>163</sup>. In TPH2 activation by Ser19 phosphorylation, a residue not conserved in TPH1, was reported. 14-3-3 protein family has been shown to bind and structure phosphorylated TRP<sup>164</sup>. This protein-protein interaction is still studied nowadays. Due to its relatively low in-vitro instability, only TPH catalytic domain was crystalized<sup>165</sup>. Therefore, there is no structural basis to study in detail the regulatory and oligomerization domain mechanisms. TPH substrates have been reported to bind in the active site in a random fashion before undergoing hydroxylation. TPH is regulated *in-vivo* by serotonin and 5-HT via competitive inhibition.

### ***1.4.2 Nitric Oxide Synthesis***

Due to its importance in biological processes, nitric oxide (NO) is nowadays a hot topic generating in 2016 more than 1500 publications containing “nitric oxide” in their titles. Here, only mechanical and



structural information on NO synthases (NOS) and effects resulting from BH4 deficiencies or linked to BH4 are discussed. Physiologically, NO has several crucial functional roles<sup>166</sup>. NO is a polyvalent molecule, in neurons it acts as neurotransmitter, in activated macrophages it is generated as antimicrobial agent, in endothelial cells it regulates apoptosis while it is also a vasodilator and inhibitor of platelet aggregation.

NO is synthesized by NOS by abstraction of a nitroso group from the Arg guanidino moiety to yield L-citrulline<sup>167</sup>. Three forms of NOS exist: endothelial NOS (eNOS), neuronal NOS (nNOS) and induced NOS (iNOS) all structurally similar (50-60% homology) and BH4 dependent<sup>168</sup>. eNOS and iNOS supply the basal NO in a  $\text{Ca}^{2+}$ /calmodulin(CaM) modulated fashion. iNOS, as its name implies, is induced in case of inflammatory immune response and is  $\text{Ca}^{2+}$ , but not CaM, independent<sup>169,170,171</sup>. Mechanistically, NOS is dependent on NADPH, flavin mononucleotide (FMN), flavin adenine dinucleotide (FAD), iron heme b, molecular oxygen and BH4 substrates. BH4 is not consumed during NO synthesis and acts as a structural cofactor essential in forming active dimeric NOS. Bound in proximity to the heme ring, BH4 is in a cationic state and gives a proton and an electron to the heme iron- $\text{O}_2$  complex. The heme bound  $\text{Fe}^{2+}$  and BH4 are regenerated by electrons supplied by NADPH via a cascade involving FAD and FMN. Furthermore, the dimer and BH4 reduced state is maintained by a tetrahedrally coordinated Zn ion. Structurally, NOSs are composed of two domains: an oxygenase and a reductase domain. The oxygenase domain, located at the N-terminus, possesses a CaM-recognition site and binding sites for BH4, heme and Arg. The C-terminal reductase domain contains the FAD, DMN and NADPH binding sites. Several structural features differ between each NOS isoforms such as the size of their domains, loop organization between the different binding pockets and a PDZ recognition domain only found in iNOS. The PDZ domain, a protein interaction motif, is believed to be binding to glutamate or melatonin receptors<sup>172</sup>.

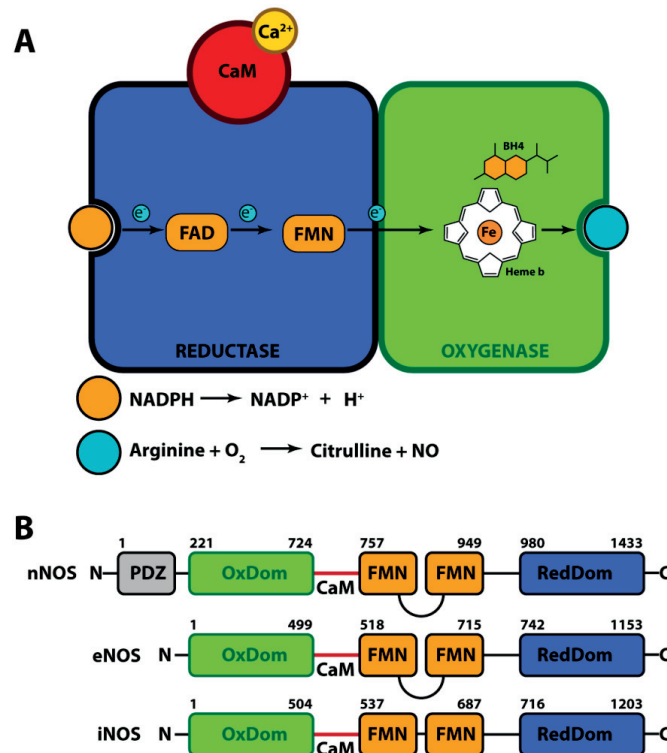


**Fig 13 Global structural features of NOSs.** (A) NOSs are composed of two main domains: the reductase (blue) and oxygenase (green) domains. Electrons are carried from the oxidation of NADPH through FAD and FMN to the Heme b. Arginine binds into the oxygenase domain of the BH4 stabilized NOS to be converted to citrulline and release NO. A CaM binding pocket exists in between the two main domains regulating the structure and electron flow. (B) Schematic description of NOSs individual features. The two main domains are structurally similar but vary in size. Loop organization of the FMN binding pocket. nNOS is the only synthase possessing a PDZ domain for protein interaction.

BH4 and BH2 have both been shown to bind with an equal and high affinity of  $K_d = 80 \text{ nM}$  to all forms of NOS<sup>173</sup>. BH4 and BH2 bound NOS have been respectively termed “coupled” and “uncoupled” NOS catalyzing different reactions. In the coupled form, NOS promotes the synthesis of NO while the BH2-bound enzyme will promote the formation of superoxide. As no electron can be shared with heme, the oxygenase domain becomes inactivated. NO and superoxide can rapidly combine to form peroxynitrite, a reactive nitrogen compound. At physiological levels, ROSs such as peroxides, free oxygen radicals and oxygen ions have a role of signaling molecules and regulators of several cellular processes<sup>174</sup>. Pathological conditions, in the case of BH4 deficiencies, arise when the ratio of BH4 over BH2 becomes close to unity. It has been shown that the relative amount of BH4 towards BH2 and not the absolute BH4

amount is the determining factor in NOS uncoupling<sup>173</sup>. Consequent superoxide anion release is often followed by oxidative stress mostly due to the formation of peroxynitrite, the molecule formed via NO and superoxide reaction. The latter has a propensity to oxidize BH<sub>4</sub>, classically leading to further NOS uncoupling which in turn worsens the oxidative stress condition. Nitrosative stress further increases as peroxynitrite triggers the release of zinc from eNOS<sup>175</sup>. Additionally, peroxynitrite can cause S-nitrosylation of proteins, lipids and DNA. Generally, cardiovascular complications and atherosclerosis arise as a result of this oxidative stress. Evidence of the implication of iNOS generated peroxynitrite in Alzheimer's disease has been demonstrated<sup>176</sup>.

It was shown that NOS activity increases in cases of immune response<sup>177</sup>. As a consequence to inflammatory stimulation, GCH1 upregulation directly impacts levels of BH<sub>4</sub>. Increase in iNOS activity seems to be linked specifically to BH<sub>4</sub> levels. In endothelial cells, iNOS mRNA was decreased upon stimulation but a six fold increase in NO production was measured indicating that BH<sub>4</sub> concentration is the determining factor in this process<sup>78</sup>. Yet, this model is hard to confirm on humans<sup>178</sup>, shows to be species dependent, and culture method and state of the cells appears to have an impact as well<sup>179</sup>.

### ***1.4.3 Phenylketonuria***

Classical PKU results from an inborn genetic mutation in the phenylalanine hydroxylase codon. Phenotypical consequences range from mild (120 – 600 µmol Phe/L blood) to pronounced hyperphenylalaninaemia (HPA, > 1200 µmol Phe/L blood)<sup>180</sup>. Statistically, PKU prevalence is of 1 over 10000 live birth in Europe<sup>181</sup>. Usually, patients with mild PKU are on a strict phenylalanine-restricted diet with a tolerance between 250 to 400 mg/day<sup>182</sup> whereas in classic, severe, PKU the daily phenylalanine intake must not exceed 250 mg. Atypical PKU represents as little as 2% of the global PKU cases. These cases can be caused by mutations in enzymes responsible for BH<sub>4</sub> biosynthesis or regeneration such as GCH1, PTPS, SPR, PCD and finally DHPR<sup>183</sup>. It has been reported that 29 mutations in the QDPR gene

(encoding for DHPR) are responsible for the enzyme's partial or total loss of function. DHPR function deficiency leads generally, despite the phenylalanine-restricted diet, to crescent physical and mental impairment. These symptoms can be followed by basal ganglia calcification and death. A mechanism can explain such devastating syndromes: BH2, being an hydroxylase and NOS inhibitor, accumulates<sup>184</sup> leading to the decreased production of L-Dopa, 5-OH-tryptophan<sup>113,185</sup>. Another form of atypical PKU, detected by excretion of 7 substituted pterins, PAH inhibitors as well, is due to PCD deficiency. These chemical rearrangements are usually minimized by PCD<sup>144,186</sup>.

#### **1.4.4 Dopamine-Responsive Dystonia**

Dopamine-responsive dystonia (DRD) also known as Segawa's disease is a disorder induced by critically low doses of L-dopamine (L-DOPA). This phenotype is generally linked to autosomal dominant mutations of the *gch1* gene in priority and infrequently the *tyh* and *spr* genes<sup>187</sup>. Traditionally, dystonia is observed at a young age with mild Parkinsonism. Occurrences of *tyh* and *spr* related cases of DRD often lead to more dramatic syndromes such as mental retardation, Parkinsonism and oculogyric crises. Generally, such atypical clinical syndromes fall in the DRD-plus category<sup>188</sup>. Newborns with DRD sometimes present HPA, detected at birth neonatal PKU screening. However, DRD in HPA-free patients is only detected later by classical symptoms. A biochemical marker is the significantly reduced levels of total biopterin and neopterin in the cerebro-spinal fluid<sup>189</sup>. SPR deficiency is believed to be the main factor in HPA-free DRD. Complete BH4 synthesis can be performed out of the CNS without SPR (discussed previously – SPR chapter). As DHFR is weakly expressed in the cerebrospinal fluid, BH2 generated via the salvage pathway cannot be converted and accumulates, consequently inhibiting TYH and TPH<sup>113</sup>. Other reports indicate an increased vulnerability of nigrostriatal dopaminergic neurons towards BH4 deficiencies compared to liver cells. BH4 was shown to stimulate gene expression of TYH, therefore its low levels obstruct TYH enzyme activity<sup>190</sup>. As improvement in patient condition is usually obtained upon treatment with L-DOPA, DRD is not a neurodegenerative but a biochemical disorder.

### **1.4.5 Neuropathic Pain**

Neuropathic pain is usually associated with tissue and nerve injury and is often a chronic pathology. In opposition to classical inflammation, nerve injury is therapeutically hard to tackle. Classically, in healthy mammals, BH4 production from the *de novo* pathway is low and tightly regulated while recycling and salvage pathways maintain homeostasis<sup>191</sup>. Following nerve damage, BH4 levels have been reported to significantly increase in sensory neurons and macrophages<sup>192</sup>. The consequence of this cellular stress is an increase in transcription, translation and therefore activity of GCH1, usually the rate limiting enzyme in BH4 synthesis. It has been revealed, through patients with GCH1 genetic polymorphism, that decreased levels of BH4 reduced pain<sup>192</sup>. This was confirmed by inhibiting GCH1 with DAHP in rats with nerve injury and inflammation. Consequently, elaboration of SPR specific inhibitors for the development of analgesics was undertaken. A summary of those drugs can be found in the “SPR” chapter. Inhibition of SPR still allows production of BH4 to basal levels via the salvage pathway while GCH1 inhibition would reduce total BH4 amount on the long run. Treatment with the SPR-inhibitors SSZ or SPRi3 for extended periods of rats with nerve injury and inflammation, prevented and reversed hypersensitivity, providing evidence that SPR inhibition might have therapeutic utility<sup>193,115</sup>.

Mechanistically, in the sensory neurons of a naïve reporter mice low levels of GCH1 are present. Following peripheral nerve injury and persisting after 7 days, *gch1* transcription is increased proximal to the injury in all major sensory neuron classes as well as in macrophages. In both cells, significant BH4 overproduction was measured. Injured mice were tested for chemical (capsaicin) as well as radiant and contact heat and showed that high level of BH4 affects the sensitivity of somatosensory neurons. It was shown that BH4 sensitizes TRPV1 channels via nitrosylation due to increased NO synthesis<sup>115</sup>. Increased pain manifestation such as allodynia and hyperalgesia is a direct consequence of these sensitized receptors.

### **1.4.6 Alkylglycerol Monooxygenase**

Alkylglycerol monooxygenase (AGMO), also known as glyceryl ether monooxygenase, is the enzyme responsible for the BH<sub>4</sub>-dependent hydroxylation of alkylglycerols. AGMO cleaves the ether bond of alkylglycerols ether phospholipids yielding, via an unstable hemiacetal, the resultant glycerol derivative and a fatty aldehyde (Fig 14A). Generally, saturated lipids from 14 to 22 carbons are processed by the enzyme<sup>194</sup>. These ether lipids can be found in the brain structure, the cataract and in the development of semen<sup>195</sup>. They are also believed to influence platelet-activating factor inflammation<sup>196</sup>. 6MPH4 was also shown to be a suitable substrate<sup>197</sup>.

Being an integral membrane enzyme, no purification has been successful so far and therefore little structural insight is known. A bioinformatic model, partial bacterial and mammalian cell expression as well as mutagenesis allowed proposing a global structure and a putative binding site (Fig 14B). Furthermore, the enzyme lacks homology with any known BH<sub>4</sub>-dependent enzyme. Structurally AGMO appears to be composed of nine transmembrane helices covering roughly half of the enzyme sequence. A structural motif composed of eight His are reported to be crucial for catalysis<sup>198</sup> indicating a di-iron center, classical in BH<sub>4</sub> and O<sub>2</sub> mediated hydroxylation, is involved in the catalytic process. Similarly to other BH<sub>4</sub> binding proteins, anchoring of BH<sub>4</sub> is performed via the Glu137 residue ( $K_M \approx 33.5 \mu\text{M}$ ) located in proximity to the His motif<sup>199</sup>.

Recently, a report highlighted the importance of BH<sub>4</sub> in lipid homeostasis in a murine macrophage model<sup>200</sup>. AGMO was in the case of M1 (INF- $\gamma$  & LPS activated) and M2 (interleukin 4 activated) bone marrow macrophages respectively down and upregulated. No tangible explanation for this regulation has been proposed as for now. These regulations were shown to reverberate directly on the lipidome and beyond ether lipids.

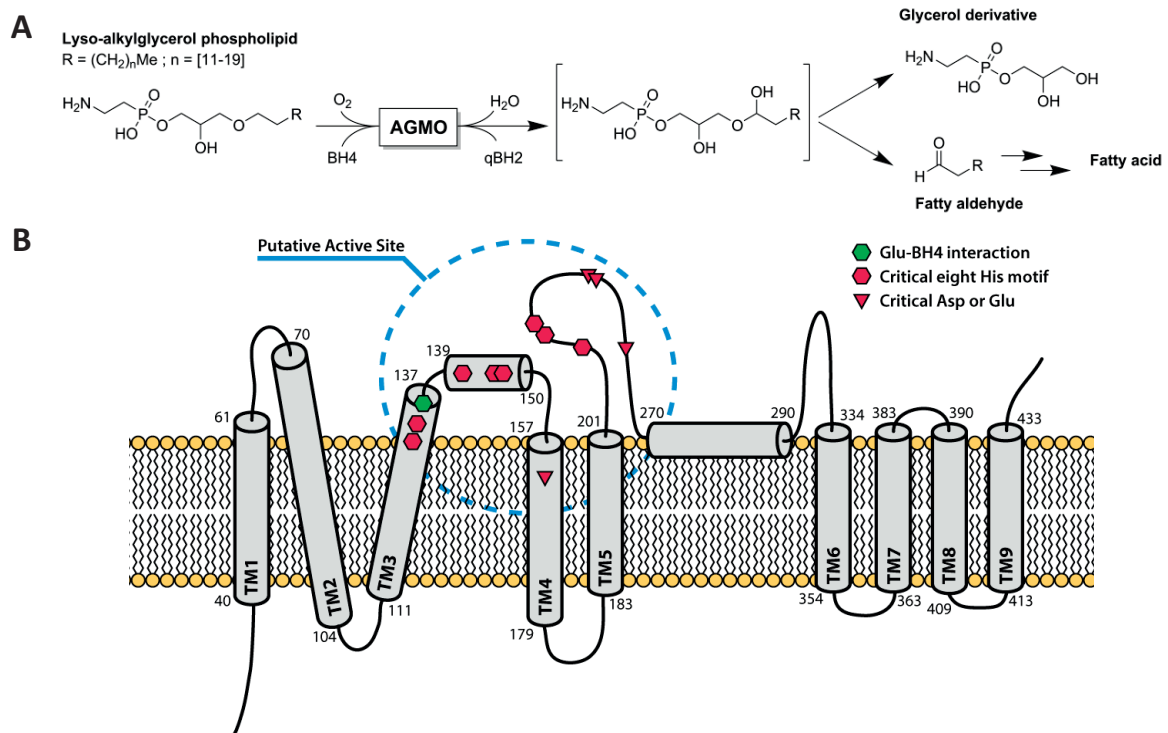


**Fig 14 AGMO catalytic mechanism and schematic structure.** (A) AGMO promotes, in a BH4 dependent fashion, alkylglycerol cleavage yielding a fatty aldehyde and a glycerol derivative. (B) Schematic structure of AGMO. AGMO being transmembranar, no crystal structure exists.

### 1.4.7 Vitiligo

Vitiligo is a skin condition characterized by local depigmentation of the epidermis due to melanocytes loss of function<sup>201</sup>. Several combined mechanism such as genetic, immunologic and environmental factors, seem to generate melanocyte destruction<sup>202</sup>. The most accepted mechanism is based on an interplay between oxidative stress and autoimmune response<sup>203</sup>.

Dermal accumulation of  $H_2O_2$  to mM levels coupled with low catalase activity, decrease of antioxidant agents and increase in 6- and 7-biopterin concentration is believed to be a main cause of vitiligo generation<sup>204</sup>. As previously presented, accumulation of 7-isomers of biopterin has been linked to impairment of PCD. The low PCD activity is worsened as critical catalytic residues are oxidized in the presence of high  $H_2O_2$  concentration<sup>205</sup>. In patients with vitiligo, PCD activity was significantly lower than the other BH4 metabolic pathway enzymes<sup>206</sup>. In addition, isomerization of 4HTP is favored under the

presence of H<sub>2</sub>O<sub>2</sub>. These 7-pterin have been reported to be potent PAH competitive inhibitors (K<sub>i</sub> in low μM range)<sup>205</sup> directly being reflected by the PAH activity decrease and Phe concentration increase in patients<sup>207,208</sup>. This inhibition in turns favors the formation of H<sub>2</sub>O<sub>2</sub>. Consequently, Tyr depletion leads to a decrease in tyrosinase produced melanins.

Furthermore, at such levels H<sub>2</sub>O<sub>2</sub> deactivates catalase and oxidizes the tetrahydro form of pterin isomers. Moreover, H<sub>2</sub>O<sub>2</sub> concentrations as high as 30 μM have been shown to significantly decrease DHPR activities, diminishing BH<sub>4</sub> recycling<sup>204</sup>. Accumulation of this oxidized pterin can be observed by skin fluorescence at 351 nm<sup>206</sup>. Additionally, high local H<sub>2</sub>O<sub>2</sub> concentration leads to increased intracellular ROS by initiation of NOS driven oxidative stress. Prolonged and extensive oxidative stress leads to peroxynitrite and ROS driven protein aberration potentially serving as autoantigens leading to autoimmunity in parallel to cytokine induced apoptosis<sup>209</sup>.

In retrospect, it appears that oxidative stress is the initiating event in the cascade leading to vitiligo<sup>210</sup>. Finally, it has been shown that substitution of the defective epidermal catalase leads to repigmentation of the skin<sup>206</sup>.

## ***1.5 In Vivo Pterin Quantification***

### ***1.5.1 Chemical Oxidation***

Chemical oxidation has been widely used in the early studies of pterins biological relevance as it is a simple alternative for the indirect quantification of BH<sub>4</sub> and BH<sub>2</sub>. The physical property of BH<sub>4</sub> renders it non fluorescent while BH<sub>2</sub> only has 4% of biopterin fluorescence and is therefore hardly detectable. Traditionally BH<sub>4</sub>, BH<sub>2</sub> were chemically oxidized to be later detected by fluorescence<sup>211</sup>. In one hand, acidic oxidation in the presence of iodine transforms both BH<sub>4</sub> and BH<sub>2</sub> to biopterin<sup>212</sup> (1 M HCl, 10 mg/ml I<sub>2</sub>, 20 mg/ml KI, 1 h, RT). On the other hand, using basic conditions in the presence of iodine (1 M



NaOH, 10 mg/ml I<sub>2</sub>, 20 mg/ml KI, 30 min, RT) would transform, non-quantitatively, BH4 to pterin, a highly fluorescent molecule, while BH2 would oxidize to biopterin. This method was used in the study of small molecule inhibitors on SPR<sup>119</sup> and quantification of pterins in living organisms and tissues.

### **1.5.2 Electrochemical Detection**

Methods employing reverse phase HPLC separation followed by post-column electrochemical oxidation and detection coupled with fluorescence were developed following the chemical oxidation method<sup>213,214</sup>. This application relies on the capacity of coulometric electrochemical detectors to quantitatively oxidize compounds flowing through the high surface-area porous working electrode<sup>215</sup>. Advantage of such a method is sensitivity and linearity over pico- to micromolar concentrations. Furthermore, the additional dimension brought by the different oxidation potentials applied post-column allows for differentiation and quantification of co-eluting molecules. Experimentally speaking this method is robust and apparatus maintenance is limited to column cleaning from cellular debris.

### **1.5.3 Liquid Chromatography Mass Spectrometry**

The latest quantification methods rely on hydrophilic interaction liquid chromatography (HILIC) based separation<sup>216</sup> followed by mass spectrometry quantification<sup>217,218,219</sup>. HILIC columns were developed to efficiently separate tens of closely related pterin compounds allowing one to draw the complete pteroidic metabolic landscape. Adequate separation by HILIC, coupled to the sensitivity of triple quadrupole modules is the state of the art. This method is however more expensive and requires dedicated instruments as the types of buffers and columns are not routinely used in chemical synthesis.

## **1.6 Semi-Synthetic Sensors**

Sensing metabolite concentration and quantifying competitive enzymatic inhibition both *in vivo* and *in vitro* provides a large pool of information in the study of biological processes. Sensors based on fusion proteins and chemical linkers are able to achieve such performances. Several technologies are

combined together in order to build a functional and reliable sensor<sup>220</sup>: (i) genetically encoded scaffolds are built by the assembly of several protein sub-units, (ii) self-labeling proteins such as SNAP, CLIP or Halo are used as said sub-units in order to shape the sensor's functionality. (iii) Small molecules, synthetic probes and tag substrates are assembled by organic synthesis. (iv) Those sensors most often rely on the Förster Resonance Energy Transfer (FRET) and Bioluminescence Resonance Energy Transfer (BRET) obtained by the rational design of the sensor scaffold. Fig 15,A/B pictures one of the most common designs of a SNIFIT (SNAP-tag based Indicator protein with a Fluorescent Intramolecular Tether)<sup>221,222</sup>. The scaffold is assembled part by part in order to yield the functional sensor. The sensor is closed when no competitive substrate is present thus allowing the donor and acceptor to be in close proximity to each other, yielding high FRET efficiencies. In the presence of a free analyte, the tethered substrate will be displaced therefore lowering the FRET interaction between the donor and acceptor which can be monitored using a spectrofluorometer. In the case of a BRET sensor<sup>223</sup>, a luciferase replaces the genetically encoded fluorophore in the sensor. In the presence of additional luciferin the bioluminescence emitted by the luciferase is bright enough to be captured on a common camera. Several important features have to be noted: The proline 30 (P30) linker, expected to form a rigid helix, is used to increase the distance between the FRET donor and acceptor therefore strongly decreasing the FRET when the internal substrate is unbound. The FRET efficiency difference between the open and the closed sensor is therefore expected to be strongly increased. However, in the case where a more flexible linker is required, the P30 linker can, by insertion of several glycine-glycine-serine (GGS) units, adopt different conformations. Another important factor in the design of sensors is the choice of an efficient FRET pair. Usually tetramethylrhodamine (TMR) and silicon rhodamine (SiR) are used for the large spectral overlap and the red-shifted signals they emit (570 nm and 650 nm, respectively). Furthermore, the proteins can be modified to accommodate an unnatural amino-acid<sup>224</sup> which can later be conjugated to a synthetic dye in order to replace a bulky self-labeling protein<sup>225</sup>(Fig 15C).

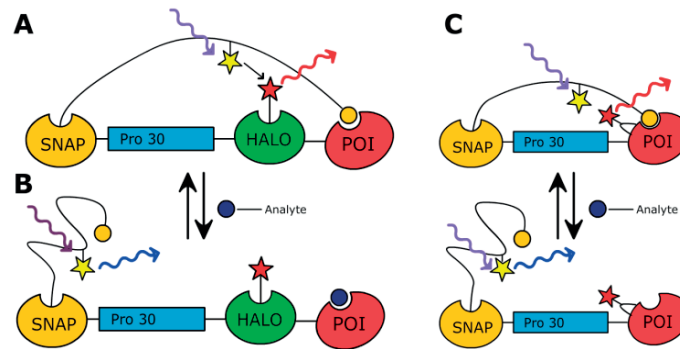


**Fig 15 Typical Snifit scaffold.** The base structure is genetically assembled and expressed. The tags and the fluorophores are chemically synthesized and self-assembled. The sensor is closed (A) and high FRET is emitted when no competitive substrate (blue dot) is present. The competitive substrate can displace the tethered ligand and open the sensor (B) and therefore low FRET is emitted. (C) Scaffolds bearing an unnatural amino acid can be bound to a synthetic dye in order to replace a self-labeling protein.

The main advantage of such sensors in screening campaigns is the ratiometric nature of their readout. This generally translates to better reproducibility of the results as concentration of the sensor in solution doesn't impact on quantification of a molecule towards the protein of interest. The quality of the readout is dependent of the distance and orientation between the two fluorophores. Indeed, when in close proximity the FRET efficiency will be higher. Furthermore, optimal FRET occurs when the excitation dipole of the donor dye is parallel to the absorbance dipole of the acceptor dye. Finally the spectral overlap between the donor and acceptor dyes as well as their spectral overlap lay an important role with respect to the amount of transferred energy<sup>226</sup>.



## Chapter 2. Results

### 2.1 A Sensor for DHPR Inhibitors

A semi-synthetic FRET based sensor was developed in order to screen for competitive DHPR inhibitors. The theoretical design principle is introduced in the following section followed by the sensor creation.

#### 2.1.1 Sensor Development Strategy

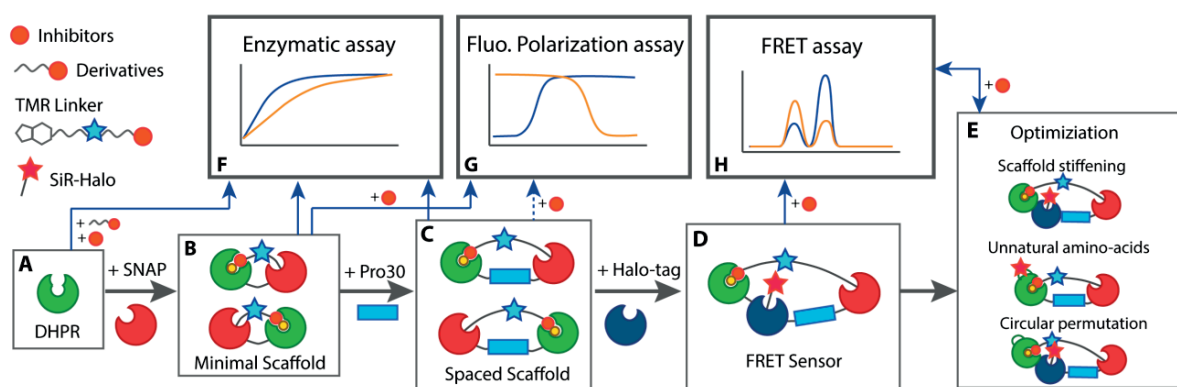


**Fig 16 Scheme for the development of semisynthetic FRET sensors.** (A) The enzyme of interest, here DHPR, is first studied in an enzymatic assay. (F) Different known inhibitors are tested via the enzymatic assay. The compounds are derivatized and tested to ensure their conserved potency. A dye (TMR) and a self-labeling tag (BG) are then added to form a complete linker. (B) The enzyme is modified by fusing it to a self-labeling protein to form the minimal scaffold. Its catalytic activity is assessed to confirm its integrity. The minimal scaffold is labeled and tested for fluorescent polarization (G) and enzymatic assay. The capacity of the tethered inhibitor for binding and unbinding is assessed via this experiment. (C) A poly-proline spacer is added to increase the distance between the protein of interest and the self-labeling protein to form the spaced scaffold. The spaced scaffold binding ability is tested again via enzymatic assay and fluorescent polarization. (D) A second self-labeling enzyme is fused and linked to a second dye (SiR) to form the FRET sensor. (H) FRET is recorded in the bound (closed) and unbound (opened) situation. (E) The first FRET sensor is optimized using various methods

The final sensor design was obtained through a step-by-step approach consisting of testing each parameter before obtaining a robust sensor that could be used in a large drug screen. As seen in Fig 16 the first step (Fig 16A) is to test known inhibitors in an enzymatic assay (Fig 16F). Generally, inhibitors possessing moieties that are easily derivatized and that possess the strongest binding potentials are preferred. Further on, the effect of chemical modification on their inhibition potential is investigated. This allows for quantification of a compound's loss of potential and directs the development of the

linkers further. Indeed, the latest step is to incorporate a dye such as TMR, a spacer (polyethylene glycol) and a self-labeling tag such as BG.

DHPR is fused to the self-labeling protein SNAP on either C or N-termini and tested enzymatically (Fig 16B). The catalytic ability of the construct, here denominated *minimal scaffold*, is assessed via the enzymatic assay. This experiment ensures complete preservation of DHPR functionality. These small fusion proteins are then labeled with a linker bearing a tethered inhibitor and a fluorophore. The highest possible local concentration of inhibitor in fusion proteins is obtained this way. These scaffolds are tested enzymatically in order to evaluate the intramolecular inhibition from the tethered drug. Through this assay it is possible to estimate the local concentration of tethered inhibitor.

Binding and displacement of the tethered inhibitor from the active site is then investigated by fluorescence polarization (Fig 16G). Free inhibitor is added, in solution, to a labeled minimal scaffold, displacing its tethered counterpart allowing the fluorophore to regain mobility. The assay allows to test opening (unbinding of the tethered inhibitor) and closing (binding of the inhibitor) of the minimal scaffold. The enzymatic assay and FP steps can be repeated after the insertion of a P30 spacer between the protein of interest and SNAP. (Fig 16C) The objective is to verify that binding still occurs in a *spaced scaffold*, a system where the binding site is further from the SNAP attachment point.

Finally, a Halo self-labeling protein is added in order to accommodate the FRET acceptor dye SiR. (Fig 16D) The efficiency of the two dyes to perform FRET is assayed (Fig 16H). Ratio of signal of the acceptor dye over the donor dye is measured in the closed and open sensor conformation. The first iteration of the FRET sensor can be optimized using various methods such as scaffold stiffening, circular permutation, and insertion of unnatural amino acids serving as handle for fluorophore coupling.

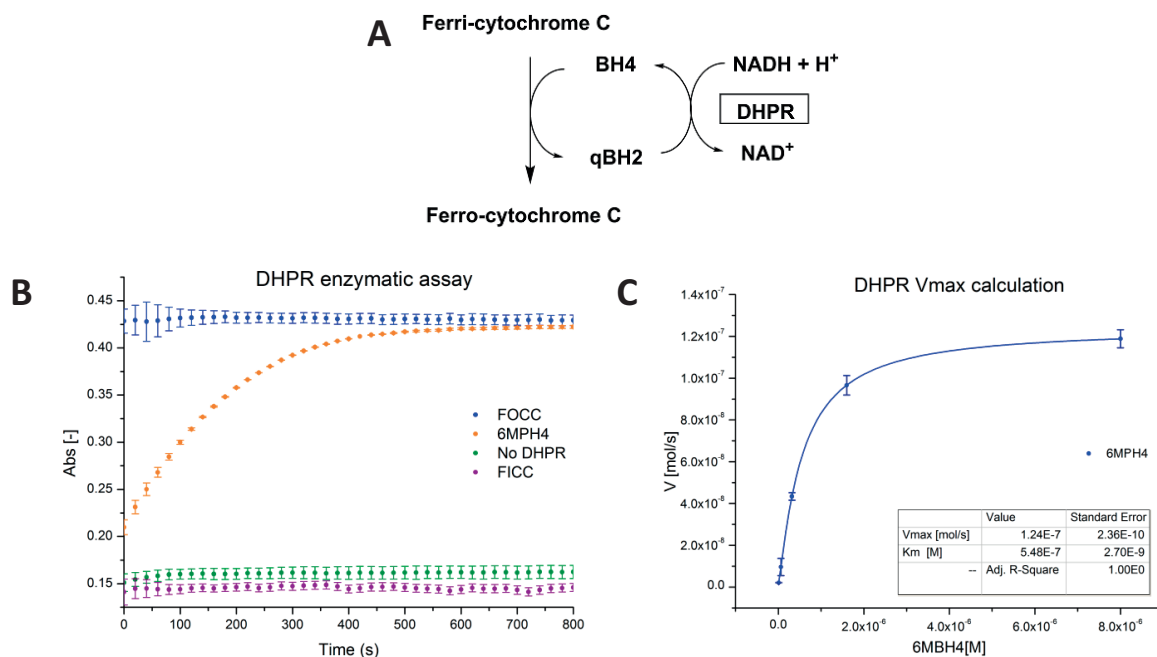


**Fig 17 DHRP assay and  $K_M$  determination.** (A) Scheme of the assay. FICC is rapidly reduced by BH4 to FOCC to yield qBH2. qBH2 is then reduced enzymatically by DHRP. (B) Results of the DHRP enzymatic assay. 6MPH4 is used as substrate. As controls independent wells lacking DHRP and containing only FOCC are assayed. (C)  $K_M$  constant measurement. Each point is the average of 3 measurement  $\pm$  SD.

### 2.1.2 DHRP Assay

The assay was run on human DHRP as described in material and methods. Briefly, ferricytochrome-c (FICC) and BH4 (in the experimental case 6MPH4) quickly react to form ferrocycytochrome-c (FOCC) and qBH2 (in the experimental case 6MqBH2). qBH2 is then reduced by DHRP to complete the cycle (Fig 17A). FICC and FOCC were also added to separated wells to determine the reaction starting and ending points. Upon total conversion of FICC, by the enzymatic reaction, the plateau reached the FOCC signal level (Fig 17B). Conditions without DHRP showed that non-enzymatic reduction of FICC could take place as previously reported. This was due to the relatively slow non-enzymatic conversion of qBH2 to BH4 by NADH. However the enzymatic reaction rate was roughly 70 times faster and can be afterwards corrected to measure the exact enzymatic rate. Influence of DMSO on the assay was tested and no noticeable change in the reaction rate could be observed with up to 10% V/V DMSO. Nevertheless, care was taken to keep DMSO concentrations constant over the whole assay

and set to a maximum of 1%. The  $K_M$  was measured by titrating 6MPH4 at five concentrations. Upon fitting with a Hill function, the estimated  $K_M$  was found to be 0.55  $\mu\text{M}$  (Fig 17,C). This value was in accordance with reported values of 0.15 to 18  $\mu\text{M}$ . This difference might be due to the choice of synthetic cofactor 6MBH4 whereas the reported values were measured with either BH4 or 6,7MPH4. Furthermore our assay used 50 $\mu\text{M}$  NADH instead of 100 $\mu\text{M}$  used in the literature. Inhibition of the enzyme was performed as a control with APT and MTX (Fig 18). The reported higher affinity of APT for DHPR in comparison to MTX was verified.  $K_i$  of 31 and 102  $\mu\text{M}$  for APT and MTX respectively were found.

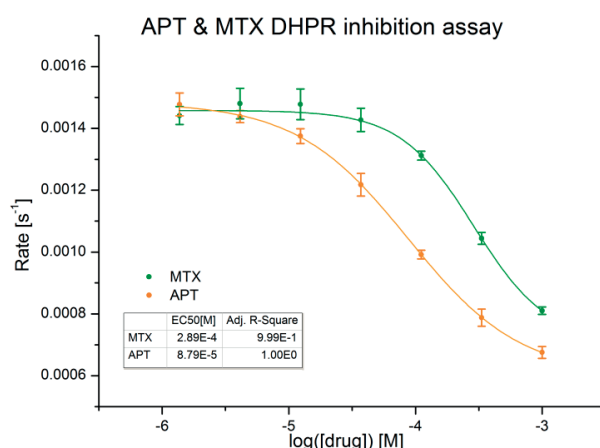


**Fig 18 Inhibition assay of DHPR with APT and MTX.** Inhibition potential of APT (orange) and MTX (was) against DHPR. A titration was made starting from 1mM. Each point is the average of 3 measurement  $\pm$  SD.

Through this assay it was seen that DHPR is a relatively robust enzyme, stable at room temperature and unaffected by low concentrations of DMSO. Values obtained for the enzyme characterization were consistent with the values reported in literature. The best known inhibitor was assayed in an inhibition assay and the  $K_i$  was measured.  $K_i$  for APT was similar to what has been reported ( $K_{i(\text{repo})} = 20\mu\text{M}$ ,  $K_{i(\text{found})} = 31\mu\text{M}$ ) while  $K_i$  for MTX diverges by a factor of three ( $K_{i(\text{repo})} = 38\mu\text{M}$ ,  $K_{i(\text{found})} = 102\mu\text{M}$ ).



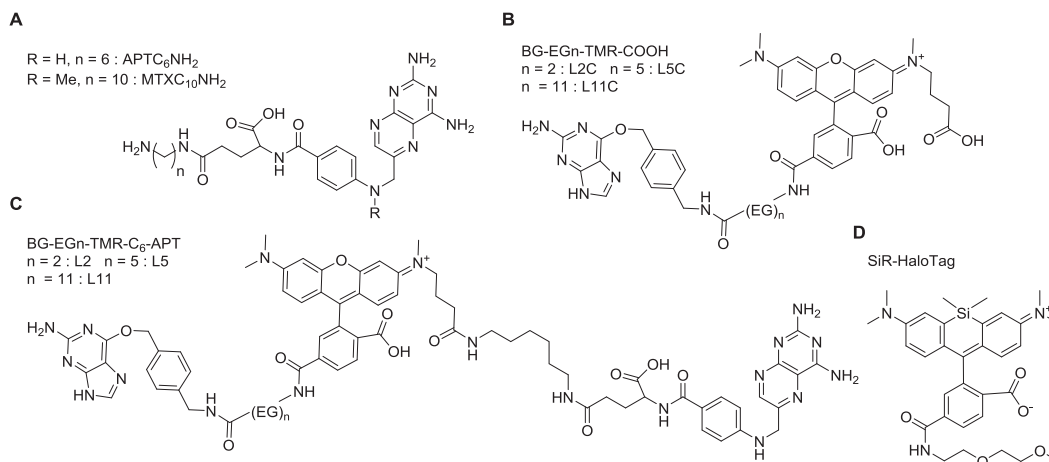


**Fig 19 Inhibitor derivatives and fluorescent linkers.** (A) Derivatized inhibitors are modified on one of their carboxylic acid moiety. (B) Small fluorescent SNAP binders based on the TMR dye are synthesized and used as controls for unspecific inhibition (C) Full linkers of various size were made based on APT. (D) SiR-Halo is used to couple SiR to the Halo-tag self-labeling protein

However, it was impossible to increase the inhibitors concentrations to obtain complete enzyme inhibition due to their insolubility at higher concentrations.

The used inhibitors possess two carboxylic acid moieties that can later be used for derivatization and linker design. The affinity of these compounds is, in comparison to those that were used before in literature for the design of sensors, similar to weaker. DHFR and SPR based sensors have been using nM range tethered inhibitors while a sensor for glutamate has been reported with similar tethered substrate affinity<sup>223,222</sup>.

### 2.1.3 Drug Derivatization and Linker Synthesis

In order to create a functional linker for the complete sensor, primary aminohexyl conjugates of MTX and APT were synthesized (Fig 19, A). These drugs possess accessible carboxylic acid moieties for straightforward amide bond formation. Both derivatized drugs were tested in order to assess the loss of inhibitory potential towards DHPR. The enzymatic assay was run with 250  $\mu$ M of APT, APTC<sub>6</sub>NH<sub>2</sub>, MTX and MTXC<sub>10</sub>NH<sub>2</sub>. A control containing no drug is run in parallel (Fig 20). The observed reaction rates for DHPR only, MTX and ATP are similar to what was observed in previous enzymatic assays. It is observed

that APT and APTC<sub>6</sub>NH<sub>2</sub> both decrease the reaction rate to a larger extent compared to MTX and MTXC<sub>10</sub>NH<sub>2</sub>. A similar affinity for both MTXC<sub>10</sub>NH<sub>2</sub> and APTC<sub>6</sub>NH<sub>2</sub> towards their respective original compound was observed. The retained affinity seemed suitable for sensor construction. Since APTC<sub>6</sub>NH<sub>2</sub> was shown to be a more potent inhibitor than MTXC<sub>10</sub>NH<sub>2</sub> all further synthesis were performed with this compound. Three linkers L2, L5 and L11 (Fig 19C) of various lengths were synthesized. All linkers contain a BG group for labeling of SNAP-tag, a TMR fluorescent dye as emitting FRET partner and ethylene glycol spacers of various sizes. Control linkers L2C, L5C and L11C (Fig 19B) lacking the tethered APT were synthesized, to assess unspecific interactions.

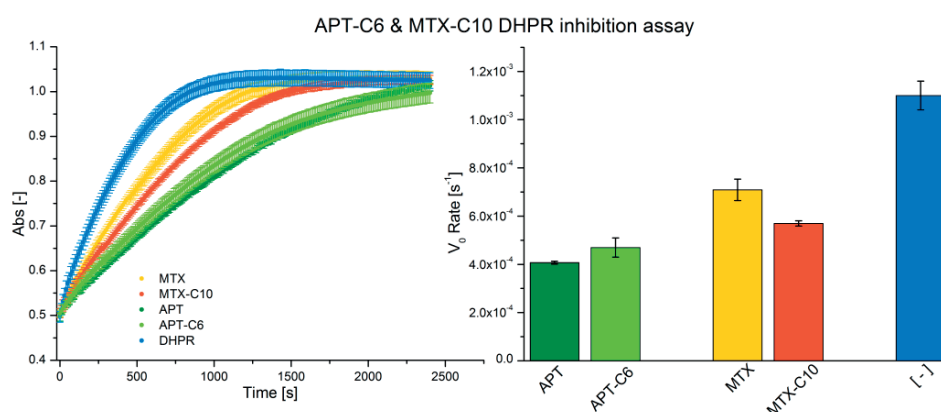


**Fig 20** Inhibition assay of DHPR with derivatives of APT and MTX. DHPR rate of reaction was compared with 250  $\mu$ M of unmodified and derivatized APT and MTX. Each point is the average of 3 measurement  $\pm$  SD.

Binding of the tethered drug to DHPR, once attached to SNAP, is a requirement in order to obtain a functional FRET sensor. As a mean to study this interaction the fusions SNAP-DHPR and DHPR-SNAP were expressed as so-called minimal-scaffolds. Labeled and unlabeled minimal scaffolds were assayed in standard enzymatic conditions and rates were compared to native DHPR. As seen on Fig 21 the  $V_0$  rates for DHPR and unlabeled SNAP-DHPR are comparable. DHPR-SNAP showed a slightly increased rate versus DHPR rate, but the difference might be due to the errors in the estimation of protein extinction coefficient. Rate of labeled versus unlabeled construct are roughly two times smaller in the case of SNAP-DHPR. The local inhibition due to the presence of tethered APT would correspond to an effective concentration of approximately 1 mM APT or 4 mM APTC<sub>6</sub>NH<sub>2</sub>. The change of reaction rate

indicates a semi-closed conformation of the constructs. Theoretically, the system was approximated as a set of two spheres in which a ligand is tethered to one of them. Using PyMOL, the linker length was estimated to be approximately 57 Å. Taking the linker length as a sphere radius giving one molecule in the sphere allowed us to estimate an effective molarity of ~10 mM. Using a more sophisticated random-coil polymer model to measure intramolecular molarity, a concentration of 5 to 15 mM (depending on the linker size) should be expected<sup>227</sup>. These predictions are in close correspondence to the measured values presented above.

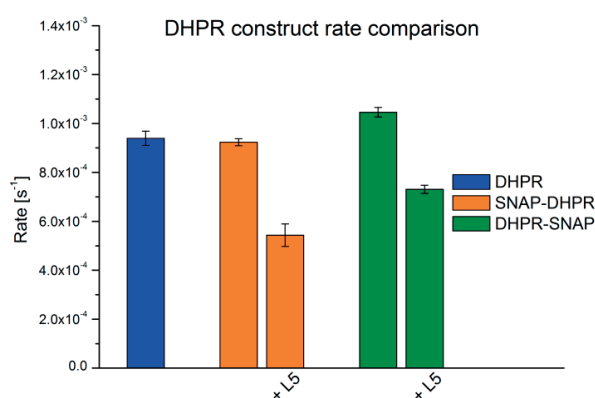


**Fig 21 Comparison between DHPR, labeled and unlabeled minimal scaffolds.** SNAP-DHPR and DHPR-SNAP were tested, labeled and unlabeled, in an enzymatic assay. The rates were compared to wild type DHPR. Each point is the average of 3 measurement ± SD.

It was observed that no loss of inhibition potential took place upon drug derivatization, yielding suitable precursors for the synthesis of complete linkers. Additionally fusing SNAP to both DHPR N and C termini did not affect the enzyme reaction rate. Furthermore, in the case of the tethered inhibitor, due to the high local concentration, binding could be observed via the enzymatic assay. The rate of reaction remained fairly high indicating partial binding of the tethered inhibitor to the DHPR fusion protein. In order to consolidate these observations the system was tested in fluorescence polarization (FP) assay.

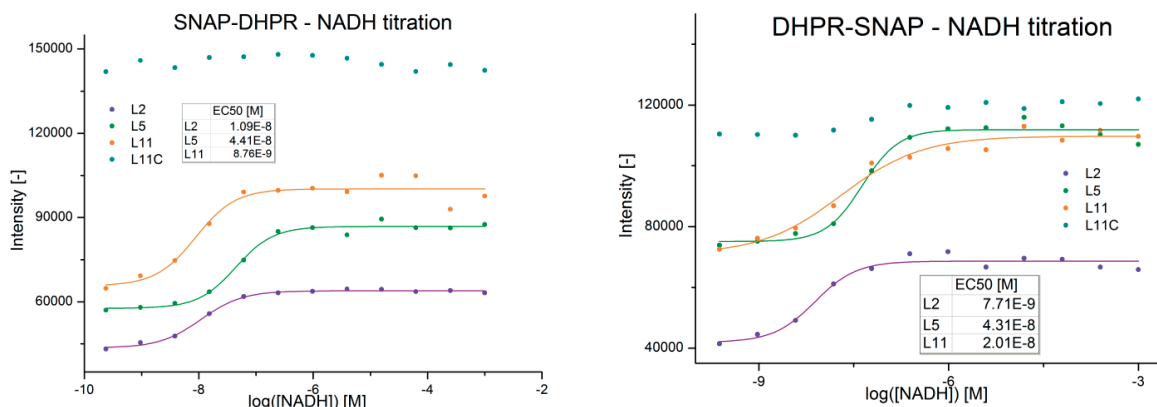


**Fig 22 Fluorescence intensity assay of labeled minimal constructs.** SNAP-DHPR (left) and DHPR-SNAP (right) were labeled with the linkers (L2,L5 & L11) and the control linkers (L2C, L5C & L11C) and titrated with various NADH concentrations. No signal in anisotropy could be observed but a total intensity change could. For the controls only L11C is shown for the sake of clarity.

### 2.1.4 Anisotropy Study of the Binding

DHPR requires first binding of NADH in order to bind its second cofactor qBH2. This could not be verified in the enzymatic assay, but could instead be tested with the FP assay. SNAP-DHPR and DHPR-SNAP were labeled with L2, L2C, L5, L5C, L11 and L11C and polarization was measured at different NADH concentration. No polarization change could be observed in any conditions. However, as seen in Fig 22, a change in total intensity could be observed. This change can be translated as an environmental effect on the dye. It can be observed that this change of intensity occurs for all linkers at roughly the same concentration with similar amplitude. All the control linkers were tested and showed a comparable intensity and linearity over the whole concentration range. Hence, for the sake of clarity only L11C is shown. The observed low nM IC50 corresponds to a mix between sensor titration and linker binding. Indeed, in the assay the sensor concentration was 50 nM. The affinity of DHPR for NADH being  $K_d = 20$  nM it cannot be concluded that the observed change are strictly due to NADH binding. It can be observed that the signal reaches plateau at 1  $\mu$ M NADH indicating saturation of the system closed state.

In order to confirm that the observed intensity change was due to binding of the tethered drug to the active site, displacement of the ligand was attempted by titrating APT at a fixed NADH concentration. Both constructs were labeled with L5 and L5C, NADH was kept at 50  $\mu$ M and APT was

titrated from mM to nM concentration. As seen on Fig 23, there is a clear unspecific effect from APT on the system. It was observed that the effect takes place close to 1 mM. It cannot be excluded that the drug at this range of concentration is not totally dissolved and therefore might influence the system. However, the decrease in intensity observed for SNAP-DHPR starts in the  $\mu\text{M}$  range, significantly before the drop due to APT. If the intensities are normalized over the L5C signal a dose response curve can be fitted. A smaller intensity change is observed for DHPR-SNAP in comparison to SNAP-DHPR. Furthermore, the EC50 for DHPR-SNAP is at high  $\mu\text{M}$  concentrations. Both the relatively weak intensity change and the high EC50 values point towards a less favorable protein conformation for the tethered drug to bind in the case of DHPR-SNAP. In order to investigate the implication of DHPR in these unspecific effects L5 and L5C were attached to a SNAP-CLIP construct. An APT titration was performed and similar effects could be observed on the high  $\mu\text{M}$  intensity decrease. This indicates a probable interaction of the drug with either the dye or SNAP.

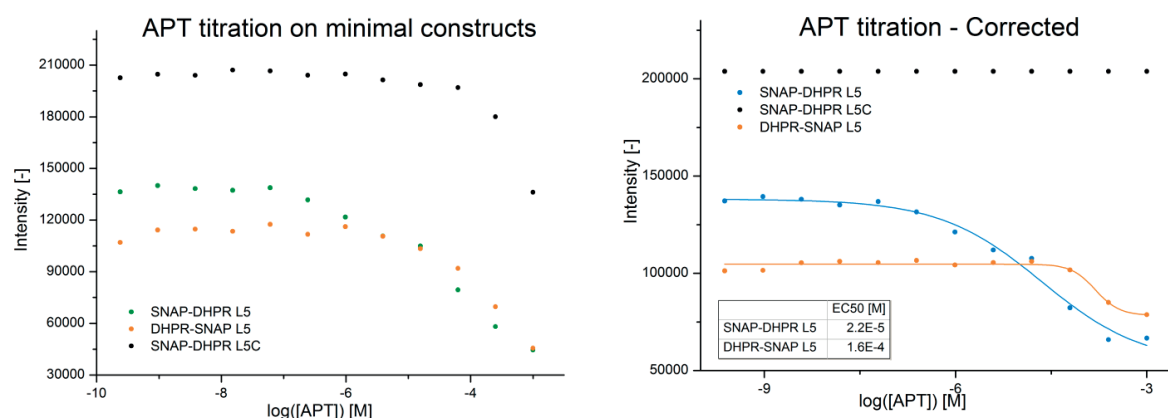


**Fig 23 Fluorescence polarization, tethered ligand unbinding by APT.** SNAP-DHPR and DHPR-SNAP were labeled with L5 and L5C. APT was titrated at a fixed NADH concentration in order to open the minimal constructs. Significant unspecific effects were observed on the control (left) the signal was corrected for those (right).

Through this FP experiment no anisotropy changes could be observed. However, upon measuring total fluorescent intensity a signal increase was seen when titrated with NADH. Such artifacts point towards an interaction of the dye with its environment, most probably with DHPR upon binding. Indeed, the relatively short spacer (12 atoms) used between TMR and APT could force the dye to enter in

contact with residues close to the active site. The ability of the system to close in the presence of NADH was confirmed but it was impossible to distinguish which of the three linkers was the most suitable. The slightly better signal change of DHPR-SNAP upon NADH titration suggests this protein fusion might be more appropriate. Furthermore, displacement of the bound tethered drug was attempted with APT. In light of the unspecific effects observed upon titration of APT, potentially due to an interaction with TMR, it cannot be certain that the tethered drug unbinds. The constructs geometries will be investigated *in-silico* in order to rationally drive the sensor development.

### **2.1.5 In-Silico Modeling for Rational Sensor Design**

No DHPR crystal structures bound to a pterin cofactor or a drug is available. Therefore, an *in-silico* docking computational model was calculated in order to orient the sensor development. Autodock Vina, a well-established, fairly user-friendly and well documented docking algorithm was used for this purpose. Being popular, Vina has been used in a majority (32% over all other algorithms) of studies involving docking between 2010 and 2013<sup>228</sup>. The algorithm is known to be a robust tool when it comes to flexible ligand docking into macromolecular targets. Furthermore, Vina accepts threading, which diminishes computational hardware requirement allowing desktop computers to perform the calculations in a reasonable time<sup>229</sup>. The software requires a preparation of the protein (lock, described in material and methods) and molecule (key). The binding pocket location for the endogenous cofactor has been well described and was used to define the boundaries of a search box surrounding it. Both MTX and qBH2 were used as keys. As a result, qBH2 was docked in the active site with its pterin ring parallel to the Trp90 a position known to be favorable due to  $\pi$ - $\pi$  stacking (Fig 24A). The qBH2 N5 was oriented towards the NADH molecule with N5 at 4.5 Å from the nicotinamide ring C4. This distance is reasonable in order for the molecule to perform a hydride transfer. Hydride transfer studies reported 3.4 to 3.6 Å<sup>230</sup> reaction distance and as comparison sepiapterin C1' ketone has been reported to be located at 3.2 Å from the nicotinamide C4 in the SPR crystal structure<sup>107</sup>. Furthermore, N5 is also in close proximity of

Tyr150 a residue involved as proton acceptor essential for the reaction. Finally, the qBH2 1,2-dihydroxypropyl side chain is oriented above the NADH cofactor, towards the center of the enzyme. This orientation would support a fusion of DHPH on the C-termini as a linker would favorably close in such a conformation. In addition, Varughese et. al.<sup>35</sup> reported in 1992 the first DHPH crystal structure as well as a model of qBH2 binding mode. Their model supports the performed simulation and highlights the critical enzymatic active site features described in the docking.

MTX was docked with a general orientation comparable to qBH2 (Fig 24B). The side-chain was oriented towards NADH but the molecule was flipped upside-down, its N5 pointing towards the solvent. This change in vertical orientation could be due to the increased size and flexibility of the molecule. Indeed, qBH2 is a rather rigid molecule with only the 1,2-hydroxypropyl chain being flexible (2 rotating bonds). However, MTX has a larger side chain with 10 rotating bonds and a phenyl ring allowing, during docking, for more conformational freedom and interactions outside of the active site. It was speculated that the general horizontal orientation of MTX with its side-chain pointing towards the enzyme center, similar to qBH2, was correct. However, the vertical orientation predicted by the docking model was presumably erroneous. Furthermore, the distance from the termini to the active site is shorter in the C-terminal case than the N-terminal one. Generally, fusion on the termini closer to the active site yields sensors with larger FRET ratio changes. In light of the structural clues gathered through the *in-silico* model and the literature, it was decided that the future DHPH fusions would be carried on the C-termini.

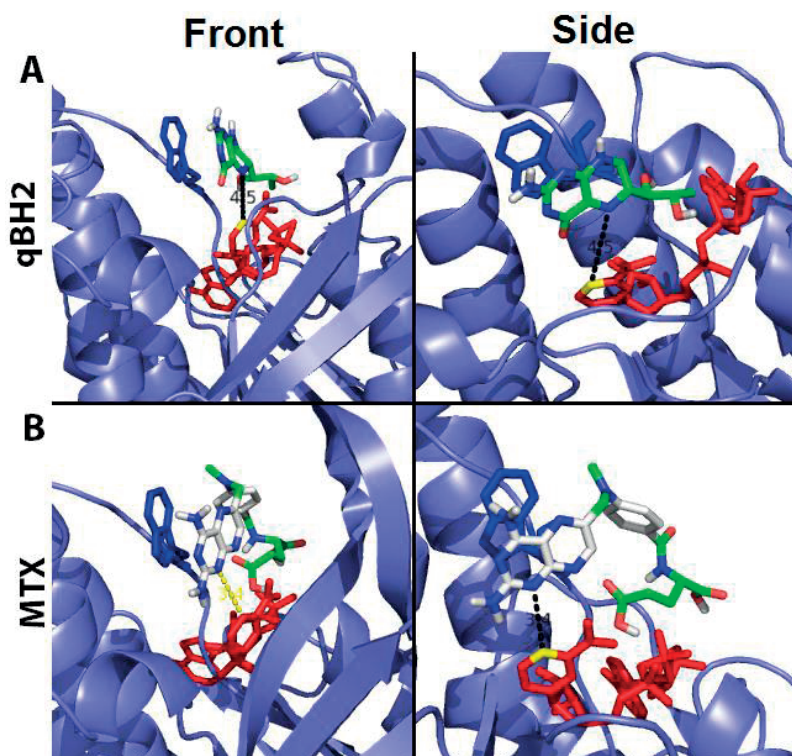


**Fig 24 Models of qBH2 and MTX docking in DHPR.** Front and side view of qBH2 (A) and MTX (both green) (B) docking. NADH is shown in red, and Trp90, a residue expected to be involved in  $\pi$ - $\pi$  stacking with the pterin ring, is shown in blue. qBH2 orientation towards the active site is similar to previously reported simulated models. MTX was docked flipped with the N5 pointing towards the solvent.

### 2.1.6 Scaffold Spacing

The next objective was to obtain the best balance between the closing capacity and the FRET signal ratio change between closed and open sensor state. Inserting rigid amino acid patches (polyproline) between DHPR and SNAP potentially increases the inter-fluorophore distance in the open sensor. In precedent published sensors, this strongly increased the signal ratio change between the open and closed sensor state<sup>231</sup>. It has been reported that a chain of 30 prolines (P30) strongly increased the maximal ratio change without significantly impacting the local concentration.



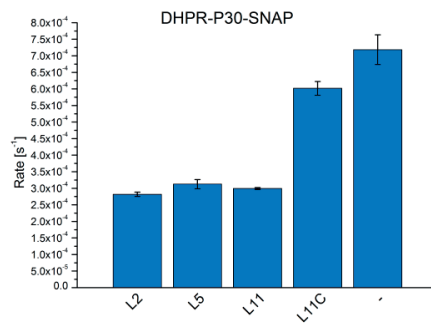


**Fig 25 Enzymatic assay with DHPR-p30-SNAP.** The construct was labeled with the linkers L2, L5, L11 and L11C and the rates of reaction were compared to the unlabeled one. Each point is the average of 3 measurement  $\pm$  SD.

To evaluate the effect of the insertions of a P30 linker the DHPR-P30-SNAP construct was expressed. The enzymatic assay was performed on the L2, L5, L11, and L11C labeled construct compared with the unlabeled one. The enzymatic rates of constructs labeled with a linker bearing a tethered drug were significantly reduced (50%) in comparison to the control (Fig 25). This was a strong indication that DHPR in the construct is bound to the tethered drug. Furthermore, the difference in conversion rate between L11C and the unlabeled construct can be explained by the fact that the labeled sensor concentration was measured by TMR absorbance while the unlabeled construct concentration was measured with its protein extinction coefficient. This could have induced significant errors in the concentrations even though the labeling efficiency was expected to be quantitative. In addition, no difference in the reaction rate for the different linkers could be observed even though theoretically L2 should be too short. The separation due to P30 was estimated to be between 60 and 90 Å<sup>232</sup> (without counting the SNAP and DHPR enzyme increasing the distance) while the L5 linker length was estimated as 57 Å and L2 was smaller. However, L11 with an estimated length of 77Å which would allow the tethered APT to reach into DHPR binding pocket should be the only linker presenting inhibitory affinity.

From this experiment it could be concluded that insertion of P30 was not deleterious to the tethered drug binding. Furthermore, it appears important to consider the linker and constructs size approximations carefully. Indeed, considering the system as rigid could be erroneous as it could actually be in a much more packed conformation allowing even short linkers to access DHPR binding pocket. DHPR-P30-SNAP was not tested in FP assay as most of the relevant information was already gathered with the minimal constructs and the current enzymatic assay. The sensor development was pursued further with the incorporation of the Halo-tag (noted only Halo in the description of fusion proteins) self-labeling protein necessary for the incorporation of the SiR acceptor dye.

### 2.1.7 First Sensor Iteration

The DHPR-Halo-p30-SNAP fusion protein was expressed and purified. This construct possessed a Halo self-labeling protein able to selectively react with chloroalkanes. SiR was selected as the FRET acceptor in this system since the TMR-SiR FRET couple has good spectral overlap for FRET. The molecule SiR-Halo was used in all further constructs to label the Halo-tag protein. The sensor was labeled on SNAP with L2, L5, L11 and L11C and SiR-Halo and was titrated with NADH and NAD<sup>+</sup>. As seen in Fig 26 the signal at 665nm (from here referred as the SiR signal) increases upon titration with NADH indicating that the sensor is closing and that TMR comes in closer proximity to SiR. Furthermore, it was observed that the

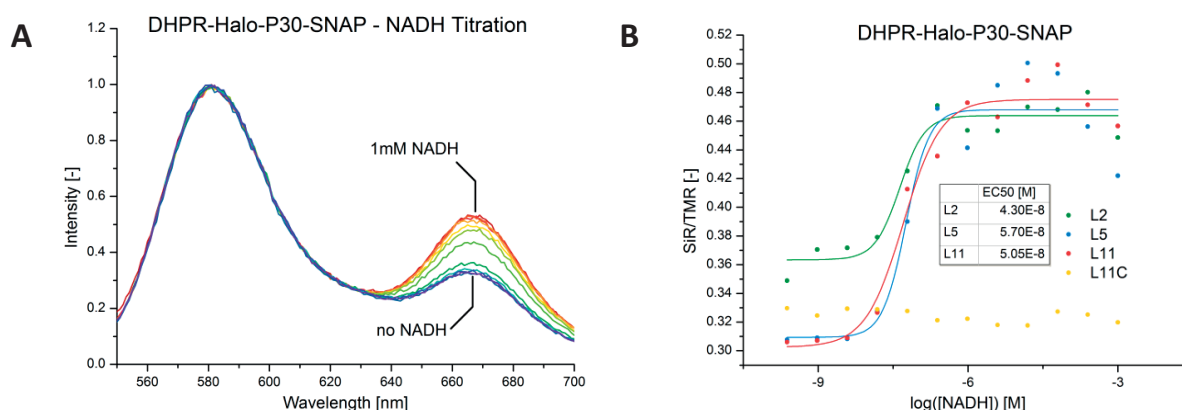


**Fig 26 Labeled DHPR-Halo-P30-SNAP titration with NADH.** The sensor was labeled with the linkers, L11C and SiR-Halo and was titrated with NADH. The SiR signal increases upon NADH concentration increase (left, L11). The 3 linkers give rise to different ratio changes (right)

ratio change was smaller with L2 compared to L5 and L11 which show larger ratio changes (Fig 26B). It was observed that the control linker ratio remained unchanged throughout the whole titration indicating that there was no interaction between NADH and the dye. Interestingly, the sensor open state (when no NADH is present) was not similar for all linkers. The observed maximal ratio change was found to be  $R_{max} = 160\%$  or 1.6 fold ratio change. Plateau in the current setup was reached above  $60 \mu\text{M}$  NADH, a value larger to what was observed in the FP experiments with SNAP-DHRP with any linker. Therefore, a  $[\text{NADH}] = 200 \mu\text{M}$  was used for all subsequent sensor opening experiments. NADH had no effect on the sensor labeled with L11C while  $\text{NAD}^+$  had no effect on the sensor labeled with L11 and L11C (data not shown). Further characterization was performed with L11.

Furthermore, the plot (Fig 26A) was normalized on the 580nm signal (from here on referred as TMR signal) as signal drifts were observed upon NADH titration. Previously, FP assay presented no anisotropy change but total intensity changes due to environmental effects. In order to understand the signal drifts, the sensor was labeled with L11 only. It was titrated with NADH and a small but significant intensity change was observed (Fig 27A). The phenomenon could be explained by the sensor closing first with TMR potentially coming close to the enzyme reaching an intensity peak close to  $1 \mu\text{M}$ . When labeling the sensor with L11 and SiR-Halo and directly exciting SiR upon NADH titration, no fluorescence

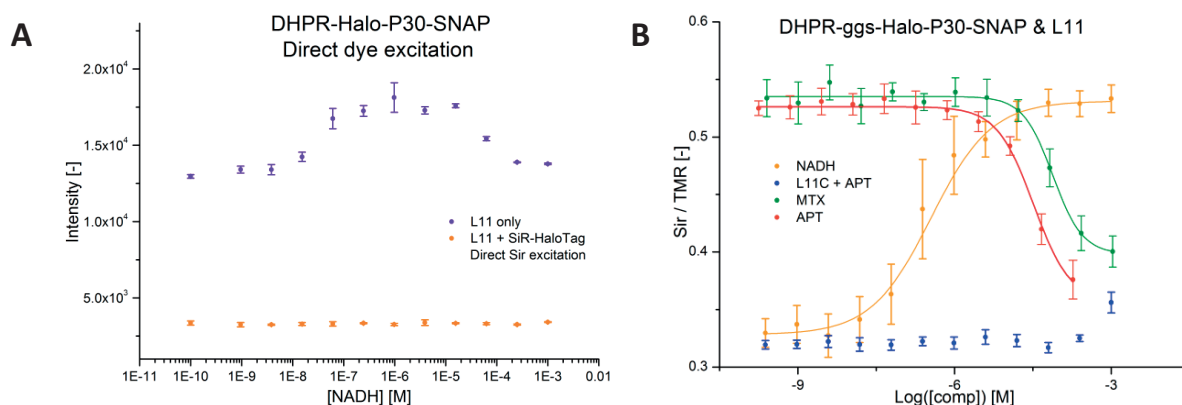


**Fig 27 Sensor TMR assay and opening.** (A) Direct excitation of the TMR dye with various concentrations of NADH as control. The sensor was tested in different conditions to assess environmental effects on the dye. (B) Closing of the sensor with NADH followed by opening with either MTX or APT. Titration with APT and MTX was performed on the sensor to assess its opening capacity. Control is performed with L11C and APT. Each point is the average of 3 measurement  $\pm$  SD.

intensity change could be observed indicating no unspecific effect on the dye either by a construct conformational change or NADH effects on the dye. The collected data indicated that the signal was composed of a part of FRET and a part of environmental effects on the TMR dye. No explanation could be given for the factors bringing the signal down and this issue was not investigated further as it did not impact the sensor development.

The sensor was labeled with L11 and was then titrated with APT and MTX at 200  $\mu$ M NADH. APT and MTX were titrated in order to displace the tethered ligand (Fig 27, right). The sensor was opened by both MTX and APT with an IC50 relatively smaller for APT than MTX showing the inhibition potential difference of both those drugs. Additionally, at high drug concentration a FRET ratio similar to the control could not be observed. It would be expected for L11C, L11 without NADH and L11 + 200  $\mu$ M NADH + drug to possess the same FRET ratios as the sensor should be open. This was indeed the case when no NADH was added to L11 but not in the presence of a drug. At high concentrations of APT, both L11 and L11C showed a ratio increase at 1mM explainable by the poor solubility of APT probably interacting with the dyes. FP experiments, more sensitive on precipitates, showed on DHPR-SNAP similar behaviors at relatively high APT concentrations.

A sensor, able to quantify the interaction of a competitive drug with DHPR was created. It was observed that the shortest linker was performing less efficiently than the longest ones probably owing to its shorter size. It would be expected for it not to be able to appropriately reach the binding pocket or having its dye not properly oriented to produce FRET in an efficient manner. Generally, sensors with a high Rmax value and Z factor give the most significant and reliable results in screening campaigns. In the current case the obtained Rmax was fairly small (1.6x ratio change) in comparison to previously reported sensors (Human carbonic anhydrase: 4x<sup>233</sup>, MTX bioluminescent sensor: 13x<sup>223</sup> & 22x<sup>234</sup>, MTX sensor

based on unnatural amino acids:  $34\times^{235}$  ) Efforts were put on increasing the Rmax value by attempting to incorporate unnatural amino acids, circularly permutating DHPR or modifying the sensor geometry.

## **2.1.8 Sensor Optimization**

### **2.1.8.1 Non Natural Amino Acids**

It was hypothesized that modifying DHPR in order to incorporate close to the active site, an unnatural amino acid, serving as handle for later derivatization with a fluorophore, could yield an efficient sensor. The structure of DHPR was investigated in order to find regions prone to modifications. Glutamic acid 46, an amino acid proximal to the active site, located in a flexible loop, was selected to be modified to an Amber stop codon (modification named further on DHPR(E46X)). The suppressor system adapted from Lemke<sup>236</sup> and Chin<sup>225</sup> had shown to be successful in our lab in a subset of experiments (see material and methods). A generally convenient handle to install was (2S)-2-Amino-6-(((1R,8S)-bicyclo[6.1.0]non-4-yn-9-ylmethoxy)carbonyl)amino)hexanoic acid (BCN-lysine) as it would react with tetrazine in a copper-free fashion. The reaction rate has been reported to be  $\sim 400 \text{ M}^{-1}\cdot\text{s}^{-1}$ , ideal for fast protein labeling with dyes coupled to tetrazine. Four plasmids, bearing an Amber stop codon replacing Glu46, DHPR(E46X), DHPR(E46X)-SNAP, SNAP-DHPR(E46X) and DHPR(E46X)-p30-SNAP were produced. Protein expression on these constructs was either inexistent or yielded truncated products that could not be labeled. A GFP with an amber mutation was expressed as control. The bacterial culture had a characteristic yellow color indicating presence of the protein. The GFP protein was not purified and the idea was discontinued.

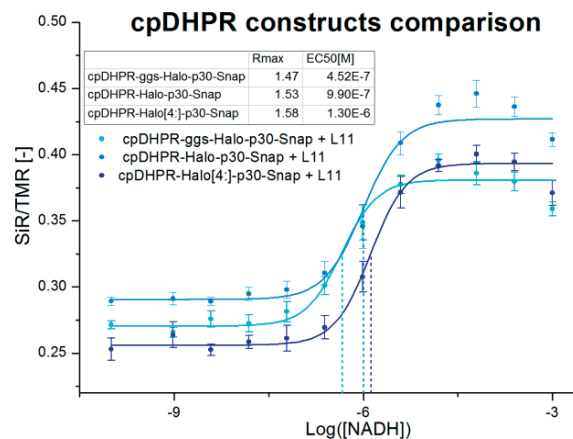


**Fig 28 cpDHPR constructs ratio change.** Three constructs based on circularly permuted DHPR were labeled with L11 and tested by NADH titration. Each point is the average of 3 measurement  $\pm$  SD.

### 2.1.8.2 Circular Permutation and Scaffold Stiffening

The concept of modifying DHPR in order to create attachment point close to its active site was further evaluated. It was envisioned that circularly permuting DHPR at E46 (cpDHPR) could yield a version able to be fused closer to the active site. It would potentially bring in closer proximity the FRET couple once the sensor closes increasing therefore the sensor Rmax. Using PyMOL, a linker able to link the N to the C termini was modeled. A (GGG)4 linker, appeared to be of the correct size and a plasmid containing the cpDHPR version was created. The protein expressed in satisfactory yields and an enzymatic assay on cpDHPR compared to DHPR was performed. Vmax and  $K_M$  were measured and were found to be similar (DHPR : Vmax = 0.124  $\mu$ M/s,  $K_M$  = 0.55  $\mu$ M ; cpDHPR : Vmax = 1.14  $\mu$ M/s,  $K_M$  = 0.95  $\mu$ M). Three sensors, cpDHPR-ggs2-Halo-P30-SNAP, cpDHPR-Halo-P30-SNAP and cpDHPR-Halo[4:]-P30-SNAP were cloned and expressed. The rationale was to decrease further the distance between cpDHPR and Halo-tag and to decrease flexibility between Halo-tag and P30. It was observed and suggested by collaborators that the 4 first Halo-tag amino acids could be removed (Halo[4:]) to reduce flexibility of the aforementioned fusion point. Increased rigidity at this point, in their case, increased the distance in the sensor open state or optimizing dye orientation yielding a larger Rmax. The three sensors were labeled with L11 and tested for closing upon NADH titration. A FRET ratio change could be observed upon titration indicating the

sensor closes. Rmax values increased when shortening the distances between cpDHPR and Halo-tag and by stiffening the Halo-tag P30 junction (Fig 28). The incorporation of Halo[4:] did increase the sensor open state and removal of the GGS linker the sensor closed state. Generally, the EC50 increased conjointly with the Rmax. However, the obtained Rmax for all of the sensors were below the value obtained with DHPR-p30-Halo-SNAP (Rmax = 1.6). Anyhow, these observed changes are small compared to what has been previously reported. Literature precedence shows that incorporation of P30 or large structural modifications such as circular permutation lead respectively to 4 to 6 fold<sup>231</sup> and roughly 7 fold change (collaborator, unpublished data) Rmax. In the current case the Rmax changes are close or within the observed error. The attempted circular permutation strategy did not yield significant improvement and was abandoned.

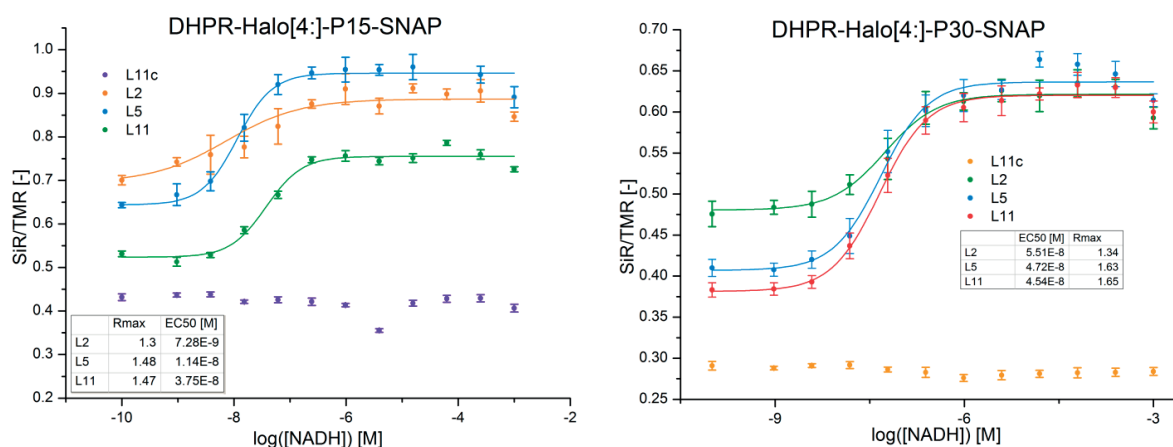


**Fig 29 Sensors optimization based on scaffold rigidification.** Two constructs lacking the (ggs)2 spacer and with different polyproline spacer (P15: left, P30:right) length were labeled and tested for closing upon NADH titration. Each point is the average of 3 measurement  $\pm$  SD.

As last attempt, the strategy involving shortening and stiffening the fusion points was applied on wild type DHPR and two constructs, DHPR-Halo[4:]-P15-SNAP and DHPR-Halo[4:]-P30-SNAP were cloned and expressed. DHPR-Halo[4:]-P15-SNAP was created by a mistake in the primer hybridization on the P30 part. The two constructs were labeled with SiR-Halo and with L2, L5, L11 and L11C. Sensor closing was tested by titrating NADH. The obtained titration curves were similar (Fig 29) between the P15 and P30

bearing constructs. Again shortening and rigidifying the fusion points had only minor impact on the Rmax. Furthermore, even deletion of 15 proline residues had only little effects on Rmax inconsistent with literature precedence. Interestingly, the control linkers in both sensors had different SiR/TMR values.

Optimization of the initial sensor was conducted applying methods that showed to be successful in previously reported sensors such as unnatural amino acids incorporation, circular permutation of the receptor protein and rigidification of the overall scaffold. However, in the current case none of these brought a substantial amelioration of the Rmax value. It was envisioned that further optimization might not be critical for a HTS.

### ***2.1.8.3 Assay validation***

The sensor and ligand couple, DHPR-Halo[4:]-P30-SNAP + L5 (Rmax = 1.63) was selected as a larger quantity of the linker was available and no substantial difference in Rmax was seen between L5 and L11. The Z factor was calculated and sample preparation and analysis was made as described in material and methods. A high statistical reproducibility<sup>263</sup> of Z' = 0.7 was found indicating that the system was suitable for HTS. Determination was made on the basis of two 96 well plates.



Name	FRET IC50 [ $\mu$ M]	Name	Remark
Triamterene	5.08	Daunorubicin hydrochloride	Fluorescent
Deoxycorticosterone	11.8	Doxorubicin hydrochloride	Fluorescent
Adrenosterone	15.9	Epirubicin hydrochloride	Fluorescent
Ebselen	17.4	Tetraethylenepentamine pentahydrochloride	Discarded
Testosterone propionate	26.4	Pentetic acid	Discarded
Corticosterone	26.5	Mitoxantrone dihydrochloride	Fluorescent
Mizolastine	32.2	Etomidate	Discarded
Zaprinast	29.1	Etifenin	Discarded
Clofazimine	31.7	Oxytetracycline dehydrate	Discarded
Progesterone	48.0	Alexidine dihydrochloride	Discarded
Exemestane	40.8	Sulfadimethoxine	Discarded
Praziquantel	39.3	Paclitaxel	Discarded
Medrysone	81.7	Methotrexate	Known
		Bephenium hydroxynaphthoate	Discarded
		Carbenoxolone disodium salt	Discarded
		Benserazide hydrochloride	Discarded

**Table 6 Summary of the drugs discovered via the HTS campaign.** In green are the drugs selected for further characterization. In white are the drugs that were found to interact with DHPR but which were not further characterized as they appeared to possess a weaker potential than APT. In red are the drugs that were discarded. A table containing all the structures can be found in the annex.

## 2.2 Prestwick Library Screen

### 2.2.1 Library Selection

The library selection was made on two criterions. (i) Compounds had to be commercially available for further testing. (ii) Evidence showed that certain drugs provoked, in patients, symptoms related to BH4 deficiency<sup>119</sup>. Screening for administered drugs was of interest. Therefore the Prestwick chemical library was selected. This library is composed of 1280 drugs approved by regulatory agencies, and is chemically diverse. Compounds and their pharmacologic effects in this library also are well detailed. The screening campaign was performed as described in the material and method section.

### 2.2.2 New DHPR Inhibitors

Thirty hits came out in the first round of selection (Table 6). Several of these hits possessed similarities. Indeed, seven compounds possessed a sterone motive (deoxycorticosterone, adrenosterone, corticosterons, progesterone, medrysone, exemestane and testosterone propionate). Four had high aromatic content (daunorubicin, doxorubicin, epirubicin and mitoxantrone) and were suspected to

interact with the assay due to their absorbance. Finally, four compounds had characteristic chelating agent structures (tetraethylene pentamine, pentetic acid, alexidine and etifenin). MTX was found to be a hit, increasing confidence in the screen results. Furthermore, the compound triamterene (TRI), stood out as its structure was similar to 4-amino substituted pterins, often proven to be decent DHPR and DHFR inhibitors. A table containing all the drugs structures can be found in the annex.

A second round of screening was performed without the fluorescent compounds and without MTX. As negative control for this round, the sensor was labeled with L11C. The rubicins and mitoxantrone were tested via the enzymatic assay and showed no inhibition potential. Out the remaining drugs, and after a second round of screening, eleven more compounds were discarded. The discarded compounds were either false positives or too weak binders to be of interest. The remaining thirteen molecules were tested for a nine points (100 to 0.78  $\mu\text{M}$  + no drug) IC50 curve. Six molecules possessing a sterol motif were found to interact with DHPR. A selection of four candidates was made based on the drugs inhibitory potential: TRI, ebselen (EBS), adrenosterone (ADR) and deoxicorticosterone (DCS) (Fig 30). Investigation of the drug effects on intracellular pterin balance was of interest. In addition, in-vitro examination of these compounds on enzymes of the BH4 metabolic network was pursued. These assays would shed light on the mechanisms behind potential pterin metabolic imbalances.

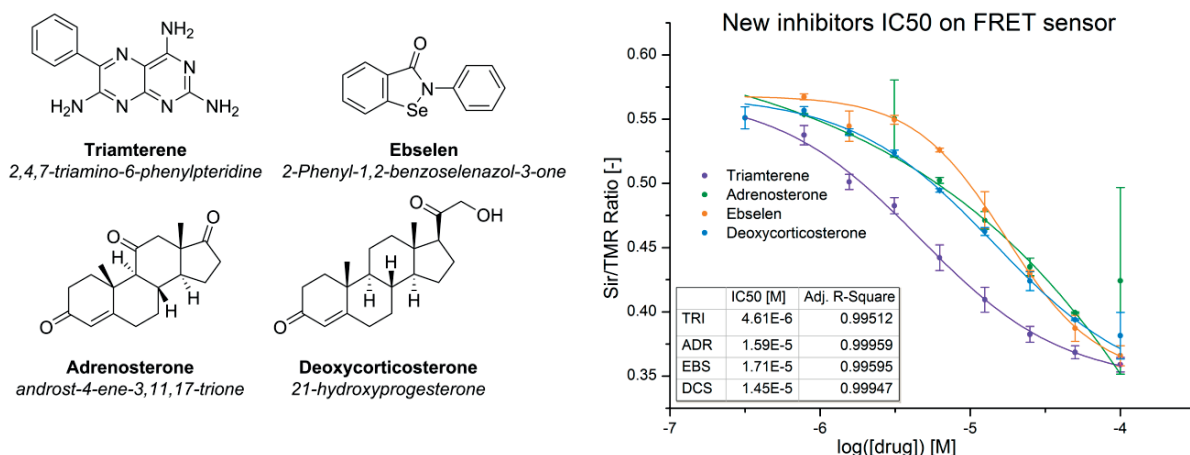


**Fig 30 Four DHPH candidates and their IC50 curve.** The four drugs were found to be the most potent DHPH inhibitors out of thirty candidates. Their IC50 curve, determined via the FRET assay is displayed on the right. Each point is the average of 3 measurement  $\pm$  SD.

## 2.3 Further Candidate Characterization

### 2.3.1 In-Vitro Characterization

The inhibitory potentials of the four drugs candidates were tested on several enzymes of the BH4 metabolic pathway. It was of interest to see if in addition to DHPH also GCH1, SPR and DHFR would be inhibited. Furthermore, knowing the selectivity of these drugs was important as to understand potential effect they might have on cell metabolism. Only drugs having an effect on the tested enzymes were discussed.

#### 2.3.1.1 DHPH & SPR & DHFR

The candidates were tested on DHPH in an enzymatic assay and showed inhibitory potential. This result indicated that the interaction observed during the FRET assay was not unspecific. All candidates possessed an IC50 smaller than APT (Fig 31 left). The found  $K_i$  were  $K_{i(\text{TRI})} = 5.57 \mu\text{M}$ ,  $K_{i(\text{ADR})} = 6.3 \mu\text{M}$ ,  $K_{i(\text{DCS})} = 20.1 \mu\text{M}$  &  $K_{i(\text{EBS})} = 28.4 \mu\text{M}$ .

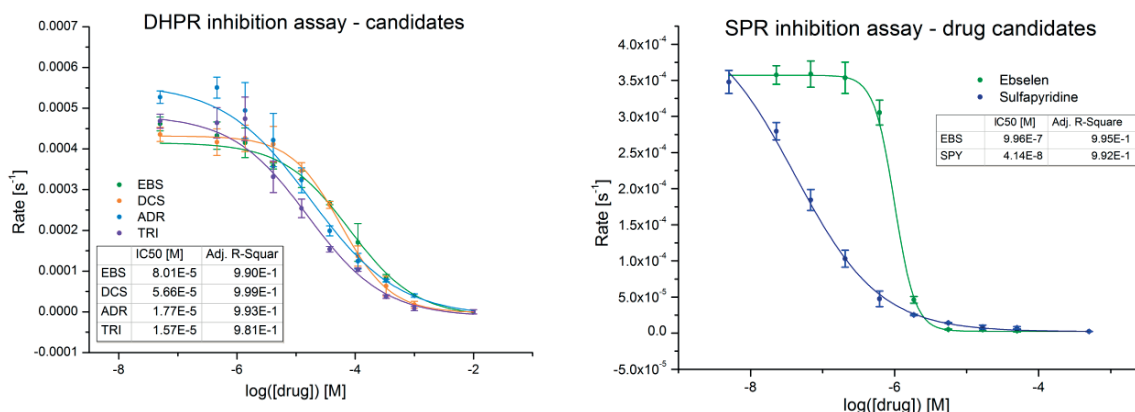


**Fig 31 Inhibition potential assessment of the four drug candidates on DHPR and SPR.** All drug candidates inhibited DHPR in the enzymatic assay. SPR was tested with another known inhibitor as no value had been experimentally acquired now. Each point is the average of 3 measurement  $\pm$  SD.

In order to assess the drug candidates inhibition potentials on SPR, they were compared to sulfapyridine (SPY) an inhibitor with a reported IC<sub>50</sub> of 82 nM in a similar type of assay. No data on SPR had been experimentally acquired so far during this work therefore this inhibitor was used as control. As a result, only EBS showed inhibition potential on SPR with an IC<sub>50</sub> of  $\sim$ 1  $\mu$ M (Fig 31 right). However, the very steep curve indicates that a potential unspecific effect is potentially taking place. This feature was not observed when interacting with DHPR in neither the FRET nor enzymatic assay.

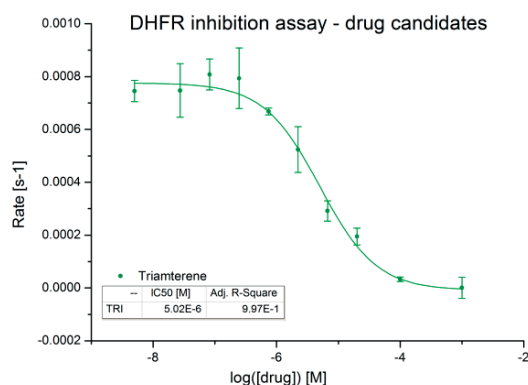


**Fig 32 DHFR inhibition assay with the drug candidates.** Out of the four drug candidates only TRI inhibited DHFR. Each point is the average of 3 measurement  $\pm$  SD.

The drugs candidates were tested on DHFR and it was observed that only TRI possessed an inhibition potential (Fig 32). An IC<sub>50</sub> of 5.02  $\mu$ M was found resulting in a K<sub>i</sub> of 0.13  $\mu$ M using the reported

$K_M$  of 2.7  $\mu\text{M}$ . The inhibition potential on DHFR is therefore roughly 40 folds higher than for DHPR. The inhibition of DHFR by TRI had already been reported<sup>237,238</sup> and  $K_{i(\text{repo})} = 0.2 \mu\text{M}$  was found to be similar to our value<sup>239</sup>.

IC50 / Ki [ $\mu\text{M}$ ]	Enzyme			
	DHPR	DHFR	SPR	GCH1
TRI	15.7 / 5.57	5.02 / 0.13	N.I	N.I
EBS	80.1 / 28.4	N.I	0.996 / -	4.67 / -
DCS	56.6 / 20.1	N.I	N.I	N.I
ADR	17.7 / 6.3	N.I	N.I	N.I

**Table 7 *In-vitro* inhibition potentials of the drug candidates towards enzymes members of the BH4 metabolic pathway.** IC50 and calculated Ki are reported as  $\mu\text{M}$ . N.I.: No inhibition observed.

When comparing the IC50s in the case of the FRET assay versus the enzymatic assay for DHPR, similar values could be observed. The obtained IC50 in the enzymatic assay were generally higher with a maximal difference of roughly fourfold. This might be explained by the difference of competition the drug faces in the two assays. In the FRET assay the tethered linker affinity for DHPR is weaker than 6MPH4 but its local concentration is much higher. ( $\sim 1\text{mM}$  tethered APT vs.  $1 \mu\text{M}$  6MPH4). Table 7 summarizes the IC50 and Ki found in *the in-vitro* characterization.

### 2.3.1.2 GCH1

GCH1 is a challenging enzyme to work with. GCH1 C-termini is buried inside the enzyme's homodecameric structure. In order to purify GCH1, the recombinant protein was cloned with only a N-termini Strep tag and a TEV cleavable sequence for post-purification removal as the enzyme's N-termini has been shown to play a role in the interaction with GFRP. GFRP was purified in the same fashion as its C-terminal peptide is also buried within its core. High salt concentration was required to stabilize the enzyme, and precipitation occurred if the enzyme was diluted with large amounts of glycerol. Several tests were performed in order to characterize the enzyme. GCH1 was tested alone and in the presence of 10eq of GFRP (Fig 33 left). The observed reaction rates were similar with and without GFRP, as reported. In order to assess the interaction of GFRP with GCH1, Phe was added in large excess. An increase of

roughly 1.5x in the reaction rate was observed similar to the reported value. Finally, temperature was increased from 25 to 37°C. Catalysis was reported to be performed faster at higher temperature as it could be observed in our case. The systems in place, the candidates were tested on GCH1 only. EBS was the only molecule impacting GCH1 reaction rate (Fig 33 right). The IC50 was found to be 4.7 μM but, as previously seen with SPR, the hill curve was steep and inhibition went from off to on. It could not be excluded that enzyme precipitation occurred at the highest concentrations even though it could not be visually confirmed.

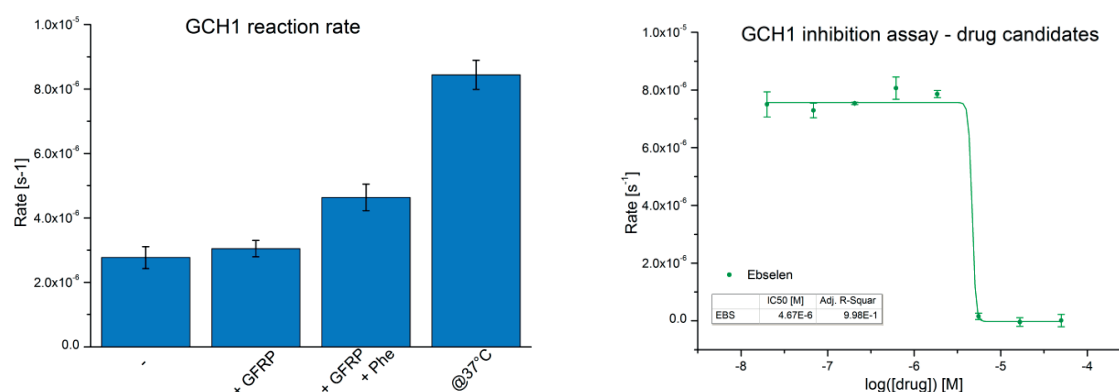


**Fig 33 GCH1 enzymatic assay and inhibition.** Reaction rates for GCH1 were compared in different conditions. GCH1 was tested alone, with additional GFRP and Phe as well as when temperature was changed (left). GCH1 alone was assayed against the drugs candidates and only EBS seemed to inhibit it. Each point is the average of 3 measurement ± SD.

Concerning the effects of EBS in-vitro, particularly with SPR and GCH1, they are the only enzyme tested possessing Cys residues close to their active site or being catalytically active. EBS has also been reported to be a Cys modifier indicating that the drug probably reacts with SPR and GCH1 by covalently modifying their Cys residues. In addition DHFR and DHPR do not possess a Cys residue close to their active site. EBS had no inhibitory effect on DHFR and the inhibition curves seen for DHPR, both in the enzymatic assay and during the FRET experiments, having regular Hill curves, point towards a non-covalent inhibition.

Overall, the drug candidates were tested on a selected set of enzymes part of the BH4 metabolic pathway. It was observed that TRI is an inhibitor of DHFR as well as DHPR. It was expected, during later

tests on cells that its effect would be similar to MTX or APT. EBS, as an inhibitor of both GCH1 and SPR as well as DHPR, was expected to present large variability in both the total amount of pterins as well as a change in the BH4 to BH2 ratio. DCS and ADR as specific DHPR inhibitors were expected to only shift the pterin balance towards an increase of oxidized biopterins. Furthermore, no tests were performed on PTPS, PCD and GCH1 + GFRP. Therefore, an effect, from the drugs, on the interaction between GCH1 and GFRP is unknown. In addition, it might be observed, during *in-vivo* experiments, a decrease in BH4 by drugs not inhibiting SPR. In this situation, it would be only an assumption to postulate that PTPS is inhibited. In case of PCD inhibition, since the dehydration of 4HTP occurs non-enzymatically, a significant change in total pterin levels or on the pterin balance was not expected. Finally, the candidates were later assayed on a cellular model in order to confirm these hypotheses.

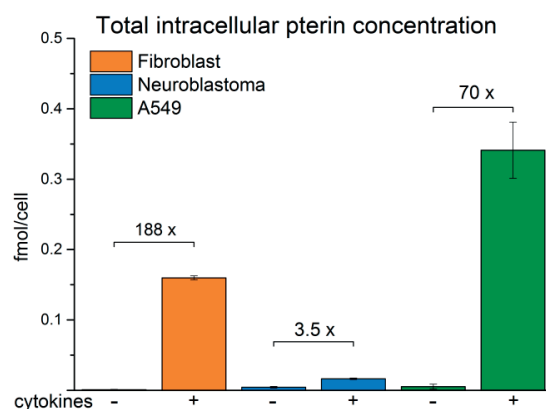


**Fig 34 Total intracellular pterin concentration.** The cultivated cells total pterin concentration was assayed for three lines (Fibroblast, Neuroblastoma and A549) with and without 100 ng/ml TNF- $\alpha$  and INF- $\gamma$ . The increase is indicated on top of the bars for each line. Each point is the average of 3 measurement  $\pm$  SD.

## 2.3.2 In-Vivo Characterization

### 2.3.2.1 Controls and Method Development

In order to test the drugs candidate *in-vivo*, a cellular model had to be chosen. Several cell lines were cultivated with cytokines for 24 h and total pterin amount was then quantified by HPLC coupled to fluorescence and electrochemical detection (see material and methods).

Human umbilical vascular endothelial cells (HUVECS) are a satisfactory choice when it comes to BH4 intracellular levels activations. This cell line has shown good applicability in terms of quantification of pterins and were used in several studies on the tetrahydrobiopterin network<sup>80,240</sup>. However on the practical level HUVECS are difficult to cultivate, expensive to maintain and proliferate relatively slowly. All attempts to cultivate them for a satisfactory period failed in our hands.

The human adult dermal fibroblast (FIB) is known to produce large amounts of BH4 when stimulated with the cytokines INF-g and TNF-a (Fig 34, 188-fold), and has, as well, been used as model in numbers of publications on BH4 and its derivatives<sup>119,212</sup>. Furthermore, knowledge and data on the model had already been acquired in house. In addition, FIB have strong contact inhibition, an advantageous feature which allows for similar numbers of confluent cell population on plates and relatively convenient storage and handling. Finally, their proliferation rate is relatively fast and the media inexpensive.

The neuroblastoma model has constitutive expression of the enzymes involved in the BH4 and 5HW biosynthesis, the precursor of serotonin. Therefore, they do not need to be activated but produce much less total amount of pterin. Increase of pterin concentration can be obtained upon cytokine activation but the increment is relatively small compared to the other model cell lines (3.5x vs. 188x).

The epithelial lung carcinoma model A549 was also tested as it was used in house for other applications. Interestingly, upon activation this model produces the largest absolute amounts of pterin. However, A549 has not, to our knowledge, been extensively used in research on BH4. Furthermore, control tests on metabolic pterin imbalance were mitigated, indicating this model was not the most suitable for our assay. Finally, the FIB model was selected to investigate the potential effects of our drug candidates.



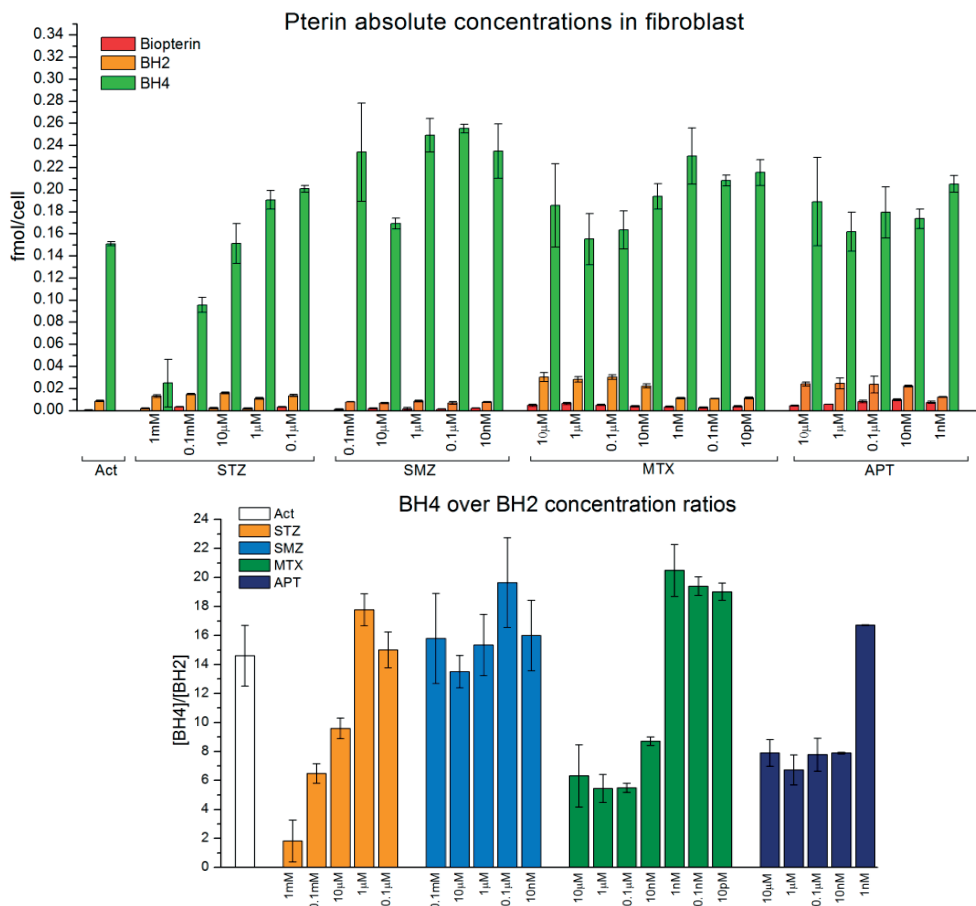


**Fig 35 Influence of drugs on pterin intracellular concentrations in FIB.** Several controls were assayed on FIB in order to assess the effect from drugs inhibiting a specific set of enzymes. The absolute pterin concentrations are plotted in the top graph while the ratio BH4/BH2 was plotted in the lower graph. STZ, a known SPR inhibitor, showed a decrease only in BH4 concentration. SMZ, usually a weak SPR inhibitor was used as negative control. No significant change in biopterin levels was observed. MTX and APT were used as DHFR and DHPR inhibitor. A slight decrease in BH4 was observed for MTX and an increase in BH2 was observed for both MTX and APT. Each point is the average of 3 measurement  $\pm$  SD.

The effect of drugs models, on the total pterin levels and balance, was first investigated. Drugs known to decrease only BH4 or to increase BH2 were tested on the selected cell line. Sulfathiazole (STZ) and sulfamethazine (SMZ) are two drugs known to inhibit respectively strongly and weakly SPR<sup>119</sup>. They were shown *in-vitro* to have IC50 at respectively 14 nM and 16  $\mu$ M. Moreover, a roughly four fold decrease in *in-vivo* BH4 production was reported upon addition of 0.1 mM STZ along with an increase in neopterin concentration indicating drug permeability towards the cell membrane. However, neither BH4 concentration decrease and neopterin increase was reported with SMZ indicating SPR inhibition was not obtained. Consequently, these two drugs were selected as positive and negative controls in order to

assess changes in absolute BH4 concentration. MTX and APT are known to inhibit *in-vitro* DHFR and DHPR and to be permeable to cell membranes<sup>124</sup>. The inhibition potentials are for MTX  $K_{i(\text{hDHFR})} = 2.3 \text{ nM}$ ;  $K_{i(\text{DHPR})} = 32 \text{ }\mu\text{M}$  and APT  $K_{i(\text{hDHFR})} = 1 \text{ nM}$ ;  $K_{i(\text{DHPR})} = 20 \text{ }\mu\text{M}$ . These two compounds were therefore selected as controls to assess increase in BH2 and change in the [BH4]/[BH2] ratio.

Each of the drugs was applied on FIB at different concentration and pterin levels were quantified after 24 h by HPLC coupled to fluorescence and electrochemical detection (see material and methods). Generally, when no drug was added, BH4 concentration was predominantly higher than BH2 and biopterin (Fig 35). Total pterin levels at low drug concentration were in each tested experiment significantly higher compared to the drug-free setup. As predicted, BH4 levels in the case of STZ, decreased in a dose dependent manner with a maximal ten fold decrease compared to the lowest drug concentration. The obtained IC50 for this titration was roughly 160  $\mu\text{M}$ , a value ten fold higher than the reported one. Over the whole titration, BH2 levels were also higher than in the drug free case. Overall, steady BH4 and BH2 concentrations were observed for SMZ indicating the drug inability to strongly inhibit SPR.

A dose dependent increase in BH2 concentration was observed upon both MTX and APT titration. However, a BH4 concentration decrease upon MTX increase could also be observed at 1  $\mu\text{M}$ . This change in BH4 concentration was unexpected as only enzymes responsible for the recycling and salvage of BH4 should be affected. However, in the case of APT no BH4 decrease was observed and the BH2 levels started decreasing at similar concentration than MTX. In both MTX and APT experiments biopterin levels were slightly higher compared to cases involving other compounds.

Finally, spiked samples injected at the first and last run consistently showed a partial transformation of BH2 to biopterin. BH4 and total amount of pterin however remained stable over the nine hours of analysis usually performed. Therefore, in all experiments, the pterin [BH4]/[BH2] ratio was compared to

the  $\frac{[BH_4]}{([BH_2] + [biopterin])}$  ratio in order to ensure no significant value discrepancy. The observed ratios were never significantly impacted by a degradation of BH<sub>2</sub>. It was also shown that the half-life of BH<sub>2</sub> degradation in the presence of 6.5 mM DTT and TCA is  $\sim 5 \text{ h}^{11}$ . Furthermore, maximal sample residence time at room temperature was of 2.25 h minimizing potential BH<sub>2</sub> conversion the solutions being stored at -80 °C. Additionally, the samples were spiked with 1  $\mu\text{M}$  pterins, a quantity largely higher than the value measured endogenously. At such concentration BH<sub>2</sub> might degrade faster.

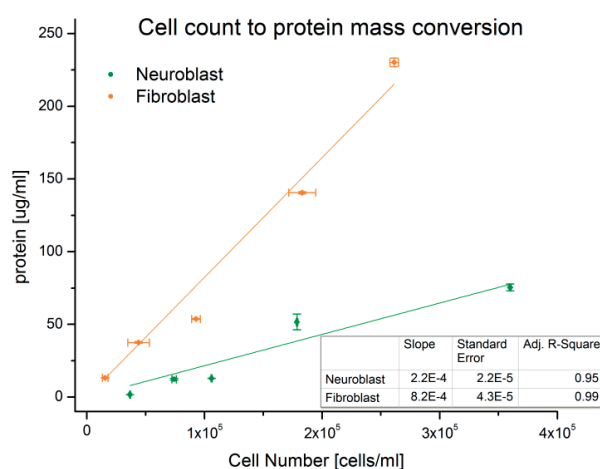


**Fig 36 Conversion from number of cells per ml to protein concentration.** A conversion scale on two models, neuroblastoma and FIB was performed. Each point is the average of 3 measurement  $\pm$  SD.

Generally, literature reports metabolite concentration in cells as nmol/mg of protein therefore a conversion scale was made in order to transform the units of fmol/cell (Fig 36). A value of  $8.2\text{E-}7 \pm 4.3\text{E-}8 \text{ mg/cell}$  was found, converting total pterin content in the order of 0.1 to 0.3 nmol/mg of protein. These values were lower but close to the reported values of 0.3 to 0.4 nmol/mg of protein in the case of fibroblasts. Total protein amount per cell was also measured for the neuroblastoma model as a comparison. A value of  $2.2\text{E-}07 \pm 2.2\text{E-}8 \text{ mg/cell}$ , coherent with the fact that this cellular model is smaller than FIB, was found.

In summary, the applied method allowed for quantification of pterins. FIB showed to be the most favorable cell line for assays on pterin metabolism. Indeed, they were shown to generate large amounts of endogenous pterins upon incubation with cytokines. Total pterin concentration was generally variable between each run and standard deviation on absolute values was rather high. Pterin ratios were usually reproducible and effects upon drug addition visible. It was seen that spiked BH2 had a tendency to oxidize to biopterin after long periods of incubation in the lysis buffer while BH4 and total pterin concentration stayed stable. This effect was negligible on authentic samples as the incubation time and BH2 concentration was much lower. Pterin levels were modified according to the drug incubated. BH4 decreased in the presence of STZ, BH2 increased in presence of with MTX and ATP and pterin levels remained unchanged with SMZ. The [BH4]/[BH2] ratio decreased in a dose dependent fashion for both MTX and STZ. The most dramatic ratio decrease for MTX was influenced by the BH2 increase while STZ was only influenced by the relatively large BH4 decrease. This observation was consistent with the drug mechanism of action. SMZ ratios stayed generally similar to those observed in the drug free case, consistent with the lack of BH4 concentration changes observed. Additionally, total pterin concentrations were found to be similar to what had been reported<sup>119</sup>. Furthermore, the IC50 found for STZ here was higher to what had been reported<sup>119</sup> due predominantly to the difference in cell type used and the detection method.

### ***2.3.2.2 Drug Candidates Assay***

The four drug candidates were applied at different concentration on FIB and incubated for 24h. TRI showed to be toxic at concentration of 100  $\mu$ M and above, which can be explained by the impairments in causes on DNA metabolism. A report showed that 80  $\mu$ M TRI was enough to cause dissolution of human lymphoma cells<sup>241</sup>. Cells were usually detached and deformed at such concentrations while 50  $\mu$ M seemed to have no significant deleterious effects. Trypan blue assay showed good cell survival and cell shape was similar to cells in the drug free condition. TRI induced a strong dose

dependent BH2 increase similar to levels observed in the case of MTX and APT. At 50  $\mu\text{M}$  BH4 concentration decreased at concentration similar to BH2 (Fig 37). This decrease was unexpected and might be linked either to unspecific effects on the *de-novo* BH4 synthesis or potentially as an indication of toxicity even though the cells were still alive. In the most extreme case the  $[\text{BH}_4]/[\text{BH}_2]$  ratio was found to be equal to unity whereas the lowest ratio observed for MTX was roughly six.

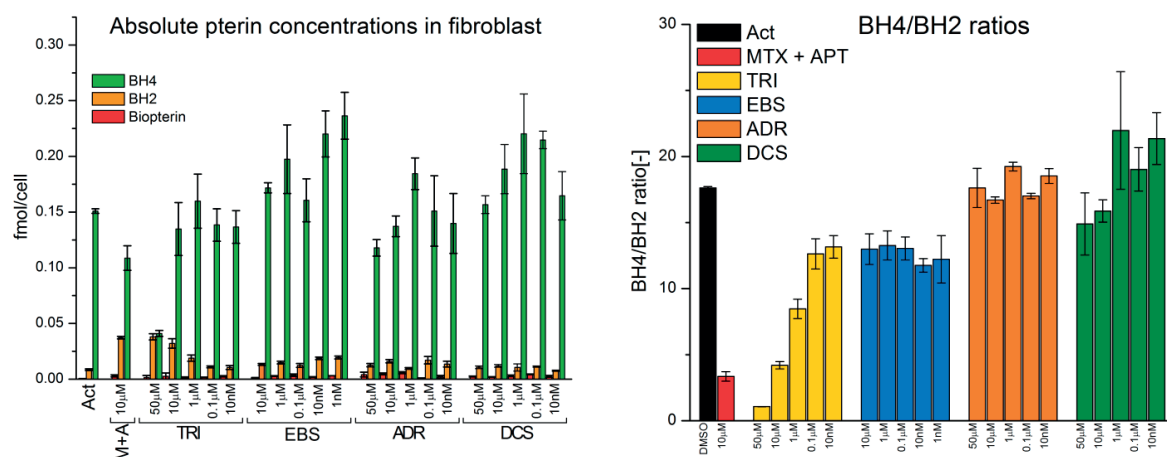


**Fig 37 Influence of drugs candidates on pterin intracellular concentrations in FIB.** An increase of BH2 takes place in a dose dependent fashion in the case of TRI. BH4 decreases only significantly at 50  $\mu\text{M}$ . The ratio  $\text{BH}_4/\text{BH}_2$  was plotted on the right. Each point is the average of 3 measurement  $\pm$  SD.

EBS showed to be toxic at concentrations above 10  $\mu\text{M}$ . At 50  $\mu\text{M}$  cells were still attached but usually broke into fragments when trypsin was applied. Pterin concentrations were not showing a significant change upon titration, more clearly reflected by the steady ratios obtained.

ADR and DCS had no notable cell toxicity at 50  $\mu\text{M}$ . This maximal drug concentration was chosen for ADR and DCS in order to be comparable with TRI. Neither of the compounds could alter pterin concentrations or ratios. Generally, biopterin was not affected by any of the drugs concentration and remained constant within all experiments. It was notable that ratios and total pterin concentration varied between analysis rounds as seen previously in the method setup. As pairs EBS and TRI did not have the same total amount of pterin with respect to ADR and DCS at their lowest concentration. Finally, the only compound showing potential in generating metabolic pterin imbalance was TRI.

## **2.4 Discussion on the Discovered Compounds**

Interest was initially put on the development of tool compounds for the inhibition of DHPR and study of administered drugs side effects that could be linked to the BH4 metabolic network. Here, the results obtained with each of the four candidate drugs are discussed and a description of their mechanisms of action or usage is provided.

### **2.4.1 On Triamterene**

#### **2.4.1.1 Mechanisms of Action**

Triamterene is a diuretic agent used for the treatment hypertension and edema<sup>242</sup>. Mechanistically, TRI blocks Na<sup>+</sup> reabsorption and lowers K<sup>+</sup> secretion. It acts on the renal transport of sodium by blocking, in the renal collecting tubules, the Na<sup>+</sup> channels. TRI also inhibits the nephrotrophic effect of aldosterone. Classically, when taken alone, 50-300 mg/day of TRI is ingested. Fifty to sixty percent of it is bound to plasma proteins and is as well rapidly metabolized. It has been reported that only 3% of the drug was excreted unchanged. Furthermore, TRI is often administered with hydrochlorothiazide an antihypertensive agent. Hydrochlorothiazide is a sulfa drug, but has not been, to our knowledge, reported as a SPR inhibitor. It does however possess similar structural features as reported sulfa drug derived SPR inhibitors.

#### **2.4.1.2 Relevance**

To our knowledge, TRI has never been reported as a DHPR inhibitor. As presented, the drug is the best DHPR inhibitor *in-vitro*. *In-vivo*, data show maximal pterin imbalance was observed in the presence of TRI. The BH4/BH2 ratio observed at 50  $\mu$ M was roughly 1, a value that is lower than the lowest ratio observed in the case of MTX and APT. However, TRI is not strictly selective to DHPR and part of its potency might be due to its effect on DHFR as well. The fact that TRI has a better potency on DHPR than MTX and APT *in-vitro* might explain lower obtained ratio value. Generation of such pterin imbalance

is of interest when studying oxidative stress in cellular models. At such low ratio, NOS becomes uncoupled and oxidative stress ensues. However, in mammalian models, at safe dosages, maximal intracellular and plasma concentration are expected to be low. Furthermore, the fast metabolization decreases as well total TRI amount. Therefore, it is not expected for TRI to have significant effects on the BH4 metabolic pathway. It would be of interest to study the effects of other bicyclic polyaza diuretics on members of the BH4 metabolic network as they might prove to be inhibitors.

## 2.4.2 On Ebselen

### 2.4.2.1 Mechanisms of Action

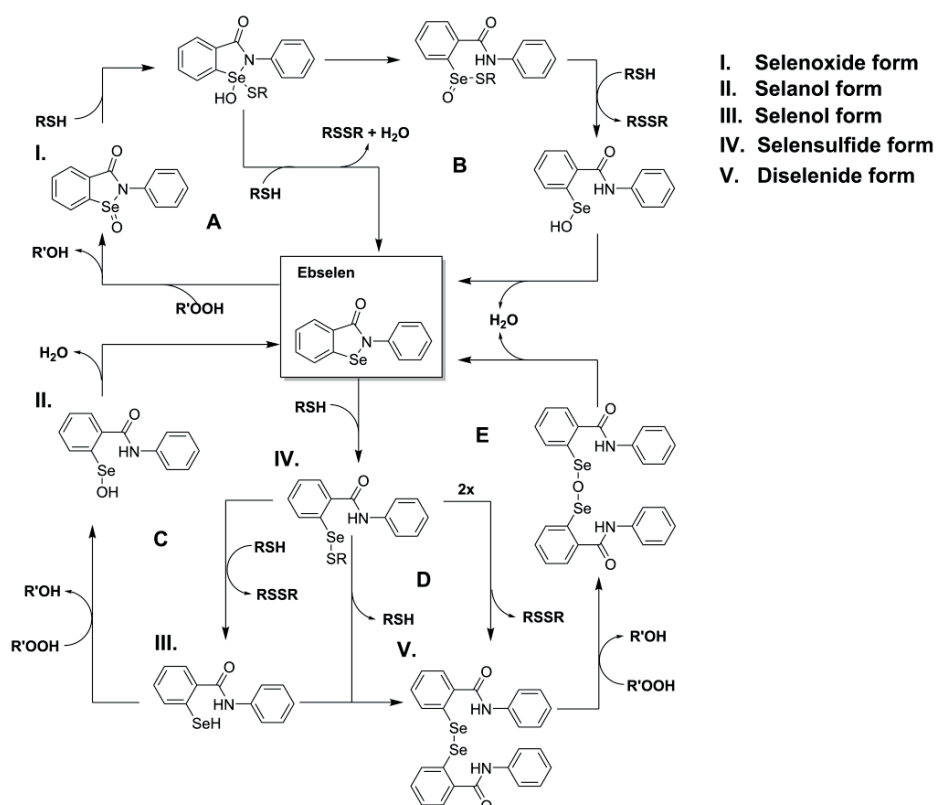


**Fig 38 EBS catalytic mechanism.** EBS peroxidase-like activity takes place via two different cycles. Cycles A & B by first reacting with and hydroperoxy, cycles C, D & E by first reacting with a thiol.

Ebselen (EBS) was first described as a seleno-organic compound with glutathione peroxidase-like (GSH Px-like) and antioxidant activity<sup>243</sup>. GSH Px, a selenocysteine bearing enzyme, was shown to be able to catalyze the degradation of several types of hydroperoxides and showed to be a potent defense against oxidative challenges. EBS performances *in vitro* as a GSH Px analogue were demonstrated with H<sub>2</sub>O<sub>2</sub>, t-butyl hydroperoxide and to a larger extent hydroperoxy-lipids in the presence of GSH, GSSG reductase and NADPH<sup>244</sup>. No activity was observed in absence of GSH. In addition, EBS has the ability to react with various other thiols such as DTT, N-acetyl-L-cysteine, dihydrolipoate. Later on, EBS propensity as being a moderate free radical and singlet oxygen quencher as well as a potent peroxynitrite scavenger was demonstrated<sup>245,246,247</sup>. Model experiments indicated that the drug could protect liposomes, microsomes and some organs against oxidative stress<sup>248</sup>. Furthermore, low toxicity in animals was observed owing to the lack of selenium bioavailability<sup>249</sup> and almost complete binding to serum albumin (90%)<sup>250</sup>. Therefore, organoselenium drugs could be of clinical interest in diseases involving oxidative stress.

Mechanistically, EBS mediated conversion of peroxides is complicated and not yet fully characterized (Fig 38). Some of the presented pathway could be favored *in-vivo* due to concentrations of thiols and peroxides differing from *in-vitro* experiments. Two main reaction paths were proposed initiated (Fig 38 top) via peroxide selenium oxidation or via the thiol adduct (Fig 38 bottom). Peroxide initiation was proposed to proceed with (cycle B) and without (cycle A) ring opening. When thiol is in excess, the reaction can process via a mix of selenol and selenulfide form (cycle D) or via the reaction of two selenulfide forming a diselenide (cycle E)<sup>251</sup>. In addition, high reactivity of selenol towards peroxides closes the cycle via the selenol intermediate (cycle C). In classical peroxidase experiments selenol was shown to be the dominant form proceeding to EBS formation via cycle C. Finally, such versatile chemical interconversions might be beneficent to EBS metabolic stability.



EBS was also shown to be an inhibitor of enzymes involved in inflammation such as NOS, protein kinase C, NADPH oxidase, lipoxygenases and H<sup>+</sup>/K<sup>+</sup>-ATPase. Furthermore, numbers of reports have shown how organic diselenides could inhibit enzyme bearing thiols vicinal to their active site<sup>252</sup>. Additionally, it was shown that EBS toxicity in mice is related to its administration means and probably owing to depletion of said endogenous thiols-bearing enzymes. EBS has been shown to be an anti-inflammatory agent in numbers of animal studies. The action mechanism is believed to be linked to an attenuation of peroxynitrite accumulation, or inhibition of certain pro-inflammatory lipoxygenases. Another effect of EBS administration is antinociceptive action. The drug was also tested for its effect on neuropathic and inflammatory pain. As example, BH4 level decrease and nitrosative stress has been observed in plasma of nephropathic type II diabetic rats, concomitant with previously described metabolic pterin imbalance and oxidative stress phenotypes<sup>253</sup>. At 22 weeks, sclerosis, proteinuria nitro-tyrosinated proteins and decreased renal levels of BH4 and an increase in BH2 were observed, a phenomenon absent in lean rats. EBS admission was shown to decrease BH2 and increase BH4 to near absolute basal levels but leave qBH2 as roughly 20% of total pterin content<sup>254</sup>. A study on the effects of EBS in acute ischemic stroke in adults showed the drug potency to slightly improve the stroke outcome. As ROS have been shown to play a role in permanent brain damage due to ischemia it was correctly postulated that EBS could be of clinical value<sup>255</sup>. Further evidence confirming EBS role as oxidative and nitrosative stress regulator has been gathered in numbers of animal model studies<sup>256</sup>.

#### **2.4.2.2 Relevance**

As mentioned previously EBS is a cysteine modifier and reacts with protein thiols. It therefore not surprising that *in-vitro* effects can be observed on several enzymes. GCH1 and SPR both possess Cys located close to the active site or needed to perform catalysis. However, no reduction of total pterin was observed *in-cellulo*. As seen for SPR and GCH1 *in-vitro*, 10 μM EBS should totally inhibit the enzyme activities. DHPR showed to be a target in both the FRET and the enzymatic assays indicating it could be a

true target. DHPR only possesses Cys that are either buried or far from any binding pocket. Furthermore, it is not surprising to see no effect on cellular assay. Reports indicate that EBS can bind to proteins such as serum albumin, be transferred in the cells and detach in the cytosol or to be transferred to other proteins<sup>250,257</sup>. However, as EBS is expected to be mostly bound to albumin, it can be expected that a large part of the added compound is not free to access the cells. Additionally, the maximal possible viable drug concentration tested of 10  $\mu\text{M}$  is not significantly higher than the  $K_i$ . Also no experiment measuring the internal cell concentration was performed therefore no conclusions can be drawn on a potential accumulation of the drug.

### ***2.4.3 On Adrenosterone and Deoxycorticosterone***

ADR is a steroid hormone produced by the adrenal cortex. As endogenous molecule, it possesses androgenic potential. ADR is commonly taken as a dietary supplement for athletes willing to drastically increase their muscular weights and fat loss<sup>258</sup>. Classically, oral dosage of such compound, for cosmetic concerns, is ranging from 0.3 to 0.9 g/day over periods of 5 to 9 weeks<sup>259</sup>. DCS is, when administered, a neuroactive steroid acting as a sedative-hypnotic agent. It inhibits the CNS excitability by interacting with  $\gamma$ -aminobutyric acid (GABA) receptors<sup>260</sup>. Endogenously, DCS is a biosynthetic precursor of corticosterone.

To our knowledge, the sterane motif has never been reported to have direct interaction with enzymes from the BH4 metabolic network. Indeed GCH1 on the transcriptional level has been reported to be impacted by estradiol<sup>82</sup> but no competitive inhibition has ever been reported, for any of the remaining enzymes. It is unexpected for endogenous steroid hormones to affect the BH4 metabolic pathway and especially not DHPR as their concentration in the cytosol is in the nM range. Classically, membrane permeability coefficient for steroid hormones is low ( $10^{-4}$  cm/s)<sup>261</sup>. It was reported that steroids are generally protein and membrane bound and that the free compound percentage was a maximum of

4%<sup>262</sup>. In the presented case fetal bovine serum composed 10% of the medium. This represents roughly 50  $\mu\text{M}$  of protein concentration in the culture medium<sup>263</sup>, equal to the maximal concentration of added drug. It is expected for ADR and DCS to have been principally accumulated at the cellular membrane or to proteins part of the culture medium. Therefore, concentration of the molecules in the cytosol is expected to be low. Consequently DHPR inhibition shall not have taken place even at larger concentration than 50  $\mu\text{M}$  since the IC50 is in the 10<sup>th</sup> of  $\mu\text{M}$ .



## **Chapter 3. Conclusion**

### **3.1 Achievements**

Based on a pipeline established in this work, a semisynthetic FRET sensor for investigating the interaction of DHPR with small molecules was developed. The pipeline consisted of increasing molecular and proteic scaffold complexity by adding elements to the system and testing the effect of each of these modifications. This approach allowed to quickly troubleshoot the development and guided the rational design of the sensor. Computational modeling was as well performed to shed light on structural clues further reinforcing planning towards a successful system. Once the sensor operational, a high throughput screen was performed in order to discover DHPR binders. Thirteen molecules were shown to interact with the enzyme. The four most potent compounds, TRI, EBS, ADR and DCS were selected for further investigation. Each of the candidates was assayed in enzymatic assays against DHPR, DHFR, SPR and GCH1. It was shown that TRI was the most potent inhibitor against DHPR but was also active against DHFR. EBS was disrupting catalytic activity of enzymes possessing Cys residues close to their active sites. ADR and DCS were selective towards DHPR. Later, a method was set up for the quantification of pterins in mammalian cells. It was possible via reversed phase HPLC coupled to fluorescence and electrochemical detection to separate and quantify biopterin, BH2, pterin, neopterin, xanthopterin and BH4. The drug candidates were incubated with cytokine activated FIB in order to study their effects on metabolic pterin balance. Biopterin, BH2 and BH4 levels were quantified and the ratio  $[BH4]/[BH2]$  was calculated. It was observed that only TRI induced a significant effect on the pterin balance oppositely to other drug candidates. It was hypothesized that the pterin imbalance, generated by incubation with TRI, is significant enough, in the case of cells, to produce partial NOS uncoupling. Such feature can be of interest in the study of cellular oxidative stress. However, TRI is not expected to have effect on vertebrate BH4 metabolic network since most of the drug is quickly metabolized.

### **3.2 Future Development**

The method used for pterin quantification did not focus on the quantification of qBH2. The quantification of the molecule could be of interest to picture the percentage of oxidized pterin generated by DHPR with respect to DHFR. A method has been reported to satisfy this requirement, could be included in the detection but would double the analysis time and diminish the overall detection sensitivity<sup>264</sup>. Furthermore, addition of an internal standard would ameliorate the reproducibility of the obtained results. Some synthetic pterin such as 6MPH4 or 6,7MPH4 could have been used.

The structural sterone motif appeared multiple times as selective inhibitor for DHPR. Development of more potent sterone derived DHPR inhibitors could be performed by structure activity relationship. This suggestion might be of interest for *in-vitro* studies. The inherent poor ability of sterones to cross the membrane will make development of cell permeable and potent candidates a challenge. Furthermore, it cannot be excluded that such molecules would in the process interact with nuclear receptors leading to unwanted side effects.

EBS, even though it did not influence the metabolic pterin imbalance in cells, could be further studied in rodent models. Indeed, several mechanistic features are of interest with respect to oxidative and nitrosative stress. In the case of neuropathic pain, quantification of nitro-peroxides and pterin balance could be of interest. EBS, in the case of vitiligo, could be a candidate for diminishing H<sub>2</sub>O<sub>2</sub> and potentially restoring pigmentation. Topical administration of EBS with thiols could reverse skin depigmentation locally. Unfortunately, this hypothesis seems incorrect as a study shown that 20 mM EBS applied topically promotes dermal depigmentation<sup>265</sup>. Furthermore, there is potentially a way for EBS to rescue BH4 oxidation. A control of interest would have been to test EBS in conjugation to TRI. BH4/BH2 ratios could potentially increase shedding light on EBS mechanism.

## **Chapter 4. Material and Methods**

### **4.1 General Methods**

#### **4.1.1 Cloning**

All the engineered plasmids were designed using the software Geneious. Gene sequences were ligated together using the Gibson Assembly method. The vectors used were based on pET-51b(+) (Novagen). PCR amplifications were carried using New England Biolab Q5 Hot Start High-Fidelity DNA Polymerase. Transformation was carried in Lucigen E. cloni 10G electrocompetent cells. The clones were sequenced using Sanger Sequencing proposed by GATC-biotech ([www.gatc-biotech.com](http://www.gatc-biotech.com)). Primers were synthesized by Microsynth AG ([www.microsynth.ch](http://www.microsynth.ch)) and were ordered as 100 ng/μl solutions.

#### **4.1.2 Protein Expression**

BL21(DE3) cells (New England Biolab) were transformed with purified plasmids by electroporation. Bacterial cultures were grown at 37°C in 100 ml auto-inducible terrific broth supplemented with 25 mM ammonium sulfate, 2 mM magnesium chloride, 0.2% lactose and 0.05% glucose for 5 hours followed by 17h at 25°C. The cells were harvested by centrifugation, the obtained pellet was lysed by sonication. The debris and insoluble parts were discarded after centrifugation. The proteins of interest were purified by Ni-NTA (Machery Nagel) and Strep-Tactin (iba) chromatography following the provided protocols. Purity was assessed by electrophoresis on polyacrylamide gels. Quantification of protein concentration was performed by absorbance measurement at 280 nm. The extinction coefficients were estimated using Geneious' statistics tool.

#### **4.1.3 Protein Labeling**

4 μM of self-labeling protein was allowed to react for 90 minutes at room temperature with 8 μM of its corresponding TMR-conjugated tag. The reaction was performed in 400 μl Tris-HCl 40 mM, pH 7.4, 0.5

mg/ml BSA buffer. The proteins were purified from the excess tag by centrifugal filter. The obtained concentrated solution was washed four times with Tris-Cl 40 mM, pH 7.4 to ensure total removal of the excess tag. The protein concentration, in the resulting solution, was measured on the TMR absorbance. Control of labeling efficiency was performed by adding a dye of different color (BG-Alexa488 and Halo-Alexa488) to a purified labeled sample. The quantification was performed by running the samples on polyacrylamide gels. (See appendix protein gels and yields)

## **4.2 Enzymatic Assays**

If not explicitly specified, the buffer used in all the enzymatic assays was Tris-Cl 40 mM, pH 7.4, 0.5 mg/ml BSA and the temperature was 22°C. All assays were performed in a transparent Greiner 96-well plate and measured with a Tecan Infinite M1000 spectrophotometer.  $K_i$  was calculated for DHFR and DHPR based on the equation (eq 1)

$$K_i = \frac{IC_{50}}{1 + \frac{[S]}{K_m}} \quad (\text{eq 1})$$

Where  $IC_{50}$  is the concentration at half inhibition,  $[S]$  is the substrate concentration,  $K_M$  is the Michaelis-Menten constant. This approximation is only valid in the case of competitive inhibition<sup>266</sup>.

### **4.2.1 DHPR Cytochrome-c Based Assay**

DHPR enzymatic activity was assayed following Arai et. al. method<sup>267</sup>. The enzymatic conversion of qBH2 to BH4 is followed by the quick reduction of FICC to FOCC by BH4. FICC reduction is followed by reading the increasing FOCC absorbance signal at 550nm. The experiment is run for 40 minutes and recorded at 10 seconds intervals in 200  $\mu$ l buffer containing 50  $\mu$ M FICC, 1  $\mu$ M 6MPH4, 20 nM DHPR, 50  $\mu$ M NADH and selected inhibitor concentration. A control lacking DHPR is ran in parallel to assess the rate of non-enzymatic reduction of qBH2 by NADH. The extinction coefficient used for FOCC and NADH



are respectively 29500 (reduced, 550 nm, H<sub>2</sub>O) and 6220 (340 nm, H<sub>2</sub>O) L·mol<sup>-1</sup>·cm<sup>-1</sup>. Generally, 50 μM of FOCC and FICC in buffer are measured in isolated wells to assess reaction completion.

#### **4.2.2 DHFR Assay**

The enzymatic conversion of dihydrofolate (FH<sub>2</sub>) to tetrahydrofolate (FH<sub>4</sub>) is followed by the resulting decrease in signal at 284 nm. The experiment is run for 30 minutes and recorded at 10 seconds intervals in 200 μl buffer containing 50 nM DHFR, 100 μM FH<sub>2</sub>, 300 μM NADPH and selected inhibitor concentration. A control lacking DHFR is ran in parallel. The extinction coefficients used for FH<sub>2</sub> and NADPH are respectively 28000 (284 nm, H<sub>2</sub>O pH 12) and 6220 (340 nm, H<sub>2</sub>O) L·mol<sup>-1</sup>·cm<sup>-1</sup>.

#### **4.2.3 SPR Assay**

The enzymatic conversion of sepiapterin to BH<sub>2</sub> is followed by the resulting decrease in signal at 420 nm. The experiment is run for 30 minutes and recorded at 10 seconds intervals in 200 μl buffer containing 50 nM SPR, 100 μM sepiapterin, 300 μM NADPH and selected inhibitor concentration. A control lacking SPR is ran in parallel. The extinction coefficient used for sepiapterin is 10400 L·mol<sup>-1</sup>·cm<sup>-1</sup> (420 nm, H<sub>2</sub>O).

#### **4.2.4 GCH1 Assay**

The assay was adapted from Hussein et al.<sup>72</sup>. The buffer was 100 μM Tris-Cl, 100 μM NaCl, pH 7.3. Reaction was ran with 0.25 μM GCH1, 100 μM GTP and selected inhibitor concentration. When added, [GFRP] = 2.5 μM & Phe = 100 μM. Total reaction volume was 200 μl. Reaction rate was followed by appearance of the H<sub>2</sub>NTP at 340 nm. The experiment was run for 60 min and recorded as 10 s intervals. The extinction coefficient used for GTP was 14200 L·mol<sup>-1</sup>·cm<sup>-1</sup> (252 nm, H<sub>2</sub>O pH 7).

### 4.3 Fluorescence Polarization

FP assays are performed in a black opaque Greiner 96 half-well volume, non-binding, plate using the Envision 2103 Multilabel Reader. The assay was run at 50 nM labeled enzyme concentration in a total volume of 40ul. The buffer used was Tris-Cl 40 mM, pH 7.4, 0.5 mg/ml BSA and measurement was performed at 22°C. The filters are used according to the dye emission and excitation characteristics.

### 4.4 High Throughput Screen

The DHPR-[4:]HALO-pro30-SNAP sensor labeled with Sir-Halo and BG-EG<sub>5</sub>-TMR-(CH<sub>2</sub>)<sub>6</sub>-APT (L5) was screened against the Prestwick library (1280 compounds). Screening took place at the Biomolecular Screening Facility in EPFL. The plates used were black opaque Greiner 96 half-well volume and read with Tecan Infinite F500 (excitation 520 nm, emission 667 nm). Z' factor<sup>263</sup> determination was calculated following equation 2 with 96 positive and 96 negative control measurements homogeneously spread on two plates.

$$Z' = 1 - \frac{3(dev_{pos} + dev_{neg})}{ABS(avg_{pos} - avg_{neg})} \quad (\text{eq 2})$$

Where *dev* is the standard deviation, *ABS* is the absolute value and *avg* is the average. Z values between 0.5 and 1 denote an excellent assay. The negative control was 40 µl Tris-Cl 40 mM, pH 7.4, 0.5 mg/ml BSA, 200 µM NADH, 50 nM sensor. 200 µM APT was supplemented to the previous solution for the positive control. 80 compounds at 10 µM were tested per plate. The compounds were kept as 100 mM DMSO stocks and were diluted to 10 µM working concentration. 16 wells were used for positive and negative controls. Each plate was made in duplicate. The obtained hits, defined as a compound inducing FRET change more than 3x the standard deviation of the positive control measurement, were tested a second time and confirmed against a different control: DHPR-[4:]HALO-pro30-SNAP labeled with Sir-Halo and BG-EG<sub>11</sub>-TMR-COOH (L11C) . A titration curve for each confirmed hit was performed in triplicate between 100 µM and 0.78 µM.

## **4.5 Cell Culture**

Adult human dermal FIB were purchased from Lonza. Human neuroblastoma (SK-N-BE(2)) and A549 were purchased from ATCC. The aliquots were thawed at 37°C directly after reception and were transferred in a 75 cm<sup>2</sup> plate containing for FIB and A549 25 ml, 37°C DMEM Glutamax + 10% heat inactivated FBS (all from Gibco) and for the neuroblastoma 25 ml DMEM/F-12, Glutamax + 10% heat inactivated FBS (all from Gibco). Cells were cultivated as a main seed plate in 75 cm<sup>2</sup> plates (TPP) and at each passage cells were split 10 times. Prior to analysis cells were cultivated in 6well plates (9.8 cm<sup>2</sup> / well) in 2 ml of their respective medium.

## **4.6 HPLC Fluorescence and Electrochemical Detection**

The analytical setup consisted of the Shimazu Prominence system coupled to a Thermo Scientific Ultimate 3000 RS electrochemical detector (Fig 39 A). The whole system was controlled using Chromeleon 7.2 with Shimadzu drivers for Chromeleon. HPLC running buffer was prepared as follows: A mQ water solution of 6.5 mM NaH<sub>2</sub>PO<sub>4</sub>, 6 mM Citric acid, 1 mM sodium octyl sulfate (OSA), 1.5 mM diethylenetriaminepentaacetic acid was prepared and brought to pH 3.0 and 3.5% v/v ACN was added. The solution was flown circularly during 48 h at 2 ml/min over two 5011 ESA electrochemical cells set at 1 V & 100 µA in order to oxidize all contaminants. To this solution DTT was added to 1 mM prior usage. The HPLC run was conducted in isocratic mode over a 4.6x150 mm Waters Atlantis dC18, 3 µm column protected with Vanguard cartridges at 1.6 ml/min. The column was thermostated at 30°C and injection volume was 50 µl. The column allowed separation of several types of pterins. Biopterin, BH<sub>2</sub>, BH<sub>4</sub>, xanthopterin, neopterin and pterin were all separated to baseline. Furthermore, a clear conversion of BH<sub>2</sub> to biopterin took place upon passage in the electrochemical detector (Fig 39 B). The shoulders observed in Fig 39 B were later corrected using ThermoFisher Viper Fingertight fitting to obtain small width symmetrical peaks (Fig 39 C). Fluorescence was recorded with the excitation wavelength set at 350 nm and the emission wavelength set at 450 nm. Detector sensitivity and gain were set to medium and

4x. The two dual channel 5011A electrochemical cells were set at 450, 600, 800 & 1000 mV with automatic current parameterization. Determination for the oxidation voltage of BH4 was confirmed by performing an hydrodynamic voltage curve. Biopterin, BH2 and BH4 retention times were compared with authentic samples (Schirks Laboratory) (Fig 39 B,C). Biopterin was quantified via fluorescence; BH2 was converted post-column via electrochemical oxidation (800 mV) to biopterin and quantified via fluorescence. Finally, BH4 was quantified on the 450 mV electrochemical detector channel. Detection limit of BH2 and biopterin was 1 nM being linear at least up to 1  $\mu$ M. Detection limit of BH4 was 40 nM being linear at least up to 10  $\mu$ M. Samples are usually run as batches of 9 aliquots while the next batch is kept at -80°C in order to preserve the samples from oxidation.

#### **4.7 Pterin Quantification**

Pterin quantification was made by means of HPLC coupled to electrochemical and fluorescence detection. The protocol was adapted from Biondi et al.<sup>10</sup>, Howells et al.<sup>214</sup> and Fismen<sup>218</sup> et al. FIB were cultivated in 6 well plates (9.8 cm<sup>2</sup>) until reaching 50% confluence. Medium was removed and replaced with 1 ml fresh medium supplemented with 100 ng/ml recombinant human interferon- $\gamma$  (INF-g, R&D Systems Europe Ltd), 100 ng/ml recombinant human tumor necrosis factor- $\alpha$  (TNF-a, Sigma Aldrich) and drugs of interest (triamterene, ebselen, aminopterin, methotrexate, adrenosterone, deoxycorticosterone, sulfatiazole and sulfametazine). Cells were incubated for 24 h. Medium was removed and wells were washed with 1 ml PBS without Ca<sup>2+</sup> and Mg<sup>2+</sup> (Lonza). Cells were detached with 300  $\mu$ l trypsin (Sigma), collected, and the remaining cells were collected by addition of 700  $\mu$ l PBS per well. The cells were quantified using Scepter Cell Counter (Millipore), 60  $\mu$ m sensor and gating from 13 to 31  $\mu$ m. The collected cells were pelleted by centrifugation (2.5 min, 2500 RCF, 4°C) and the supernatant was discarded. The pellet was washed and centrifuged (2.5 min, 2500 RCF, 4°C) once with 150  $\mu$ l ice cold of 50 mM Tris-Cl, 1 mM DTT, pH 7.4. Cells were lysed using 90  $\mu$ l of ice cold 200 mM trichloroacetic acid, 40 mM ascorbic acid, 1 mM EDTA, 5 mM DTT. The solution was sonicated for 10

seconds in a sonication bath to dissolve the cell pellet before being centrifuged (10 min, 20000 RCF, 4 °C). The supernatant was transferred to HPCL analysis vials and 50 µl were injected.

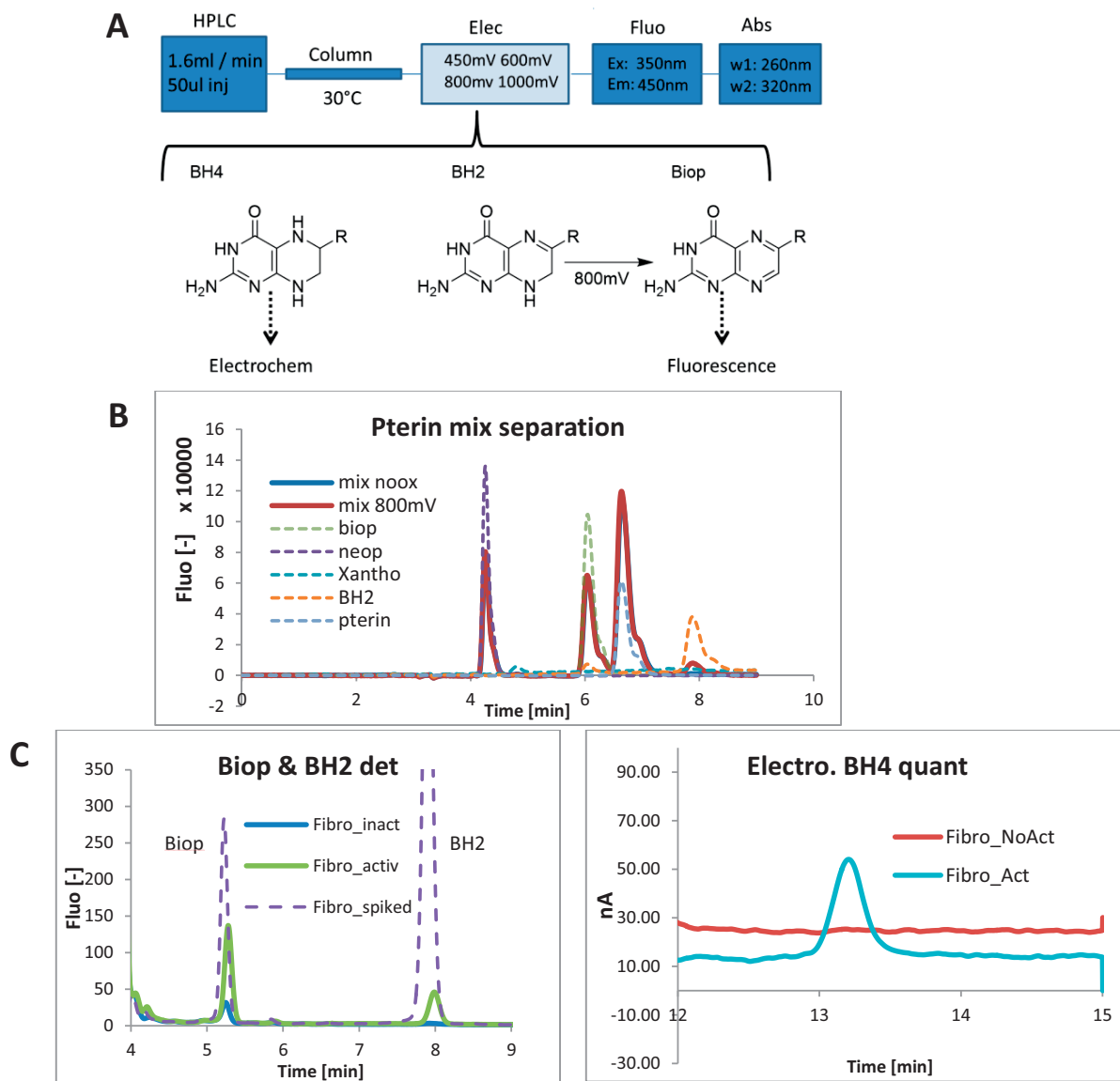


**Fig 39 Pterin quantification method based on HPLC coupled to fluorescence and electrochemical detection. (A)** Schematic view of the process. The HPLC is run in isocratic mode at 1.6 ml/min and 50 µl of sample is injected. The column is thermostated to 30 °C and the four analytical cells on the electrochemical detector is set to 450, 600, 800 and 1000 mV. On the fluorescence detector the excitation and emission wavelengths are set to 350 nm and 450 nm, respectively. Two wavelengths for the absorbance are set to 260 and 320 nm. BH4 is detected on the analytical cell at 450 mV. Biopterin is detected by fluorescence. BH2 is oxidized by the analytical cell to biopterin at 800 mV and detected by fluorescence (B) Separation of a solution in water of 5 pterins. Biopterin (biop), neopterin (neop), xanthopterin (Xantho) BH2 and pterin were injected separately and separated as a mixture with and without electrical potential applied. (C) Cell lysis sample (left) Biopterin and BH2 are detected by fluorescence and BH4 is detected (right) by electrochemical detection at 450 mV.

Routinely, 24 samples are run in a day and a sample spiked with Biopterin, BH2 and BH4 is run at the first and last daily injection to control for potential degradation. The column is then flushed with decreasing polarity solvents with 10 volumes of ACN, 10 vol. 80:20 MeOH:ACN, 20 vol 10:90 MeOH:DCM and reversed back to ACN. This ensures removal of hydrophobic cell lysate residues and keeps reproducibility in retention times.

#### ***4.8 In-Silico Docking***

The in-silico docking of qBH2 in DHPR was performed with the AutoDock Vina algorithm (<http://vina.scripps.edu>). qBH2 and MTX were drawn in 2D using ChemDraw 15.0 and then converted to 3D objects in \*.pdb format using Chem3D (<http://www.cambridgesoft.com>). \*.pdb molecule structures were optimized using OpenBabel (<http://openbabel.org>) and the force field algorithm Ghemical. DHPR (pdb: 1HDR) was prepared as lock using MGLTools (<http://mgltools.scripps.edu>). Water molecules on the structure were removed and polar hydrogen atoms were added. The modified DHPR structure was saved as \*.pdbqt files, an enhanced \*.pdb format taking into account bond flexibility, atom polarity and charge. Using MGLTools all rotational and rigid bonds within the small molecules were defined. The structures were saved as \*.pdbqt as well. The search space box was defined around DHPR's active site using MGLTools enclosing all vital residues as well as NADH. The configuration file was written as presented on the official website and calculations were performed on a desktop computer (Intel(R) Core(TM) i5-2550K CPU @ 3.40 GHz (4 CPUs), ~3.4 GHz, 8192 MB RAM, AMD Radeon HD 6450) running under Linux Mint 17.1. Results were visualized using PyMOL (<https://pymol.org/>)

#### ***4.9 Unnatural Amino Acids Incorporation***

The used method was adapted from the Lemke<sup>236</sup> and Chin<sup>225</sup> groups. Two plasmids were used. The pEvolv-pyIRS/AF plasmid was carrying the modified tRNA/synthetase pair while the pBAD carried the gene of interest. Modification of DHPR Glu 46 in pET-51b(+) plasmids was performed by point mutation

with a NEB Q5 Site-Directed Mutagenesis Kit Quick Protocol (E0554) to insert an Amber stop codon. The gene of interest was afterwards cloned into pBAD. The transformed cells were 50  $\mu$ l of DH10B cells transformed with 5 ng of pEvol-pyIRS/AF (Chloramphenicol (CMP) resistance) and 5 ng of pBAD (Ampicillin (AMP) resistance). Pre-culture was performed adding 500  $\mu$ l transformed bacteria to 3 ml LB medium containing 50  $\mu$ g/ml AMP and 25  $\mu$ g/ml CMP at 37 °C overnight. The pre-culture (1 ml) was added to 30 mL TB medium with AMP (50  $\mu$ g/ml) CMP (25  $\mu$ g/ml) and incubated at 37°C. When culture reached OD = 0.4, 2 ml freshly prepared 1 mM BCN-lysine was added. Culture was induced with 0.2% arabinose at OD = 0.6. After 5 h incubation at 37 °C the cells were centrifuged at 4000 g, 15 min, 4 °C. Purification was performed as previously explained. No BCN-lysine click-coupling was performed as no protein was obtained.

#### ***4.10 Protein content per Cell***

Cells were cultivated upon confluence in a 75 cm<sup>2</sup> plate and detached. The plate content was transferred in a 12 ml tube and centrifuged (1000 g, 5 min, 4 °C). The supernatant was discarded, the pellet suspended with 2 ml PBS to be centrifuged again (1000 g, 5 min, 4 °C). This operation was repeated 3x to remove all protein and amino acids content. The pellet was suspended in 2 ml PBS and a 2x dilution series was performed. Cell count was measured with Scepter Cell Counter (Millipore), 60  $\mu$ m sensor and grating from 13 to 31  $\mu$ m and 6 to 20  $\mu$ m for FIB and Neuroblastoma respectively. Cell count was performed in triplicate. Protein concentration was measured using the bicinchoninic acid (BCA) protein assay (AppliChem). 10  $\mu$ l of sample was added to 190  $\mu$ l of BCA solution. A 3x BSA dilution standard starting at 1.5 mg/ml was used as reference. The samples were incubated 30 min at 37 °C. The assay was performed in a transparent Greiner 96-well plate and absorbance measured at 560 nm with a Tecan Infinite M1000 spectrophotometer.

	Dilution step	D1	D2	D3	D4	D5
<b>FIB</b>	Cell count [-]	261205	183064	92701	43939	15533
	Cell count deviation	3640.962	11527.17	3701.147	9078.252	2488.685
	Protein concentration [ $\mu\text{g/ml}$ ]	230.1759	140.5078	53.75903	37.51295	13.09721
	Protein concentration dev	2.960035	0.74614	0.422329	0.489173	0.1421
<b>Neuroblast.</b>	Cell count [-]	359779	178542	106043	74144	36687
	Cell count deviation	840.0389	639.85	493.1453	1756.162	467.4495
	Protein concentration [ $\mu\text{g/ml}$ ]	75.40909	51.70722	12.79547	12.27656	1.673821
	Protein concentration dev	2.357113	5.382547	0.054777	0.540845	0.015922

**Table 8 Conversion table from cells to protein content in FIB and neuroblastoma.** For each cell concentration 3 measurements were made and total resulting protein concentration was calculated by means of BCA assay.

### 4.11 Chemical Synthesis

**Reaction conditions** All reactions were carried in oven dried glassware at room temperature. All Fmoc-NH-EG<sub>n</sub>-COOH (8, 15, 21) were purchased (PurePEG). APT (3) was purchased from TCL and N-1-Fmoc-1,6-diaminohexane (4) was purchased from Fluorochem. Anhydrous DMSO was from Acros. Purchased chemicals and solvents were purchased from Sigma-Aldrich, Fisher Scientific, Merck, Alfa Aesar or Acros and were not analyzed or further purified before usage.

**Purification** Reaction mixtures were purified by reverse-phase preparative HPLC (HPLC-prep) on a Dionex system equipped with an UltiMate 3000 pump and an UV D170U UV-Vis detector for product visualization on a Waters SunFire Prep C18 OBD 5  $\mu\text{m}$  19 $\times$ 150 mm column. Typical gradient was H<sub>2</sub>O/ACN 90:10 to 0:100 in 30 minutes at 4 ml/min. Fractions were automatically collected using Dionex UltiMate 3000 fraction collector. The system was operated by the Chromeleon 6.8 software.

**Lyophilization** Solutions of ACN and water were frozen in liquid nitrogen and placed in round bottom flasks. The flask was connected to an alpha 1-2 LD plus lyophilizer connected to a Vacubrand RC6 pump and a gaz trap and left to sublime overnight.

**NMR analysis** Proton NMR spectra were recorded at room temperature on a Bruker Avance-III 400 or on a Bruker DRX-600 equipped with a cryoprobe, with chemical shifts ( $\delta$ ) reported in ppm relative to



the solvent residual signals. DMSO-d<sub>6</sub>: δH 2.5 ppm; CD<sub>3</sub>OD: δH 3.31 ppm. Coupling constants are reported in Hz.

**Routine compound analysis:** Reaction progress and compound purity was assessed by LC-MS on a Nexera X2 Shimadzu system. The mass spectrometer was a LCMS 2020 module and both systems were connected via a FCN 20AH2 valve. Compounds were separated on a Waters Aquity UPLC BEH C18 50X2.1 mm column preceded by a Waters Vanguard cartridge. Typical gradient was H<sub>2</sub>O/ACN 90:10 to 0:100 within 6 minutes at 0.5 ml/min. Compounds were analyzed in positive mode. Hardware was operated via Shimadzu LabSolution software.

#### ***4.11.1 General Procedures***

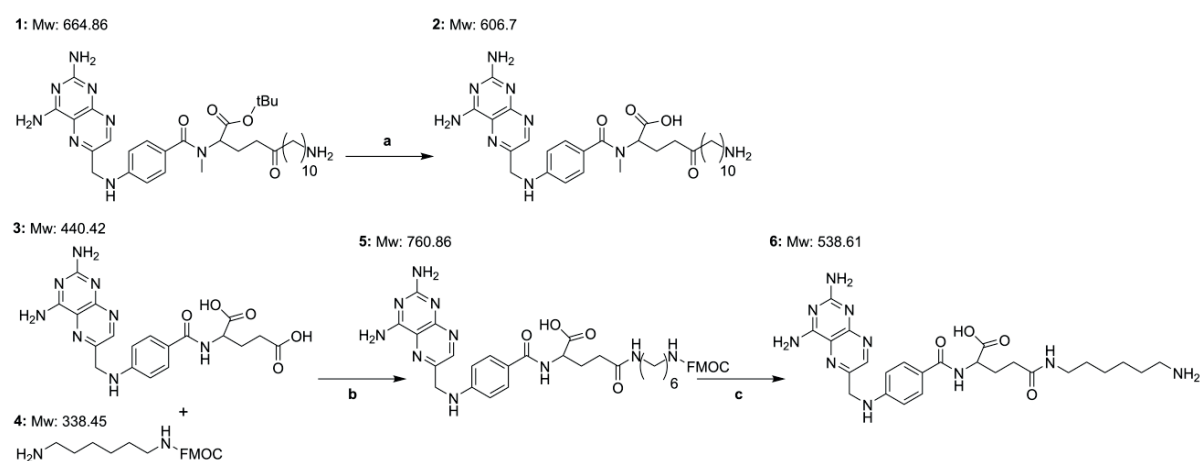
**Amide bond formation** Amide bond formation was performed first by activation of the respective carboxylic acid with N,N-diisopropylethylamine (DIPEA) and O-(N-succinimidyl)-N,N,N,N'-tetramethyluronium tetrafluoroborate (TSTU) in dry DMSO. Routinely, were prepared as separate DMSO solutions: (i) 50 mM to 100 mM carboxylic acid starting material with 10 eq DIPEA; (ii) 0.1 mg/ml TSTU and (iii) 0.1 mg/ml amine bearing compound. A volume of TSTU solution corresponding to 1eq is added to the reaction mixture and stirred. Carboxylic acid activation was followed by LC-MS by looking for a compound of additional 98 g/mol with respect to the starting material. A volume of amine bearing solution corresponding to 1.1 eq is added to the activated reaction mixture and stirred further. The coupling was followed by LC-MS until completion. The reaction mixture was quenched by the addition of 1 volume of water and 12 equivalent of AcOH. The reaction mixture was purified by HPLC-prep. The fractions were collected, combined and lyophilized overnight.

**Fmoc deprotection** Dry compounds were dissolved in DMF to 50 to 100 mM. 20% v/v of piperidine was added and the reaction mixture was stirred. The deprotection was followed by LC-MS until completion. 1 volume of water and 2 equivalent of AcOH are added to precipitate the 1-((9H-fluoren-9-

yl)methyl)piperidine. The solution is centrifuged for 3 minutes at 20000 rpm and the supernatant is collected. The collected supernatant is purified by HPLC-prep and lyophilized.

**Tert-butyl and methyl deprotection** The dry product is dissolved in a solution of 1:1 water MeOH as a 50 mM solution. 20% V/V of 1 M aq NaOH is added and the reaction mixture is stirred. The reaction is followed by LC-MS until completion. 2 equivalent of AcOH are added. The product is purified by HPLC-prep and lyophilized as previously explained.

#### 4.11.2 MTX and APT Derivatives

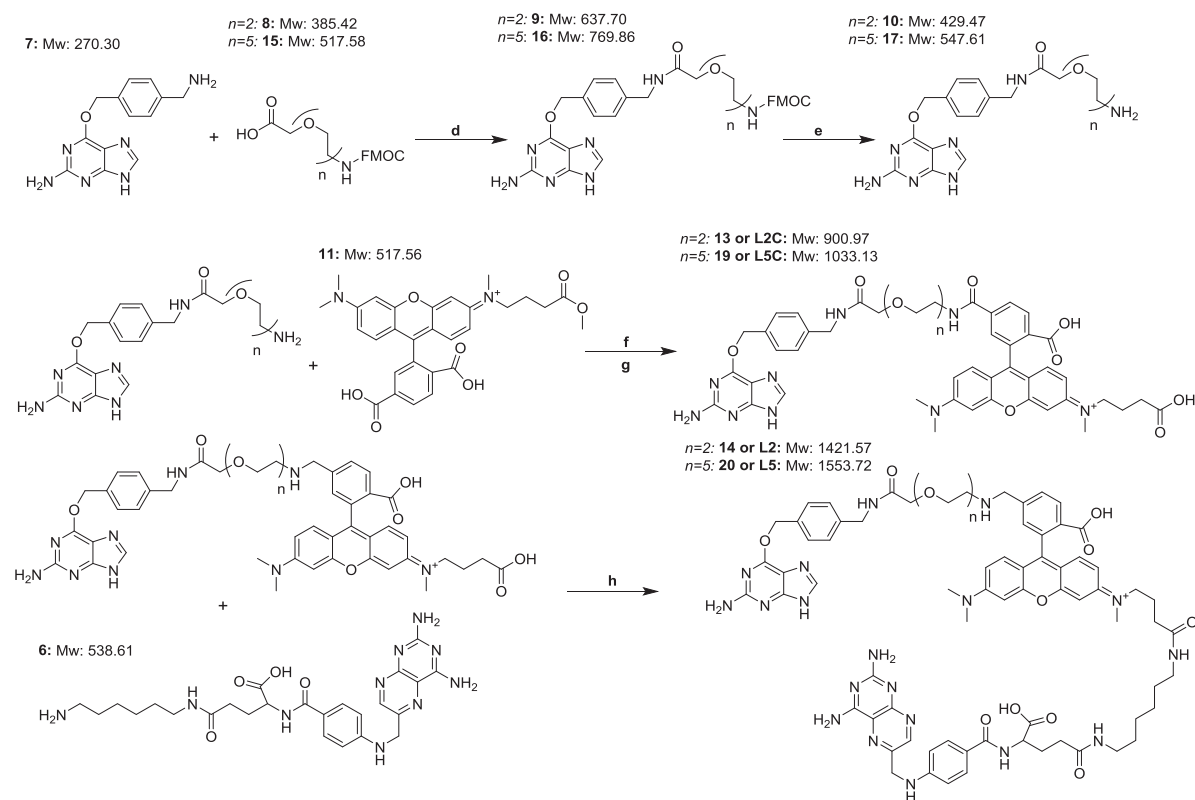


**Synthesis of MXT-(CH<sub>2</sub>)<sub>10</sub>-NH<sub>2</sub> (2)** tBu protected MXT-(CH<sub>2</sub>)<sub>10</sub>-NH<sub>2</sub> (1) was a gift from Dr. Stefan Pitsch. Purity of 1 was assessed by LC-MS before usage. The compound (17 mg, 25.6 μmol) was deprotected according to the tert-butyl deprotection procedure (a). The resulting MXT-(CH<sub>2</sub>)<sub>10</sub>-NH<sub>2</sub> (2, 82%, 12.4 mg) was analyzed by mass spectrometry and NMR. <sup>1</sup>H NMR (400 MHz, DMSO-d<sub>6</sub>) δ 12.50 (s, 1H), 9.23 (s, 1H), 9.02 (s, 1H), 8.72 (s, 1H), 8.54 (s, 1H), 8.31 (d, J = 7.5 Hz, 1H), 8.00 (s, 1H), 7.86 – 7.70 (m, 3H), 6.87 – 6.80 (m, 2H), 4.88 (s, 2H), 4.29 (ddd, J = 9.5, 7.4, 4.8 Hz, 1H), 3.26 (s, 3H), 3.01 (q, J = 6.6 Hz, 2H), 2.84 – 2.71 (m, 2H), 2.55 (s, 1H), 2.19 (t, J = 7.8 Hz, 2H), 2.13 – 2.00 (m, 1H), 1.92 (ddt, J = 13.9, 9.2, 7.2 Hz, 1H), 1.51 (p, J = 7.3 Hz, 2H), 1.37 (s, 1H), 1.24 (d, J = 13.2 Hz, 14H). HDMS (ESI): 609.3617 m/z, exp Em: 608.3547 m/z

**Synthesis of APT-(CH<sub>2</sub>)<sub>6</sub>-NH<sub>2</sub> (6)** APT (3, 14 mg, 31.8 μmol) and NH<sub>2</sub>-(CH<sub>2</sub>)<sub>6</sub>-NH-FMOC (4, 10.7 mg, 31.8 μmol) were coupled according to the amide bond formation procedure (b) to yield APT-(CH<sub>2</sub>)<sub>6</sub>-NH-FMOC (5, 65%, 15.7 mg, 20.6 μmol). The purity was assessed by LC-MS and no further analysis was performed. yield APT-(CH<sub>2</sub>)<sub>6</sub>-NH-FMOC (5, 15.7 mg, 20.6 μmol) FMOC protecting group was removed via the FMOC deprotection procedure (c) to yield APT-(CH<sub>2</sub>)<sub>6</sub>-NH<sub>2</sub> (6, 97%, 10.8 mg, 20 μmol). The compound was analyzed by mass spectrometry and NMR. <sup>1</sup>H NMR (600 MHz, DMSO-d<sub>6</sub>) δ 13.15 (s, 1H), 12.36 (s, 1H), 9.17 (s, 2H), 8.83 (s, 1H), 7.86 (t, J = 5.7 Hz, 1H), 7.73 (d, J = 8.4 Hz, 2H), 6.75 (d, J = 8.3 Hz, 2H), 4.61 (s, 2H), 4.38 – 4.26 (m, 1H), 3.05 – 3.00 (m, 2H), 2.77 (t, J = 6.8 Hz, 3H), 2.19 (s, 1H), 1.92 (h, J = 7.1, 6.1 Hz, 1H), 1.52 (dp, J = 22.1, 7.7, 6.7 Hz, 3H), 1.37 (dd, J = 14.4, 7.0 Hz, 3H), 1.26 (ddt, J = 20.2, 14.2, 6.5 Hz, 7H). HDMS (ESI): 539.2839 m/z, exp Em: 538.2764 m/z

### 4.11.3 Linkers and Control Linkers

#### Synthesis of BG-EG<sub>2</sub>-TMR-C<sub>6</sub>-APT and BG-EG<sub>5</sub>-TMR-C<sub>6</sub>-APT



**Synthesis of BG-EG<sub>2</sub>-NH<sub>2</sub> (10):** BG (7) was a gift from Dr. Luc Reymond and purity was analyzed by LC-MS before usage. NH<sub>2</sub>-EG<sub>2</sub>-NH-FMOC (8, 4.39 mg, 11  $\mu$ mol) and BG (7, 3 mg, 11  $\mu$ mol) were coupled according to the amide bond formation procedure (d). BG-EG<sub>2</sub>-NH-FMOC (9, 91%, 6.4 mg, 10.1  $\mu$ mol) was recovered and deprotected according to the Fmoc deprotection procedure (e). BG-EG<sub>2</sub>-NH<sub>2</sub> (10, 98%, 9.9  $\mu$ mol) was recovered and analyzed. BG-EG<sub>2</sub>-NH<sub>2</sub> NMR 1H NMR (600 MHz, DMSO-d<sub>6</sub>)  $\delta$  8.35 (t, J = 6.2 Hz, 1H), 8.27 (s, 1H), 7.49 (d, J = 8.0 Hz, 2H), 7.30 (d, J = 7.9 Hz, 2H), 5.51 (s, 2H), 4.33 (d, J = 6.2 Hz, 2H), 3.97 (s, 2H), 3.59 (t, J = 5.3 Hz, 4H), 2.97 (h, J = 5.6 Hz, 2H). MS (ESI) : 416.1 m/z (M<sup>+1</sup>)

**Synthesis of BG-EG<sub>2</sub>-TMR-COOH (13):** TMR (11) was a gift from Dr. Lin Xue and was analyzed by NMR and LC-MS. TMR (11, 4.6 mg, 8.8  $\mu$ mol) and BG-EG<sub>2</sub>-NH<sub>2</sub> (10, 4.1 mg, 9.77  $\mu$ mol) were coupled according to the amide bond formation procedure (f). BG-EG<sub>2</sub>-TMR-COOME (12, 60%, 4.7 mg, 5.2  $\mu$ mol) was

recovered and deprotected according to the methyl deprotection procedure (g). BG-EG<sub>2</sub>-TMR-COOH (13, quantitative, 5.1 μmol) was recovered and analyzed. Half of the quantity was kept as control ligand for later experiments. TMR (11) 1H NMR (400 MHz, Methanol-d<sub>4</sub>) δ 8.47 – 8.36 (m, 2H), 8.00 (d, J = 1.5 Hz, 1H), 7.16 (dd, J = 9.5, 2.0 Hz, 2H), 7.13 – 6.99 (m, 3H), 6.97 (d, J = 2.4 Hz, 1H), 3.70 (s, 1H), 3.68 (s, 4H), 3.31 (s, 6H), 3.28 (s, 3H), 2.47 (t, J = 6.8 Hz, 2H), 1.99 (p, J = 7.0 Hz, 2H). BG-EG<sub>2</sub>-TMR-COOH (13) 1H NMR (600 MHz, DMSO-d<sub>6</sub>) δ 8.37 – 8.10 (m, 4H), 7.89 (s, 1H), 7.45 (d, J = 7.7 Hz, 2H), 7.26 (d, J = 7.7 Hz, 2H), 7.15 – 6.90 (m, 6H), 5.46 (s, 2H), 4.27 (d, J = 6.2 Hz, 2H), 3.64 (d, J = 8.7 Hz, 2H), 3.54 (t, J = 6.0 Hz, 3H), 3.43 (d, J = 5.7 Hz, 1H), 3.00 (d, J = 1.3 Hz, 1H), 2.45 (s, 3H), 2.34 (s, 1H), 2.19 (s, 1H), 1.82 (s, 2H). HDMS (ESI): 900.3675 m/z, exp Em: 900.3681 m/z

**Synthesis of BG-EG<sub>2</sub>-TMR-(CH<sub>2</sub>)<sub>6</sub>-APT (14):** BG-EG<sub>2</sub>-TMR-COOH (13, 2.3 mg, 2.6 μmol) and APT-(CH<sub>2</sub>)<sub>6</sub>-NH<sub>2</sub> (7, 1.5 mg, 2.8 μmol) were coupled according to the amide bond formation procedure (h). BG-EG<sub>2</sub>-TMR-(CH<sub>2</sub>)<sub>6</sub>-APT (14, 12%, 0.5 mg, 0.4 μmol) was recovered and analyzed. BG-EG<sub>2</sub>-TMR-(CH<sub>2</sub>)<sub>6</sub>-APT 1H NMR (600 MHz, DMSO-d<sub>6</sub>) 8.91 – 8.78 (m, 2H), 8.31 – 8.23 (m, 3H), 7.88 (s, 1H), 7.73 (d, J = 8.3 Hz, 2H), 7.45 (d, J = 7.8 Hz, 2H), 7.26 (d, J = 7.7 Hz, 2H), 7.12 – 6.99 (m, 5H), 6.96 (d, J = 8.6 Hz, 1H), 6.75 (d, J = 8.3 Hz, 2H), 5.46 (s, 2H), 4.62 (s, 2H), 4.40 – 4.32 (m, 1H), 4.27 (d, J = 6.2 Hz, 2H), 3.91 (s, 2H), 3.56 (d, J = 27.3 Hz, 8H), 3.24 (d, J = 21.8 Hz, 11H), 3.01 (dq, J = 19.9, 6.9 Hz, 4H), 2.39 (t, 2H), 2.17 (dd, J = 12.2, 6.8 Hz, 4H), 1.87 – 1.77 (m, 2H), 1.41 – 1.30 (m, 4H), 1.29 – 1.15 (m, 4H). HDMS (ESI): 1420.6340 m/z, exp Em: 1420.6339 m/z

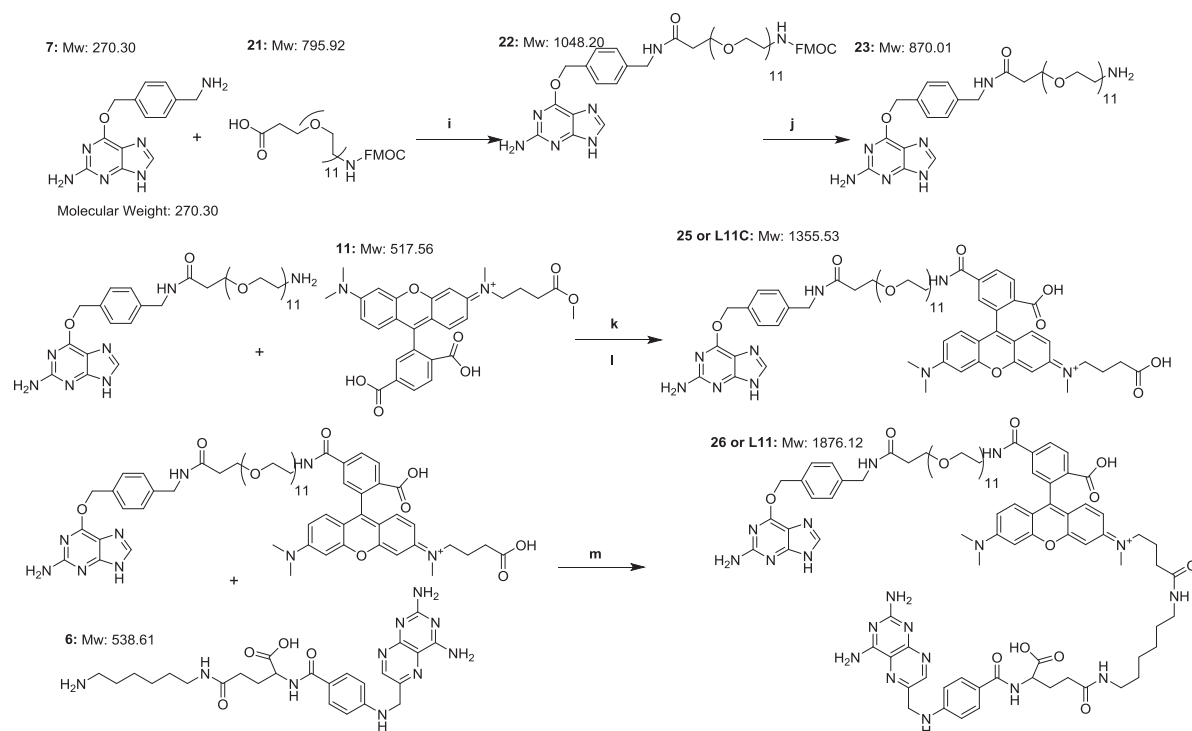
**Synthesis of BG-EG<sub>5</sub>-NH<sub>2</sub> (17):** NH<sub>2</sub>-EG<sub>5</sub>-NH-FMOC (15, 5.74 mg, 11 μmol) and BG (7, 3 mg, 11 μmol) were coupled according to the amide bond formation procedure (d). BG-EG<sub>5</sub>-NH-FMOC (16, 91%, 5.8 mg, 10.1 μmol) was recovered and deprotected according to the Fmoc deprotection procedure (e). BG-EG<sub>5</sub>-NH<sub>2</sub> (17, quantitative, 10 μmol) was recovered and analyzed by NMR. BG-EG<sub>5</sub>-NH<sub>2</sub> 1H NMR (600 MHz, DMSO-d<sub>6</sub>) δ 8.32 (t, J = 6.2 Hz, 1H), 8.20 (s, 1H), 7.51 – 7.46 (m, 2H), 7.30 (d, J = 8.1 Hz, 2H), 5.50 (s, 2H), 4.33 (d,

J = 6.2 Hz, 2H), 3.96 (s, 2H), 3.64 – 3.54 (m, 14H), 3.56 – 3.46 (m, 4H), 2.98 (p, J = 5.6 Hz, 2H), 2.61 – 2.52 (m, 2H). MS (ESI): 548.2 m/z ( $M^{+1}$ )

**Synthesis of BG-EG<sub>5</sub>-TMR-COOH (13):** TMR (11, 3 mg, 5.8  $\mu$ mol) and BG-EG<sub>5</sub>-NH<sub>2</sub> (10, 3.5 mg, 6.3  $\mu$ mol) were coupled according to the amide bond formation procedure (f). BG-EG<sub>5</sub>-TMR-COOMe (12, 86%, 4.5 mg, 5  $\mu$ mol) was recovered and deprotected according to the methyl deprotection procedure (g). BG-EG<sub>5</sub>-TMR-COOH (13, quantitative, 5  $\mu$ mol) was recovered and analyzed. Roughly half of the quantity was kept as control ligand for later experiments (L5C). BG-EG<sub>5</sub>-TMR-COOH (13) <sup>1</sup>H NMR (600 MHz, DMSO-d<sub>6</sub>)  $\delta$  8.87 (t, J = 5.7 Hz, 1H), 8.36 – 8.21 (m, 3H), 7.92 – 7.86 (m, 1H), 7.47 (d, J = 7.9 Hz, 2H), 7.28 (d, J = 7.9 Hz, 2H), 7.17 – 6.98 (m, 5H), 6.96 (d, J = 2.3 Hz, 1H), 5.48 (s, 2H), 4.31 (d, J = 6.3 Hz, 2H), 3.93 (s, 2H), 3.62 (s, 7H), 3.58 (s, 15H), 3.27 (s, 6H), 3.24 (s, 3H), 2.34 (t, J = 7.1 Hz, 2H), 1.83 (q, J = 7.5 Hz, 2H). HDMS (ESI): 1032.4463 m/z, exp Em : 1032.4467 m/z

**Synthesis of BG-EG<sub>5</sub>-TMR-(CH<sub>2</sub>)<sub>6</sub>-APT (14, L5):** BG-EG<sub>5</sub>-TMR-COOH (13, 1.8mg, 2 $\mu$ mol) and APT-(CH<sub>2</sub>)<sub>6</sub>-NH<sub>2</sub> (7, 1.2 mg, 2.2  $\mu$ mol) were coupled according to the amide bond formation procedure (h). BG-EG<sub>5</sub>-TMR-(CH<sub>2</sub>)<sub>6</sub>-APT (14, 32%, 1 mg, 0.6  $\mu$ mol) was recovered and analyzed. BG-EG<sub>5</sub>-TMR-(CH<sub>2</sub>)<sub>6</sub>-APT <sup>1</sup>H NMR (600 MHz, DMSO-d<sub>6</sub>)  $\delta$  8.80 (d, J = 23.0 Hz, 3H), 8.31 – 8.08 (m, 6H), 7.92 – 7.66 (m, 7H), 7.43 (d, J = 7.7 Hz, 2H), 7.27 (d, J = 7.7 Hz, 2H), 6.75 (d, J = 7.9 Hz, 2H), 5.43 (s, 2H), 4.59 (s, 2H), 4.31 (d, J = 6.2 Hz, 2H), 3.92 (d, J = 13.0 Hz, 2H), 3.60 – 3.56 (m, 6H), 3.54 (d, J = 4.4 Hz, 1H), 3.02 – 2.94 (m, 1H), 2.20 (q, J = 7.7 Hz, 1H), 2.13 (s, 2H), 1.78 (d, J = 27.8 Hz, 2H), 1.29 – 1.16 (m, 8H). HDMS (ESI): 1552.7120 m/z, exp Em : 1552.7126 m/z

## Synthesis of BG-EG<sub>11</sub>-TMR-C<sub>6</sub>-APT



**Synthesis of BG-EG<sub>11</sub>-NH<sub>2</sub> (23):** NH<sub>2</sub>-EG<sub>11</sub>-NH-FMOC (21, 3.9 mg, 4.9 μmol) and BG (7, 1.5 mg, 5.4 μmol) were coupled according to the amide bond formation procedure (d). BG-EG<sub>11</sub>-NH-FMOC (22, 88%, 3.7 mg, 4.3 μmol) was recovered and deprotected according to the FMOC deprotection procedure (e). BG-EG<sub>5</sub>-NH<sub>2</sub> (23, 97%, 3.7 mg, 4.2 μmol) was recovered and analyzed. BG-EG<sub>11</sub>-NH<sub>2</sub> <sup>1</sup>H NMR (600 MHz, DMSO-d<sub>6</sub>) δ 8.42 (t, J = 5.9 Hz, 1H), 8.28 (s, 1H), 7.53 – 7.41 (m, 2H), 7.36 – 7.26 (m, 2H), 5.51 (s, 2H), 4.28 (d, J = 5.9 Hz, 2H), 3.67 – 3.53 (m, ~4H), 3.53 – 3.44 (m, ~44H), 3.11 (q, J = 6.3, 5.8 Hz, 2H), 2.40 – 2.36 (m, 2H). MS (ESI): 435.8 m/z (M<sup>2+</sup>)

**Synthesis of BG-EG<sub>11</sub>-TMR-COOH (25):** TMR (11, 2.1 mg, 4.1 μmol) and BG-EG<sub>11</sub>-NH<sub>2</sub> (23, 3.6 mg, 4.1 μmol) were coupled according to the amide bond formation procedure (f). BG-EG<sub>11</sub>-TMR-COOMe (24, 76%, 4.2 mg, 3.1 μmol) was recovered and deprotected according to the methyl deprotection procedure (g) the compound was analyzed by HDMS and HNMR. BG-EG<sub>11</sub>-TMR-COOH (25, quantitative, 3.1 μmol)

was recovered and not further characterized. Roughly half of the quantity was kept as control ligand for later experiments (L11C). BG-EG<sub>11</sub>-TMR-COOMe 1H NMR (400 MHz, DMSO-d<sub>6</sub>)  $\delta$  8.83 (t, J = 5.6 Hz, 1H), 8.36 (t, J = 5.9 Hz, 1H), 8.33 – 8.21 (m, 2H), 7.88 (d, J = 1.7 Hz, 1H), 7.46 (d, J = 8.0 Hz, 2H), 7.27 (d, J = 8.0 Hz, 2H), 7.13 – 7.00 (m, 5H), 6.97 (d, J = 2.3 Hz, 1H), 5.48 (s, 2H), 4.27 (d, J = 5.9 Hz, 2H), 3.59 (s, 3H), 3.52 – 3.47 (m, ~4H), 3.47 – 3.44 (m, ~44H), 3.27 (s, 6H), 3.23 (s, 3H), 2.38 (t, J = 6.4 Hz, 2H), 1.96 – 1.76 (m, 2H). HDMS (ESI): 1368.6610 m/z, exp Em : 1368.6615 m/z

**Synthesis of BG-EG<sub>11</sub>-TMR-(CH<sub>2</sub>)<sub>6</sub>-APT (25, L11):** BG-EG<sub>11</sub>-TMR-COOH (25, 1.5 mg, 1.1  $\mu$ mol) and APT-(CH<sub>2</sub>)<sub>6</sub>-NH<sub>2</sub> (7, 0.7 mg, 1.2  $\mu$ mol) were coupled according to the amide bond formation procedure (h). BG-EG<sub>11</sub>-TMR-(CH<sub>2</sub>)<sub>6</sub>-APT (25, 13%, 0.26 mg, 0.14  $\mu$ mol) was purified, lyophilized and analyzed. EG<sub>11</sub>-TMR-(CH<sub>2</sub>)<sub>6</sub>-APT 1H NMR (600 MHz, DMSO-d<sub>6</sub>)  $\delta$  8.79 (d, J = 28.2 Hz, 2H), 8.39 (s, 3H), 7.68 (s, 1H), 7.63 (d, J = 8.4 Hz, 1H), 7.45 (d, J = 7.8 Hz, 2H), 7.27 (d, J = 7.9 Hz, 2H), 6.85 – 6.72 (m, 6H), 6.66 (s, 2H), 5.45 (s, 2H), 4.49 (s, 2H), 4.27 (d, J = 5.9 Hz, 3H), 3.63 (t, J = 6.3 Hz, 2H), 3.55 – 3.46 (m, ~48H), 3.33 – 3.28 (m, 9H), 2.95 (s, 2H), 2.92 (d, J = 8.6 Hz, 2H), 2.37 (d, J = 6.3 Hz, 2H), 2.09 (t, J = 7.0 Hz, 2H), 1.70 (d, J = 8.0 Hz, 2H), 1.36 – 1.31 (m, 4H), 1.26 – 1.19 (m, 4H). HDMS (ESI): 1874.9111 m/z, exp Em : 1874.9117 m/z



## References

1. Kaufman, S., Pteridine Cofactors. *Annu Rev Biochem* **1967**, *36*, 171-&.
2. Nichol, C. A.; Smith, G. K.; Duch, D. S., Biosynthesis and Metabolism of Tetrahydrobiopterin and Molybdopterin. *Annu Rev Biochem* **1985**, *54*, 729-764.
3. Basu, P.; Burgmayer, S. J. N., Pterin chemistry and its relationship to the molybdenum cofactor. *Coord Chem Rev* **2011**, *255* (9-10), 1016-1038.
4. Wijnen, B.; Leertouwer, H. L.; Stavenga, D. G., Colors and pterin pigmentation of pierid butterfly wings. *J Insect Physiol* **2007**, *53* (12), 1206-1217.
5. Davis, M. D.; Kaufman, S.; Milstien, S., The auto-oxidation of tetrahydrobiopterin. *Eur J Biochem* **1988**, *173* (2), 345-51.
6. Rembold, H.; Metzger, H.; Gutensohn, W., Catabolism of Pteridine Cofactors .3. Introduction of an Oxygen Function into Position 6 of Pteridine Ring. *Biochim Biophys Acta* **1971**, *230* (1), 117-+.
7. Kaufman, S.; Levenberg, B., Further Studies on the Phenylalanine-Hydroxylation Cofactor. *J Biol Chem* **1959**, *234* (10), 2683-2688.
8. Archer, M. C.; Vonderschmitt, D. J.; Scrimgeour, K. G., Mechanism of Oxidation of Tetrahydropterins. *Can J Biochem Cell B* **1972**, *50* (11), 1174-1182.
9. Nielsen, K. H., Rat Liver Phenylalanine Hydroxylase - a Method for Measurement of Activity with Particular Reference to Distinctive Features of Enzyme and Pteridine Cofactor. *Eur J Biochem* **1969**, *7* (3), 360-&.
10. Biondi, R.; Ambrosio, G.; De Pascali, F.; Tritto, I.; Capodicasa, E.; Druhan, L. J.; Hemann, C.; Zweier, J. L., HPLC analysis of tetrahydrobiopterin and its pteridine derivatives using sequential electrochemical and fluorimetric detection: Application to tetrahydrobiopterin autoxidation and chemical oxidation. *Arch Biochem Biophys* **2012**, *520* (1), 7-16.
11. Mortensen, A.; Lykkesfeldt, J., Kinetics of acid-induced degradation of tetra- and dihydrobiopterin in relation to their relevance as biomarkers of endothelial function. *Biomarkers* **2013**, *18* (1), 55-62.
12. Mayer, B.; Klatt, P.; Werner, E. R.; Schmidt, K., Kinetics and Mechanism of Tetrahydrobiopterin-Induced Oxidation of Nitric-Oxide. *J Biol Chem* **1995**, *270* (2), 655-659.
13. Nielsen, K. H.; Simonsen, V.; Lind, K. E., Dihydropteridine Reductase - a Method for Measurement of Activity, and Investigations of Specificity for Nadh and Nadph. *Eur J Biochem* **1969**, *9* (4), 497-&.
14. Vignoni, M.; Cabrerizo, F. M.; Lorente, C.; Claparols, C.; Oliveros, E.; Thomas, A. H., Photochemistry of dihydrobiopterin in aqueous solution. *Org Biomol Chem* **2010**, *8* (4), 800-810.
15. Gorren, A. C. F.; Kungl, A. J.; Schmidt, K.; Werner, E. R.; Mayer, B., Electrochemistry of pterin cofactors and inhibitors of nitric oxide synthase. *Nitric Oxide-Biol Ch* **2001**, *5* (2), 176-186.
16. (a) Capeillere-Blandin, C.; Mathieu, D.; Mansuy, D., Reduction of ferric haemoproteins by tetrahydropterins: a kinetic study. *Biochem J* **2005**, *392*, 583-587; (b) Kim, H. L.; Choi, Y. K.; Kim, D. H.; Park, S. O.; Han, J.; Park, Y. S., Tetrahydropteridine deficiency impairs mitochondrial function in Dictyostelium discoideum Ax2. *Febs Lett* **2007**, *581* (28), 5430-5434.
17. Bailey, S. W.; Dillard, S. B.; Thomas, K. B.; Ayling, J. E., Changes in the Cofactor Binding Domain of Bovine Striatal Tyrosine-Hydroxylase at Physiological Ph Upon Camp-Dependent Phosphorylation Mapped with Tetrahydrobiopterin Analogs. *Biochemistry-US* **1989**, *28* (2), 494-504.
18. Tschesche, R.; Machleidt, H.; Hess, B.; Ziegler, I., Uber Pteridine .17. Trennung Von Synthetischem Biopterin Und Isobiopterin. *Liebigs Ann Chem* **1962**, *658* (Oct), 193-+.
19. Pfeleiderer, W.; Liedek, E.; Lohrmann, R.; Rukwied, M., Pteridine .10. Zur Struktur Des Pterins. *Chem Ber-Recl* **1960**, *93* (9), 2015-2024.

20. Hyland, S. J. R. H. K., Production of Stable Solutions of 7,8-Dihydropterin *Pteridines* **1989**, *1*, 151-153.
21. Raghavan, R.; Dryhurst, G., Redox Chemistry of Reduced Pterin Species. *J Electroanal Chem* **1981**, *129* (1-2), 189-212.
22. Archer, M. C.; Scrimgeour, K. G., Reduction Potentials of Tetrahydropterins. *Can J Biochem Cell B* **1970**, *48* (4), 526-+.
23. Kaufman, S., Enzymatic Conversion of Phenylalanine to Tyrosine. *Fed Proc* **1957**, *16* (1), 203-203.
24. Kaufman, S., The Enzymic Conversion of Phenylalanine to Tyrosine. *Biochim Biophys Acta* **1957**, *23* (2), 445-446.
25. Kaufman, S., Phenylalanine Hydroxylation Cofactor in Phenylketonuria. *Science* **1958**, *128* (3337), 1506-1508.
26. Kaufman, S., New Cofactor Required for the Enzymatic Conversion of Phenylalanine to Tyrosine. *J Biol Chem* **1958**, *230* (2), 931-939.
27. Kaufman, S., The Participation of Tetrahydrofolic Acid in the Enzymic Conversion of Phenylalanine to Tyrosine. *Biochim Biophys Acta* **1958**, *27* (2), 428-429.
28. Kaufman, S., Studies on the Mechanism of the Enzymatic Conversion of Phenylalanine to Tyrosine. *J Biol Chem* **1959**, *234* (10), 2677-2682.
29. Kaufman, S., On Structure of Phenylalanine Hydroxylation Cofactor. *J Biol Chem* **1962**, *237* (8), 2712-&.
30. Kaufman, S., The structure of the phenylalanine-hydroxylation cofactor. *P Natl Acad Sci USA* **1963**, *50* (6), 1085.
31. Kaufman, S., Studies on Structure of Primary Oxidation Product Formed from Tetrahydropteridines during Phenylalanine Hydroxylation. *J Biol Chem* **1964**, *239* (1), 332-&.
32. Kaufman, S., Coenzymes and Hydroxylases - Ascorbate and Dopamine-Beta-Hydroxylase - Tetrahydropteridines and Phenylalanine and Tyrosine Hydroxylases. *Pharmacol Rev* **1966**, *18* (1p1), 61-&.
33. Kaufman, S., Structure of Phenylalanine-Hydroxylation Cofactor. *P Natl Acad Sci USA* **1963**, *50* (6), 1085-&.
34. Brennema, Ar; Kaufman, S., Characteristics of Hepatic Phenylalanine-Hydroxylating System in Newborn Rats. *J Biol Chem* **1965**, *240* (9), 3617-&.
35. Varughese, K. I.; Skinner, M. M.; Whiteley, J. M.; Matthews, D. A.; Xuong, N. H., Crystal-Structure of Rat-Liver Dihydropteridine Reductase. *P Natl Acad Sci USA* **1992**, *89* (13), 6080-6084.
36. Matthews, D. A.; Webber, S.; Whiteley, J. M., Preliminary-X-Ray Diffraction Characterization of Crystalline Rat-Liver Dihydropteridine Reductase. *J Biol Chem* **1986**, *261* (8), 3891-3893.
37. Aksnes, A.; Skotland, T.; Flatmark, T.; Ljones, T., Bovine Dihydropteridine Reductase - Purification by Affinity Chromatography and Comparison of Enzymes from Liver and Adrenal-Medulla. *Neurochem Res* **1979**, *4* (3), 385-398.
38. Su, Y.; Varughese, K. I.; Xuong, N. H.; Bray, T. L.; Roche, D. J.; Whiteley, J. M., The Crystallographic Structure of a Human Dihydropteridine Reductase NADH Binary Complex Expressed in Escherichia-Coli by a Cdna Constructed from Its Rat Homolog. *J Biol Chem* **1993**, *268* (36), 26836-26841.
39. Symersky, J.; Li, S.; Carson, M.; Luo, D.; Luan, L. H.; Luo, M., Structural genomics of Caenorhabditis elegans: Structure of dihydropteridine reductase. *Proteins* **2003**, *53* (4), 944-946.
40. Chen, C.; Seo, K. H.; Kim, H. L.; Zhuang, N. N.; Park, Y. S.; Lee, K. H., Crystallization and preliminary characterization of dihydropteridine reductase from Dictyostelium discoideum. *Acta Crystallogr F* **2008**, *64*, 1013-1015.
41. Persson, B.; Kallberg, Y., Classification and nomenclature of the superfamily of short-chain dehydrogenases/reductases (SDRs). *Chem-Biol Interact* **2013**, *202* (1-3), 111-115.

42. Eklund, H.; Samama, J. P.; Wallen, L.; Branden, C. I.; Akesson, A.; Jones, T. A., Structure of a Triclinic Ternary Complex of Horse Liver Alcohol-Dehydrogenase at 2.9 Å Resolution. *J Mol Biol* **1981**, *146* (4), 561-587.
43. Webb, L. E.; Hill, E. J.; Banaszak, L. J., Conformation of Nicotinamide Adenine-Dinucleotide Bound to Cytoplasmic Malate Dehydrogenase. *Biochemistry-U S A* **1973**, *12* (25), 5101-5109.
44. White, J. L.; Hackert, M. L.; Buehner, M.; Adams, M. J.; Ford, G. C.; Lentz, P. J.; Smiley, I. E.; Steindel, S. J.; Rossmann, M. G., Comparison of Structures of Apo Dogfish M-4 Lactate-Dehydrogenase and Its Ternary Complexes. *J Mol Biol* **1976**, *102* (4), 759-779.
45. Presnell, S. R.; Cohen, F. E., Topological Distribution of 4-Alpha-Helix Bundles. *P Natl Acad Sci USA* **1989**, *86* (17), 6592-6596.
46. Chou, K. C.; Maggiora, G. M.; Nemethy, G.; Scheraga, H. A., Energetics of the Structure of the 4-Alpha-Helix Bundle in Proteins. *P Natl Acad Sci USA* **1988**, *85* (12), 4295-4299.
47. Armarego, W. L. F., Hydrogen Transfer from 4-R and 4-S (4-H-3)Nadh in the Reduction of D,L-Cis-6,7-Dimethyl-6,7(8h)-Dihydropterin with Dihydropteridine Reductase from Human-Liver and Sheep Liver. *Biochem Bioph Res Co* **1979**, *89* (1), 246-249.
48. Craine, J. E.; Kaufman, S.; Hall, E. S., Isolation and Characterization of Dihydropteridine Reductase from Sheep Liver. *J Biol Chem* **1972**, *247* (19), 6082-&.
49. Korri, K. K.; Chippel, D.; Chauvin, M. M.; Tirpak, A.; Scrimgeour, K. G., Quinonoid Dihydropterin Reductase from Beef-Liver. *Can J Biochem Cell B* **1977**, *55* (11), 1145-1152.
50. Varughese, K. I.; Xuong, N. H.; Kiefer, P. M.; Matthews, D. A.; Whiteley, J. M., Structural and Mechanistic Characteristics of Dihydropteridine Reductase - a Member of the Tyr-(Xaa)(3)-Lys-Containing Family of Reductases and Dehydrogenases. *P Natl Acad Sci USA* **1994**, *91* (12), 5582-5586.
51. Armarego, W. L. F.; Randles, D.; Taguchi, H., Km and Kcat Values for [6,6,7,7-H-2]7,8(6h)-Dihydropterin and 2,6-Diamino-5-Iminopyrimidin-4-One with Dihydropteridine Reductase. *Biochem J* **1983**, *211* (2), 357-361.
52. Yu, Q. R.; Heikal, A. A., Two-photon autofluorescence dynamics imaging reveals sensitivity of intracellular NADH concentration and conformation to cell physiology at the single-cell level. *J Photobiophotobio B* **2009**, *95* (1), 46-57.
53. Valsecchi, F.; Monge, C.; Forkink, M.; de Groof, A. J. C.; Benard, G.; Rossignol, R.; Swarts, H. G.; van Emst-de Vries, S. E.; Rodenburg, R. J.; Calvaruso, M. A.; Nijtmans, L. G. J.; Heeman, B.; Roestenberg, P.; Wieringa, B.; Smeitink, J. A. M.; Koopman, W. J. H.; Willems, P. H. G. M., Metabolic consequences of NDUFS4 gene deletion in immortalized mouse embryonic fibroblasts. *Bba-Bioenergetics* **2012**, *1817* (10), 1925-1936.
54. Albe, K. R.; Butler, M. H.; Wright, B. E., Cellular Concentrations of Enzymes and Their Substrates. *J Theor Biol* **1990**, *143* (2), 163-195.
55. Firgaira, F. A.; Cotton, R. G. H.; Danks, D. M., Isolation and Characterization of Dihydropteridine Reductase from Human-Liver. *Biochem J* **1981**, *197* (1), 31-43.
56. Armarego, W. L. F.; Randles, D.; Waring, P., Dihydropteridine Reductase (Dhpr), Its Cofactors, and Its Mode of Action. *Med Res Rev* **1984**, *4* (3), 267-321.
57. Shen, R.; Smith, R. V.; Davis, P. J.; Abell, C. W., Inhibition of Dihydropteridine Reductase by Apomorphine and Related-Compounds. *Fed Proc* **1983**, *42* (7), 2108-2108.
58. Shen, R. S., Inhibition of Dihydropteridine Reductase by Catecholamines and Related-Compounds. *Biochim Biophys Acta* **1983**, *743* (1), 129-135.
59. Shen, R. S.; Abell, C. W., Inhibition of Dihydropteridine Reductase by Catechol Estrogens. *J Neurosci Res* **1983**, *10* (3), 251-259.
60. Burg, A. W.; Brown, G. M., Biosynthesis of Folic Acid .8. Purification and Properties of Enzyme That Catalyzes Production of Formate from Carbon Atom 8 of Guanosine Triphosphate. *J Biol Chem* **1968**, *243* (9), 2349-&.

61. Wolf, W. A.; Brown, G. M., Biosynthesis of Folic Acid .10. Evidence for an Amadori Rearrangement in Enzymatic Formation of Dihydroneopterin Triphosphate from Gtp. *Biochim Biophys Acta* **1969**, *192* (3), 468-&.
62. Bracher, A.; Eisenreich, W.; Schramek, N.; Ritz, H.; Gotze, E.; Herrmann, A.; Gutlich, M.; Bacher, A., Biosynthesis of pteridines - NMR studies on the reaction mechanisms of GTP cyclohydrolase I, pyruvoyltetrahydropterin synthase, and sepiapterin reductase. *J Biol Chem* **1998**, *273* (43), 28132-28141.
63. Nar, H.; Huber, R.; Auerbach, G.; Fischer, M.; Hosl, C.; Ritz, H.; Bracher, A.; Meining, W.; Eberhardt, S.; Bacher, A., Active site topology and reaction mechanism of GTP cyclohydrolase I. *P Natl Acad Sci USA* **1995**, *92* (26), 12120-12125.
64. Nar, H.; Huber, R.; Meining, W.; Schmid, C.; Weinkauff, S.; Bacher, A., Atomic-Structure of Gtp Cyclohydrolase-I. *Structure* **1995**, *3* (5), 459-466.
65. Harada, T.; Kagamiyama, H.; Hatakeyama, K., Feedback-Regulation Mechanisms for the Control of Gtp Cyclohydrolase-I Activity. *Science* **1993**, *260* (5113), 1507-1510.
66. Hatakeyama, K.; Harada, T.; Suzuki, S.; Watanabe, Y.; Kagamiyama, H., Purification and Characterization of Rat-Liver Gtp Cyclohydrolase-I - Cooperative Binding of Gtp to the Enzyme. *J Biol Chem* **1989**, *264* (36), 21660-21664.
67. Maita, N.; Hatakeyama, K.; Okada, K.; Hakoshima, T., Structural basis of biopterin-induced inhibition of GTP cyclohydrolase I by GFRP, its feedback regulatory protein. *J Biol Chem* **2004**, *279* (49), 51534-51540.
68. Maita, N.; Okada, K.; Hatakeyama, K.; Hakoshima, T., Crystal structure of the stimulatory complex of GTP cyclohydrolase I and its feedback regulatory protein GFRP. *Proc Natl Acad Sci U S A* **2002**, *99* (3), 1212-7.
69. Kolinsky, M. A.; Gross, S. S., The mechanism of potent GTP cyclohydrolase I inhibition by 2,4-diamino-6-hydroxypyrimidine - Requirement of the GTP cyclohydrolase I feedback regulatory protein. *J Biol Chem* **2004**, *279* (39), 40677-40682.
70. Rebelo, J.; Auerbach, G.; Bader, G.; Bracher, A.; Nar, H.; Hosl, C.; Schramek, N.; Kaiser, J.; Bacher, A.; Huber, R.; Fischer, M., Biosynthesis of pteridines. Reaction mechanism of GTP cyclohydrolase I. *J Mol Biol* **2003**, *326* (2), 503-516.
71. Yoneyama, T.; Brewer, J. M.; Hatakeyama, K., GTP cyclohydrolase I feedback regulatory protein is a pentamer of identical subunits - Purification, cDNA cloning, and bacterial expression. *J Biol Chem* **1997**, *272* (15), 9690-9696.
72. Hussein, D.; Starr, A.; Heikal, L.; McNeill, E.; Channon, K. M.; Brown, P. R.; Sutton, B. J.; McDonnell, J. M.; Nandi, M., Validating the GTP-cyclohydrolase 1-feedback regulatory complex as a therapeutic target using biophysical and in vivo approaches. *Brit J Pharmacol* **2015**, *172* (16), 4146-4157.
73. Yoneyama, T.; Hatakeyama, K., Decameric GTP cyclohydrolase I forms complexes with two pentameric GTP cyclohydrolase I feedback regulatory proteins in the presence of phenylalanine or of a combination of tetrahydrobiopterin and GTP. *J Biol Chem* **1998**, *273* (32), 20102-20108.
74. Huang, A. N.; Zhang, Y. Y.; Chen, K.; Hatakeyama, K.; Keaney, J. F., Cytokine-stimulated GTP cyclohydrolase I expression in endothelial cells requires coordinated activation of nuclear factor-kappa B and Stat1/Stat3. *Circ Res* **2005**, *96* (2), 164-171.
75. Werner, E. R.; Wernerfeldmayer, G.; Fuchs, D.; Hausen, A.; Reibnegger, G.; Yim, J. J.; Pfeleiderer, W.; Wachter, H., Tetrahydrobiopterin Biosynthetic Activities in Human Macrophages, Fibroblasts, Thp-1, and T-24 Cells - Gtp-Cyclohydrolase-I Is Stimulated by Interferon-Gamma, and 6-Pyruvoyl Tetrahydropterin Synthase and Sepiapterin Reductase Are Constitutively Present. *J Biol Chem* **1990**, *265* (6), 3189-3192.
76. Schoedon, G.; Troppmair, J.; Fontana, A.; Huber, C.; Curtius, H. C.; Niederwieser, A., Biosynthesis and Metabolism of Pterins in Peripheral-Blood Mononuclear-Cells and Leukemia Lines of Man and Mouse. *Eur J Biochem* **1987**, *166* (2), 303-310.

77. Wernerfeldmayer, G.; Prast, H.; Werner, E. R.; Philippu, A.; Wachter, H., Induction of Gtp Cyclohydrolase-I by Bacterial Lipopolysaccharide in the Rat. *Febs Lett* **1993**, *322* (3), 223-226.
78. Rosenkranzweiss, P.; Sessa, W. C.; Milstien, S.; Kaufman, S.; Watson, C. A.; Pober, J. S., Regulation of Nitric-Oxide Synthesis by Proinflammatory Cytokines in Human Umbilical Vein Endothelial-Cells - Elevations in Tetrahydrobiopterin Levels Enhance Endothelial Nitric-Oxide Synthase Specific Activity. *J Clin Invest* **1994**, *93* (5), 2236-2243.
79. Hirayama, K.; Kapatos, G., Regulation of Gtp Cyclohydrolase-I Gene-Expression and Tetrahydrobiopterin Content by Nerve Growth-Factor in Cultures of Superior Cervical-Ganglia. *Neurochem Int* **1995**, *27* (2), 157-161.
80. Wernerfeldmayer, G.; Werner, E. R.; Fuchs, D.; Hausen, A.; Reibnegger, G.; Schmidt, K.; Weiss, G.; Wachter, H., Pteridine Biosynthesis in Human Endothelial-Cells - Impact on Nitric Oxide-Mediated Formation of Cyclic-Gmp. *J Biol Chem* **1993**, *268* (3), 1842-1846.
81. Hattori, Y.; Gross, S. S., Gtp Cyclohydrolase-1 Messenger-Rna Is Induced by Lps in Vascular Smooth-Muscle - Characterization, Sequence and Relationship to Nitric-Oxide Synthase. *Biochem Bioph Res Co* **1993**, *195* (1), 435-441.
82. Sun, X. T.; Kumar, S.; Tian, J.; Black, S. M., Estradiol Increases Guanosine 5'-Triphosphate Cyclohydrolase Expression Via the Nitric Oxide-Mediated Activation of Cyclic Adenosine 5'-Monophosphate Response Element Binding Protein. *Endocrinology* **2009**, *150* (8), 3742-3752.
83. Shimizu, S.; Hiroi, T.; Ishii, M.; Hagiwara, T.; Wajima, T.; Miyazaki, A.; Kiuchi, Y., Hydrogen peroxide stimulates tetrahydrobiopterin synthesis through activation of the Jak2 tyrosine kinase pathway in vascular endothelial cells. *Int J Biochem Cell B* **2008**, *40* (4), 755-765.
84. Stegenga, S. L.; Hirayama, K.; Kapatos, G., Regulation of GTP cyclohydrolase I gene expression and tetrahydrobiopterin content in cultured sympathetic neurons by leukemia inhibitory factor and ciliary neurotrophic factor. *J Neurochem* **1996**, *66* (6), 2541-2545.
85. H., R. B. F. D. K. W. W., Course of Immune Activation Markers In Patients after Severe Multiple Trauma *Pteridines* **1990**, *2*, 95-97.
86. Fuchs, D.; Weiss, G.; Reibnegger, G.; Wachter, H., The Role of Neopterin as a Monitor of Cellular Immune Activation in Transplantation, Inflammatory, Infectious, and Malignant Diseases. *Crit Rev Cl Lab Sci* **1992**, *29* (3-4), 307-341.
87. Yoneyama, T.; Hatakeyama, K., Ligand binding to the inhibitory and stimulatory GTP cyclohydrolase I/GTP cyclohydrolase I feedback regulatory protein complexes. *Protein Science* **2001**, *10* (4), 871-878.
88. Hesslinger, C.; Kremmer, E.; Hultner, L.; Ueffing, M.; Ziegler, I., Phosphorylation of GTP cyclohydrolase I and modulation of its activity in rodent mast cells - GTP cyclohydrolase I hyperphosphorylation is coupled to high affinity IgE receptor signaling and involves protein kinase C. *J Biol Chem* **1998**, *273* (34), 21616-21622.
89. Thony, B.; Auerbach, G.; Blau, N., Tetrahydrobiopterin biosynthesis, regeneration and functions. *Biochem J* **2000**, *347*, 1-16.
90. Bogdan, C.; Werner, E.; Stenger, S.; Wachter, H.; Rollinghoff, M.; Wernerfeldmayer, G., 2,4-Diamino-6-Hydroxypyrimidine, an Inhibitor of Tetrahydrobiopterin Synthesis, down-Regulates the Expression of Inos Protein and Messenger-Rna in Primary Murine Macrophages. *Febs Lett* **1995**, *363* (1-2), 69-74.
91. Krivi, G. G.; Brown, G. M., Purification and Properties of the Enzymes from Drosophila-Melanogaster That Catalyze the Synthesis of Sepiapterin from Dihydroneopterin Triphosphate. *Biochem Genet* **1979**, *17* (3-4), 371-390.
92. (a) Takikawa, S.; Curtius, H. C.; Redweik, U.; Ghisla, S., Purification of 6-Pyruvoyl-Tetrahydropterin Synthase from Human-Liver. *Biochem Bioph Res Co* **1986**, *134* (2), 646-651; (b) Takikawa, S. I.; Curtius, H. C.; Redweik, U.; Leimbacher, W.; Ghisla, S., Biosynthesis of

Tetrahydrobiopterin - Purification and Characterization of 6-Pyruvoyl-Tetrahydropterin Synthase from Human-Liver. *Eur J Biochem* **1986**, *161* (2), 295-302.

93. (a) Inoue, Y.; Kawasaki, Y.; Harada, T.; Hatakeyama, K.; Kagamiyama, H., Purification and Cdna Cloning of Rat 6-Pyruvoyl-Tetrahydropterin Synthase. *J Biol Chem* **1991**, *266* (31), 20791-20796; (b) Thony, B.; Leimbacher, W.; Burgisser, D.; Heizmann, C. W., Human 6-Pyruvoyltetrahydropterin Synthase - Cdna Cloning and Heterologous Expression of the Recombinant Enzyme. *Biochem Bioph Res Co* **1992**, *189* (3), 1437-1443.

94. Burgisser, D. M.; Thony, B.; Redweik, U.; Hunziker, P.; Heizmann, C. W.; Blau, N., Expression and Characterization of Recombinant Human and Rat-Liver 6-Pyruvoyl Tetrahydropterin Synthase - Modified Cysteine Residues Inhibit the Enzyme-Activity. *Eur J Biochem* **1994**, *219* (1-2), 497-502.

95. Nar, H.; Huber, R.; Heizmann, C. W.; Thony, B.; Burgisser, D., 3-Dimensional Structure of 6-Pyruvoyl Tetrahydropterin Synthase, an Enzyme Involved in Tetrahydrobiopterin Biosynthesis. *Embo J* **1994**, *13* (6), 1255-1262.

96. Ploom, T.; Thony, B.; Yim, J.; Lee, S.; Nar, H.; Leimbacher, W.; Richardson, J.; Huber, R.; Auerbach, G., Crystallographic and kinetic investigations on the mechanism of 6-pyruvoyl tetrahydropterin synthase. *J Mol Biol* **1999**, *286* (3), 851-60.

97. Burgisser, D. M.; Thony, B.; Redweik, U.; Hess, D.; Heizmann, C. W.; Huber, R.; Nar, H., 6-Pyruvoyl Tetrahydropterin Synthase, an Enzyme with a Novel Type of Active-Site Involving Both Zinc-Binding and an Intersubunit Catalytic Triad Motif - Site-Directed Mutagenesis of the Proposed Active-Center, Characterization of the Metal-Binding Site and Modeling of Substrate-Binding. *J Mol Biol* **1995**, *253* (2), 358-369.

98. Francini, N.; Blau, N.; Walter, R. B.; Schaffner, A.; Schoedon, G., Critical role of interleukin-1 beta for transcriptional regulation of endothelial 6-pyruvoyltetrahydropterin synthase. *Arterioscl Throm Vas* **2003**, *23* (11), E50-E53.

99. (a) Matsubara, M.; Akino, M., On Presence of Sepiapterin Reductase Different from Folate + Dihydrofolate Reductase in Chicken Liver. *Experientia* **1964**, *20* (10), 574-&; (b) Matsubara, M.; Katoh, S.; Akino, M.; Kaufman, S., Sepiapterin Reductase. *Biochim Biophys Acta* **1966**, *122* (2), 202-+.

100. Katoh, S., Sepiapterin Reductase from Horse Liver - Purification and Properties of Enzyme. *Arch Biochem Biophys* **1971**, *146* (1), 202-&.

101. Sueoka, T.; Katoh, S., Purification and Characterization of Sepiapterin Reductase from Rat Erythrocytes. *Biochim Biophys Acta* **1982**, *717* (2), 265-271.

102. Tanaka, K.; Akino, M.; Hagi, Y.; Doi, M.; Shiota, T., The Enzymatic-Synthesis of Sepiapterin by Chicken Kidney Preparations. *J Biol Chem* **1981**, *256* (6), 2963-2972.

103. Katoh, S.; Sueoka, T., Sepiapterin Reductase Exhibits a NADPH-Dependent Dicarboxyl Reductase-Activity. *Biochem Bioph Res Co* **1984**, *118* (3), 859-866.

104. Smith, G. K., On the Role of Sepiapterin Reductase in the Biosynthesis of Tetrahydrobiopterin. *Arch Biochem Biophys* **1987**, *255* (2), 254-266.

105. Katoh, S.; Sueoka, T., Isomerization of 6-Lactoyl Tetrahydropterin by Sepiapterin Reductase. *J Biochem-Tokyo* **1987**, *101* (1), 275-278.

106. Citron, B. A.; Milstien, S.; Gutierrez, J. C.; Levine, R. A.; Yanak, B. L.; Kaufman, S., Isolation and Expression of Rat-Liver Sepiapterin Reductase Cdna. *P Natl Acad Sci USA* **1990**, *87* (16), 6436-6440.

107. Auerbach, G.; Herrmann, A.; Gutlich, M.; Fischer, M.; Jacob, U.; Bacher, A.; Huber, R., The 1.25 angstrom crystal structure of sepiapterin reductase reveals its binding mode to pterins and brain neurotransmitters. *Embo J* **1997**, *16* (24), 7219-7230.

108. Oyama, R.; Katoh, S.; Sueoka, T.; Suzuki, M.; Ichinose, H.; Nagatsu, T.; Titani, K., The Complete Amino-Acid-Sequence of the Mature Form of Rat Sepiapterin Reductase. *Biochem Bioph Res Co* **1990**, *173* (2), 627-631.

109. Sueoka, T.; Katoh, S., Carbonyl Reductase-Activity of Sepiapterin Reductase from Rat Erythrocytes. *Biochim Biophys Acta* **1985**, *843* (3), 193-198.
110. Iwanami, Y.; Akino, M., Evidence for Eneiol Form of Sepiapterin. *Journal of nutritional science and vitaminology* **1975**, *21* (2), 143-145.
111. Park, Y. S.; Heizmann, C. W.; Wermuth, B.; Levine, R. A.; Steinerstauch, P.; Guzman, J.; Blau, N., Human Carbonyl and Aldose Reductases - New Catalytic Functions in Tetrahydrobiopterin Biosynthesis. *Biochem Bioph Res Co* **1991**, *175* (3), 738-744.
112. Milstien, S.; Kaufman, S., The Biosynthesis of Tetrahydrobiopterin in Rat-Brain - Purification and Characterization of 6-Pyruvoyl Tetrahydropterin (2'-Oxo)Reductase. *J Biol Chem* **1989**, *264* (14), 8066-8073.
113. Blau, N.; Bonafe, L.; Thony, B., Tetrahydrobiopterin deficiencies without hyperphenylalaninemia: Diagnosis and genetics of DOPA-responsive dystonia and sepiapterin reductase deficiency. *Mol Genet Metab* **2001**, *74* (1-2), 172-185.
114. Ferre, J.; Naylor, E. W., Sepiapterin Reductase in Cultured Human-Cells. *Biochem Bioph Res Co* **1987**, *148* (3), 1475-1481.
115. Latremoliere, A.; Latini, A.; Andrews, N.; Cronin, S. J.; Fujita, M.; Gorska, K.; Hovius, R.; Romero, C.; Chuaiphichai, S.; Painter, M.; Miracca, G.; Babaniyi, O.; Remor, A. P.; Duong, K.; Riva, P.; Barrett, L. B.; Ferreiros, N.; Naylor, A.; Penninger, J. M.; Tegeder, I.; Zhong, J.; Blagg, J.; Channon, K. M.; Johnsson, K.; Costigan, M.; Woolf, C. J., Reduction of Neuropathic and Inflammatory Pain through Inhibition of the Tetrahydrobiopterin Pathway. *Neuron* **2015**, *86* (6), 1393-1406.
116. Chidley, C.; Haruki, H.; Pedersen, M. G.; Muller, E.; Johnsson, K., A yeast-based screen reveals that sulfasalazine inhibits tetrahydrobiopterin biosynthesis. *Nature chemical biology* **2011**, *7* (6), 375-383.
117. Haruki, H.; Hovius, R.; Pedersen, M. G.; Johnsson, K., Tetrahydrobiopterin Biosynthesis as a Potential Target of the Kynurenine Pathway Metabolite Xanthurenic Acid. *J Biol Chem* **2016**, *291* (2), 652-657.
118. Katoh, S.; Sueoka, T.; Yamada, S., Direct Inhibition of Brain Sepiapterin Reductase by a Catecholamine and an Indoleamine. *Biochem Bioph Res Co* **1982**, *105* (1), 75-81.
119. Haruki, H.; Pedersen, M. G.; Gorska, K. I.; Pojer, F.; Johnsson, K., Tetrahydrobiopterin Biosynthesis as an Off-Target of Sulfa Drugs. *Science* **2013**, *340* (6135), 987-991.
120. Silverman, M.; Keresztesy, J. C.; Koval, G. J., Isolation of N-10-Formylfolic Acid. *J Biol Chem* **1954**, *211* (1), 53-61.
121. Miller, A.; Waelsch, H., The Transfer of the Formimino Group of Formamidinoglutamic Acid to Tetrahydrofolic Acid. *Arch Biochem Biophys* **1956**, *63* (1), 263-266.
122. Wright, B. E.; Anderson, M. L., Folic Acid Reductase. *J Am Chem Soc* **1957**, *79* (8), 2027-2028.
123. Osborn, M. J.; Huennekens, F. M., Folic Acid Coenzymes and Active One-Carbon Units .7. Enzymatic Reduction of Dihydrofolic Acid. *J Biol Chem* **1958**, *233* (4), 969-974.
124. Osborn, M. J.; Freeman, M.; Huennekens, F. M., Inhibition of Dihydrofolic Reductase by Aminopterin and Amethopterin. *P Soc Exp Biol Med* **1958**, *97* (2), 429-432.
125. Peters, J. M.; Greenberg, D. M., Dihydrofolic Acid Reductase. *J Am Chem Soc* **1958**, *80* (24), 6679-6682.
126. Morales, D. R.; Greenberg, D. M., Purification + Properties of Dihydrofolate Reductase of Sheep Liver. *Biochim Biophys Acta* **1964**, *85* (3), 360-&.
127. Kaufman, S., Nature of Primary Oxidation Product Formed from Tetrahydropteridines during Phenylalanine Hydroxylation. *J Biol Chem* **1961**, *236* (3), 804-&.
128. Matthews, D. A.; Alden, R. A.; Bolin, J. T.; Freer, S. T.; Hamlin, R.; Xuong, N.; Kraut, J.; Poe, M.; Williams, M.; Hoogsteen, K., Dihydrofolate-Reductase - X-Ray Structure of Binary Complex with Methotrexate. *Science* **1977**, *197* (4302), 452-455.

129. Oefner, C.; Darcy, A.; Winkler, F. K., Crystal-Structure of Human Dihydrofolate-Reductase Complexed with Folate. *Eur J Biochem* **1988**, *174* (2), 377-385.
130. Mctigue, M. A.; Davies, J. F.; Kaufman, B. T.; Kraut, J., Crystal-Structure of Chicken Liver Dihydrofolate-Reductase Complexed with NADP+ and Biopterin. *Biochemistry-Us* **1992**, *31* (32), 7264-7273.
131. Appleman, J. R.; Beard, W. A.; Delcamp, T. J.; Prendergast, N. J.; Freisheim, J. H.; Blakley, R. L., Atypical Transient State Kinetics of Recombinant Human Dihydrofolate-Reductase Produced by Hysteretic Behavior - Comparison with Dihydrofolate Reductases from Other Sources. *J Biol Chem* **1989**, *264* (5), 2625-2633.
132. Appleman, J. R.; Beard, W. A.; Delcamp, T. J.; Prendergast, N. J.; Freisheim, J. H.; Blakley, R. L., Unusual Transient-State and Steady-State Kinetic-Behavior Is Predicted by the Kinetic Scheme Operational for Recombinant Human Dihydrofolate-Reductase. *J Biol Chem* **1990**, *265* (5), 2740-2748.
133. Hawser, S.; Lociuo, S.; Islam, K., Dihydrofolate reductase inhibitors as antibacterial agents. *Biochem Pharmacol* **2006**, *71* (7), 941-948.
134. Bhabha, G.; Ekiert, D. C.; Jennewein, M.; Zmasek, C. M.; Tuttle, L. M.; Kroon, G.; Dyson, H. J.; Godzik, A.; Wilson, I. A.; Wright, P. E., Divergent evolution of protein conformational dynamics in dihydrofolate reductase. *Nat Struct Mol Biol* **2013**, *20* (11), 1243-U262.
135. Schnell, J. R.; Dyson, H. J.; Wright, P. E., Structure, dynamics, and catalytic function of dihydrofolate reductase. *Annu Rev Bioph Biom* **2004**, *33*, 119-140.
136. Davies, J. F.; Delcamp, T. J.; Prendergast, N. J.; Ashford, V. A.; Freisheim, J. H.; Kraut, J., Crystal-Structures of Recombinant Human Dihydrofolate-Reductase Complexed with Folate and 5-Deazafolate. *Biochemistry-Us* **1990**, *29* (40), 9467-9479.
137. Carroll, M. J.; Mauldin, R. V.; Gromova, A. V.; Singleton, S. F.; Collins, E. J.; Lee, A. L., Evidence for dynamics in proteins as a mechanism for ligand dissociation. *Nature chemical biology* **2012**, *8* (3), 246-252.
138. Schweitzer, B. I.; Dicker, A. P.; Bertino, J. R., Dihydrofolate-Reductase as a Therapeutic Target. *Faseb J* **1990**, *4* (8), 2441-2452.
139. Strecker, H. J.; Korke, S., Glucose Dehydrogenase. *J Biol Chem* **1952**, *196* (2), 769-784.
140. Kaufman, S., A Protein That Stimulates Rat Liver Phenylalanine Hydroxylase. *J Biol Chem* **1970**, *245* (18), 4751-&.
141. Huang, C. Y.; Max, E. E.; Kaufman, S., Purification and Characterization of Phenylalanine Hydroxylase-Stimulating Protein from Rat-Liver. *J Biol Chem* **1973**, *248* (12), 4235-4241.
142. Huang, C. Y.; Kaufman, S., Studies on Mechanisms of Action of Phenylalanine Hydroxylase and Its Protein Stimulator .1. Enzyme Concentration-Dependence of Specific Activity of Phenylalanine Hydroxylase Due to a Nonenzymatic Step. *J Biol Chem* **1973**, *248* (12), 4242-4251.
143. Lazarus, R. A.; Benkovic, S. J.; Kaufman, S., Phenylalanine-Hydroxylase Stimulator Protein Is a 4a-Carbinolamine Dehydratase. *J Biol Chem* **1983**, *258* (18), 960-962.
144. Adler, C.; Ghisla, S.; Rebrin, I.; Haavik, J.; Heizmann, C. W.; Blau, N.; Kuster, T.; Curtius, H. C., 7-Substituted Pterins in Humans with Suspected Pterin-4a-Carbinolamine Dehydratase Deficiency - Mechanism of Formation Via Nonenzymatic Transformation from 6-Substituted Pterins. *Eur J Biochem* **1992**, *208* (1), 139-144.
145. Mendel, D. B.; Khavari, P. A.; Conley, P. B.; Graves, M. K.; Hansen, L. P.; Admon, A.; Crabtree, G. R., Characterization of a Cofactor That Regulates Dimerization of a Mammalian Homeodomain Protein. *Science* **1991**, *254* (5039), 1762-1767.
146. Citron, B. A.; Davis, M. D.; Milstien, S.; Gutierrez, J.; Mendel, D. B.; Crabtree, G. R.; Kaufman, S., Identity of 4a-Carbinolamine Dehydratase, a Component of the Phenylalanine Hydroxylation System, and DcoH, a Transregulator of Homeodomain Proteins. *P Natl Acad Sci USA* **1992**, *89* (24), 11891-11894.



147. (a) Ficner, R.; Sauer, U. H.; Stier, G.; Suck, D., 3-Dimensional Structure of the Bifunctional Protein Pcd/Dcoh, a Cytoplasmic Enzyme Interacting with Transcription Factor Hnf1. *Embo J* **1995**, *14* (9), 2034-2042; (b) Cronk, J. D.; Endrizzi, J. A.; Alber, T., High-resolution structures of the bifunctional enzyme and transcriptional coactivator DCoH and its complex with a product analogue. *Protein Science* **1996**, *5* (10), 1963-1972.
148. Fitzpatrick, P. F., Mechanism of aromatic amino acid hydroxylation. *Biochemistry-U.S.* **2003**, *42* (48), 14083-14091.
149. Grenett, H. E.; Ledley, F. D.; Reed, L. L.; Woo, S. L. C., Full-Length Cdna for Rabbit Tryptophan-Hydroxylase - Functional Domains and Evolution of Aromatic Amino-Acid Hydroxylases. *P Natl Acad Sci USA* **1987**, *84* (16), 5530-5534.
150. Arturo, E. C.; Gupta, K.; Heroux, A.; Stith, L.; Cross, P. J.; Parker, E. J.; Loll, P. J.; Jaffe, E. K., First structure of full-length mammalian phenylalanine hydroxylase reveals the architecture of an autoinhibited tetramer. *P Natl Acad Sci USA* **2016**, *113* (9), 2394-2399.
151. (a) Zhang, S. N.; Roberts, K. M.; Fitzpatrick, P. F., Phenylalanine Binding Is Linked to Dimerization of the Regulatory Domain of Phenylalanine Hydroxylase. *Biochemistry-U.S.* **2014**, *53* (42), 6625-6627; (b) Roberts, K. M.; Khan, C. A.; Hinck, C. S.; Fitzpatrick, P. F., Activation of Phenylalanine Hydroxylase by Phenylalanine Does Not Require Binding in the Active Site. *Biochemistry-U.S.* **2014**, *53* (49), 7846-7853; (c) Jaffe, E. K.; Stith, L.; Lawrence, S. H.; Andrade, M.; Dunbrack, R. L., A new model for allosteric regulation of phenylalanine hydroxylase: Implications for disease and therapeutics. *Arch Biochem Biophys* **2013**, *530* (2), 73-82.
152. Meisburger, S. P.; Taylor, A. B.; Khan, C. A.; Zhang, S. N.; Fitzpatrick, P. F.; Ando, N., Domain Movements upon Activation of Phenylalanine Hydroxylase Characterized by Crystallography and Chromatography-Coupled Small-Angle X-ray Scattering. *J Am Chem Soc* **2016**, *138* (20), 6506-6516.
153. Patel, D.; Kopec, J.; Fitzpatrick, P. F.; McCorvie, T. J.; Yue, W. W., Structural basis for ligand-dependent dimerization of phenylalanine hydroxylase regulatory domain. *Sci Rep-Uk* **2016**, *6*.
154. Pey, A. L.; Martinez, A., The activity of wild-type and mutant phenylalanine hydroxylase and its regulation by phenylalanine and tetrahydrobiopterin at physiological and pathological concentrations: An isothermal titration calorimetry study. *Mol Genet Metab* **2005**, *86*, S43-S53.
155. Roberts, K. M.; Pavon, J. A.; Fitzpatrick, P. F., Kinetic Mechanism of Phenylalanine Hydroxylase: Intrinsic Binding and Rate Constants from Single-Turnover Experiments. *Biochemistry-U.S.* **2013**, *52* (6), 1062-1073.
156. Zhang, S. N.; Huang, T.; Ilangovan, U.; Hinck, A. P.; Fitzpatrick, P. F., The Solution Structure of the Regulatory Domain of Tyrosine Hydroxylase. *J Mol Biol* **2014**, *426* (7), 1483-1497.
157. Haycock, J. W., Phosphorylation of Tyrosine-Hydroxylase In situ at Serine-8, Serine-19, Serine-31, and Serine-40. *J Biol Chem* **1990**, *265* (20), 11682-11691.
158. Daubner, S. C.; Le, T.; Wang, S. Z., Tyrosine hydroxylase and regulation of dopamine synthesis. *Arch Biochem Biophys* **2011**, *508* (1), 1-12.
159. Ramsey, A. J.; Fitzpatrick, P. F., Effects of phosphorylation of serine 40 of tyrosine hydroxylase on binding of catecholamines: Evidence for a novel regulatory mechanism. *Biochemistry-U.S.* **1998**, *37* (25), 8980-8986.
160. Goodwill, K. E.; Sabatier, C.; Marks, C.; Raag, R.; Fitzpatrick, P. F.; Stevens, R. C., Crystal structure of tyrosine hydroxylase at 2.3 angstrom and its implications for inherited neurodegenerative diseases. *Nat Struct Biol* **1997**, *4* (7), 578-585.
161. Zhang, X. D.; Beaulieu, J. M.; Sotnikova, T. D.; Gainetdinov, R. R.; Caron, M. G., Tryptophan hydroxylase-2 controls brain serotonin synthesis. *Science* **2004**, *305* (5681), 217-217.
162. Walther, D. J.; Peter, J. U.; Bashammakh, S.; Hortnagl, H.; Voits, M.; Fink, H.; Bader, M., Synthesis of serotonin by a second tryptophan hydroxylase isoform. *Science* **2003**, *299* (5603), 76-76.

163. McKinney, J.; Knappskog, P. M.; Haavik, J., Different properties of the central and peripheral forms of human tryptophan hydroxylase. *J Neurochem* **2005**, *92* (2), 311-320.
164. Winge, I.; McKinney, J. A.; Ying, M.; D'Santos, C. S.; Kleppe, R.; Knappskog, P. M.; Haavik, J., Activation and stabilization of human tryptophan hydroxylase 2 by phosphorylation and 14-3-3 binding. *Biochem J* **2008**, *410*, 195-204.
165. Wang, L.; Erlandsen, H.; Haavik, J.; Knappskog, P. M.; Stevens, R. C., Three-dimensional structure of human tryptophan hydroxylase and its implications for the biosynthesis of the neurotransmitters serotonin and melatonin. *Biochemistry-Us* **2002**, *41* (42), 12569-12574.
166. Rosselli, M.; Keller, P. J.; Dubey, R. K., Role of nitric oxide in the biology, physiology and pathophysiology of reproduction. *Hum Reprod Update* **1998**, *4* (1), 3-24.
167. Tayeh, M. A.; Marletta, M. A., Macrophage Oxidation of L-Arginine to Nitric-Oxide, Nitrite, and Nitrate - Tetrahydrobiopterin Is Required as a Cofactor. *J Biol Chem* **1989**, *264* (33), 19654-19658.
168. Kwon, N. S.; Nathan, C. F.; Stuehr, D. J., Reduced Biopterin as a Cofactor in the Generation of Nitrogen-Oxides by Murine Macrophages. *J Biol Chem* **1989**, *264* (34), 20496-20501.
169. Martin, E.; Nathan, C.; Xie, Q. W., Role of Interferon Regulatory Factor-1 in Induction of Nitric-Oxide Synthase. *J Exp Med* **1994**, *180* (3), 977-984.
170. Xie, Q. W.; Kashiwabara, Y.; Nathan, C., Role of Transcription Factor Nf-Kappa-B/Rel in Induction of Nitric-Oxide Synthase. *J Biol Chem* **1994**, *269* (7), 4705-4708.
171. Geller, D. A.; Lowenstein, C. J.; Shapiro, R. A.; Nussler, A. K.; Disilvio, M.; Wang, S. C.; Nakayama, D. K.; Simmons, R. L.; Snyder, S. H.; Billiar, T. R., Molecular-Cloning and Expression of Inducible Nitric-Oxide Synthase from Human Hepatocytes. *P Natl Acad Sci USA* **1993**, *90* (8), 3491-3495.
172. Stricker, N. L.; Christopherson, K. S.; Yi, B. A.; Schatz, P. J.; Raab, R. W.; Dawes, G.; Bassett, D. E.; Bredt, D. S.; Li, M., PDZ domain of neuronal nitric oxide synthase recognizes novel C-terminal peptide sequences. *Nature biotechnology* **1997**, *15* (4), 336-342.
173. Vasquez-Vivar, J.; Martasek, P.; Whitsett, J.; Joseph, J.; Kalyanaraman, B., The ratio between tetrahydrobiopterin and oxidized tetrahydrobiopterin analogues controls superoxide release from endothelial nitric oxide synthase: an EPR spin trapping study. *Biochem J* **2002**, *362*, 733-739.
174. Zhang, D. X.; Gutterman, D. D., Mitochondrial reactive oxygen species-mediated signaling in endothelial cells. *Am J Physiol-Heart C* **2007**, *292* (5), H2023-H2031.
175. Zou, M. H.; Shi, C. M.; Cohen, R. A., Oxidation of the zinc-thiolate complex and uncoupling of endothelial nitric oxide synthase by peroxynitrite. *J Clin Invest* **2002**, *109* (6), 817-826.
176. Heneka, M. T.; Carson, M. J.; El Khoury, J.; Landreth, G. E.; Brosseron, F.; Feinstein, D. L.; Jacobs, A. H.; Wyss-Coray, T.; Vitorica, J.; Ransohoff, R. M.; Herrup, K.; Frautschy, S. A.; Finsen, B.; Brown, G. C.; Verkhratsky, A.; Yamanaka, K.; Koistinaho, J.; Latz, E.; Halle, A.; Petzold, G. C.; Town, T.; Morgan, D.; Shinohara, M. L.; Perry, V. H.; Holmes, C.; Bazan, N. G.; Brooks, D. J.; Hunot, S.; Joseph, B.; Deigendesch, N.; Garaschuk, O.; Boddeke, E.; Dinarello, C. A.; Breitner, J. C.; Cole, G. M.; Golenbock, D. T.; Kummer, M. P., Neuroinflammation in Alzheimer's disease. *Lancet neurology* **2015**, *14* (4), 388-405.
177. Nussler, A. K.; Disilvio, M.; Billiar, T. R.; Hoffman, R. A.; Geller, D. A.; Selby, R.; Madariaga, J.; Simmons, R. L., Stimulation of the Nitric-Oxide Synthase Pathway in Human Hepatocytes by Cytokines and Endotoxin. *J Exp Med* **1992**, *176* (1), 261-264.
178. Ochoa, J. B.; Udekwu, A. O.; Billiar, T. R.; Curran, R. D.; Cerra, F. B.; Simmons, R. L.; Peitzman, A. B., Nitrogen-Oxide Levels in Patients after Trauma and during Sepsis. *Ann Surg* **1991**, *214* (5), 621-626.
179. Lamas, S.; Michel, T.; Brenner, B. M.; Marsden, P. A., Nitric-Oxide Synthesis in Endothelial-Cells - Evidence for a Pathway Inducible by Tnf-Alpha. *Am J Physiol* **1991**, *261* (4), C634-C641.
180. Harding, C. O.; Blau, N., Advances and challenges in phenylketonuria. *J Inherit Metab Dis* **2010**, *33* (6), 645-648.
181. Loeber, J. G., Neonatal screening in Europe; the situation in 2004. *J Inherit Metab Dis* **2007**, *30* (4), 430-438.

182. Guttler, F., Hyperphenylalaninemia - Diagnosis and Classification of the Various Types of Phenylalanine-Hydroxylase Deficiency in Childhood. *Acta Paediatr Scand* **1980**, 1-&.
183. Thony, B.; Blau, N., Mutations in the BH4-metabolizing genes GTP cyclohydrolase I, 6-pyruvoyl-tetrahydropterin synthase, sepiapterin reductase, carbinolamine-4a-dehydratase, and dihydropteridine reductase. *Hum Mutat* **2006**, 27 (9), 870-878.
184. Heales, S.; Hyland, K., Inhibition of phenylalanine hydroxylase by dihydropterins. A mechanism for impaired aromatic amino acid hydroxylation in dihydropteridine reductase deficiency. *Pteridines* **1990**, 2, 116.
185. Ramaekers, V. T.; Blau, N., Cerebral folate deficiency. *Dev Med Child Neurol* **2004**, 46 (12), 843-851.
186. Davis, M. D.; Kaufman, S.; Milstien, S., Conversion of 6-Substituted Tetrahydropterins to 7-Isomers Via Phenylalanine Hydroxylase-Generated Intermediates. *P Natl Acad Sci USA* **1991**, 88 (2), 385-389.
187. Clot, F.; Grabli, D.; Cazeneuve, C.; Roze, E.; Castelnau, P.; Chabrol, B.; Landrieu, P.; Nguyen, K.; Ponsot, G.; Abada, M.; Doummar, D.; Damier, P.; Gil, R.; Thobois, S.; Ward, A. J.; Hutchinson, M.; Toutain, A.; Picard, F.; Camuzat, A.; Fedirko, E.; San, C.; Bouteiller, D.; LeGuern, E.; Durr, A.; Vidailhet, M.; Brice, A.; Network, F. D., Exhaustive analysis of BH4 and dopamine biosynthesis genes in patients with Dopa-responsive dystonia. *Brain* **2009**, 132, 1753-1763.
188. Lee, W. W.; Jeon, B. S., Clinical Spectrum of Dopa-Responsive Dystonia and Related Disorders. *Curr Neurol Neurosci* **2014**, 14 (7).
189. Lewitt, P. A.; Miller, L. P.; Levine, R. A.; Lovenberg, W.; Newman, R. P.; Papavasiliou, A.; Rayes, A.; Eldridge, R.; Burns, R. S., Tetrahydrobiopterin in Dystonia - Identification of Abnormal-Metabolism and Therapeutic Trials. *Neurology* **1986**, 36 (6), 760-764.
190. Hyland, K.; Gunasekara, R. S.; Munk-Martin, T. L.; Arnold, L. A.; Engle, T., The HPH-1 mouse: A model for dominantly inherited GTP-cyclohydrolase deficiency. *Ann Neurol* **2003**, 54, S46-S48.
191. Tegeder, I.; Costigan, M.; Griffin, R. S.; Abele, A.; Belfer, I.; Schmidt, H.; Ehnert, C.; Nejm, J.; Marian, C.; Scholz, J.; Wu, T. X.; Allchorne, A.; Diatchenko, L.; Binshtok, A. M.; Goldman, D.; Adolph, J.; Sama, S.; Atlas, S. J.; Carlezon, W. A.; Parsegian, A.; Lotsch, J.; Fillingim, R. B.; Maixner, W.; Geisslinger, G.; Max, M. B.; Woolf, C. J., GTP cyclohydrolase and tetrahydrobiopterin regulate pain sensitivity and persistence. *Nat Med* **2006**, 12 (11), 1269-1277.
192. Latremoliere, A.; Costigan, M., Gch1, Bh4 and Pain. *Curr Pharm Biotechno* **2011**, 12 (10), 1728-1741.
193. Berti-Mattera, L. N.; Kern, T. S.; Siegel, R. E.; Nemet, I.; Mitchell, R., Sulfasalazine blocks the development of tactile allodynia in diabetic rats. *Diabetes* **2008**, 57 (10), 2801-2808.
194. Watschinger, K.; Werner, E. R., Alkylglycerol monooxygenase. *lubmb Life* **2013**, 65 (4), 366-372.
195. Gorgas, K.; Teigler, A.; Komljenovic, D.; Just, W. W., The ether lipid-deficient mouse: Tracking down plasmalogen functions. *Bba-Mol Cell Res* **2006**, 1763 (12), 1511-1526.
196. Stafforini, D. M.; McIntyre, T. M.; Zimmerman, G. A.; Prescott, S. M., Platelet-activating factor, a pleiotrophic mediator of physiological and pathological processes. *Crit Rev Cl Lab Sci* **2003**, 40 (6), 643-672.
197. Kosarhashemi, B.; Taguchi, H.; Armarego, W. L. F., Glyceryl Ether Monooxygenase [Ec 1.14.16.5] - Stoichiometry and Inhibition. *Adv Exp Med Biol* **1993**, 338, 93-96.
198. Watschinger, K.; Keller, M. A.; Golderer, G.; Hermann, M.; Maglione, M.; Sarg, B.; Lindner, H. H.; Hermetter, A.; Werner-Felmayer, G.; Konrat, R.; Hulo, N.; Werner, E. R., Identification of the gene encoding alkylglycerol monooxygenase defines a third class of tetrahydrobiopterin-dependent enzymes. *P Natl Acad Sci USA* **2010**, 107 (31), 13672-13677.

199. Watschinger, K.; Fuchs, J. E.; Yarov-Yarovoy, V.; Keller, M. A.; Golderer, G.; Hermetter, A.; Werner-Felmayer, G.; Hulo, N.; Werner, E. R., Catalytic residues and a predicted structure of tetrahydrobiopterin-dependent alkylglycerol mono-oxygenase. *Biochem J* **2012**, *443*, 279-286.
200. Watschinger, K.; Keller, M. A.; McNeill, E.; Alam, M. T.; Lai, S.; Sailer, S.; Rauch, V.; Patel, J.; Hermetter, A.; Golderer, G.; Geley, S.; Werner-Felmayer, G.; Plumb, R. S.; Astarita, G.; Ralser, M.; Channon, K. M.; Werner, E. R., Tetrahydrobiopterin and alkylglycerol monooxygenase substantially alter the murine macrophage lipidome. *P Natl Acad Sci USA* **2015**, *112* (8), 2431-2436.
201. Ezzedine, K.; Eleftheriadou, V.; Whitton, M.; van Geel, N., Vitiligo. *Lancet* **2015**, *386* (9988), 74-84.
202. Laddha, N. C.; Dwivedi, M.; Mansuri, M. S.; Gani, A. R.; Ansarullah, M.; Ramachandran, A. V.; Dalai, S.; Begum, R., Vitiligo: interplay between oxidative stress and immune system. *Exp Dermatol* **2013**, *22* (4), 245-250.
203. Colucci, R.; Dragoni, F.; Moretti, S., Oxidative Stress and Immune System in Vitiligo and Thyroid Diseases. *Oxid Med Cell Longev* **2015**.
204. Hasse, S.; Gibbons, N. C. J.; Rokos, H.; Marles, L. K.; Schallreuter, K. U., Perturbed 6-tetrahydrobiopterin recycling via decreased dihydropteridine reductase in vitiligo: More evidence for H<sub>2</sub>O<sub>2</sub> stress. *J Invest Dermatol* **2004**, *122* (2), 307-313.
205. Schallreuter, K. U.; Wood, J. M.; Pittelkow, M. R.; Gutlich, M.; Lemke, K. R.; Rodl, W.; Swanson, N. N.; Hitzemann, K.; Ziegler, I., Regulation of Melanin Biosynthesis in the Human Epidermis by Tetrahydrobiopterin. *Science* **1994**, *263* (5152), 1444-1446.
206. Schallreuter, K. U.; Moore, J.; Wood, J. M.; Beazley, W. D.; Peters, E. M. J.; Marles, L. K.; Behrens-Williams, S. C.; Dummer, R.; Blau, N.; Thony, B., Epidermal H<sub>2</sub>O<sub>2</sub> accumulation alters tetrahydrobiopterin (6BH(4)) recycling in vitiligo: Identification of a general mechanism in regulation of all 6BH(4)-dependent processes? *J Invest Dermatol* **2001**, *116* (1), 167-174.
207. Davis, M. D.; Ribeiro, P.; Tipper, J.; Kaufman, S., 7-Tetrahydrobiopterin, a Naturally-Occurring Analog of Tetrahydrobiopterin, Is a Cofactor for and a Potential Inhibitor of the Aromatic Amino-Acid Hydroxylases. *P Natl Acad Sci USA* **1992**, *89* (21), 10109-10113.
208. Schallreuter, K. U.; Wood, J. M.; Ziegler, I.; Lemke, K. R.; Pittelkow, M. R.; Lindsey, N. J.; Gutlich, M., Defective Tetrahydrobiopterin and Catecholamine Biosynthesis in the Depigmentation Disorder Vitiligo. *Bba-Mol Basis Dis* **1994**, *1226* (2), 181-192.
209. Kuhlreber, W. M.; Hayashi, T.; Dale, E. A.; Faustman, D. L., Central role of defective apoptosis in autoimmunity. *J Mol Endocrinol* **2003**, *31* (3), 373-399.
210. Laddha, N. C.; Dwivedi, M.; Mansuri, M. S.; Singh, M.; Gani, A. R.; Yeola, A. P.; Panchal, V. N.; Khan, F.; Dave, D. J.; Patel, A.; Madhavan, S. E.; Gupta, R.; Marfatia, Z.; Marfatia, Y. S.; Begum, R., Role of oxidative stress and autoimmunity in onset and progression of vitiligo. *Exp Dermatol* **2014**, *23* (5), 352-354.
211. Fukushima, T.; Nixon, J. C., Analysis of Reduced Forms of Biopterin in Biological Tissues and Fluids. *Anal Biochem* **1980**, *102* (1), 176-188.
212. Bonafe, L.; Thony, B.; Leimbacher, W.; Kierat, L.; Blau, N., Diagnosis of dopa-responsive dystonia and other tetrahydrobiopterin disorders by the study of biopterin metabolism in fibroblasts. *Clin Chem* **2001**, *47* (3), 477-485.
213. Hyland, K., Estimation of Tetrahydro, Dihydro and Fully Oxidized Pterins by High-Performance Liquid-Chromatography Using Sequential Electrochemical and Fluorometric Detection. *J Chromatogr* **1985**, *343* (1), 35-41.
214. Howells, D. W.; Hyland, K., Direct Analysis of Tetrahydrobiopterin in Cerebrospinal-Fluid by High-Performance Liquid-Chromatography with Redox Electrochemistry - Prevention of Autoxidation during Storage and Analysis. *Clin Chim Acta* **1987**, *167* (1), 23-30.

215. Laroche, J. H., Coulometric detection in liquid chromatography. *Retrospective Theses and Dissertations* **1977**, 191.
216. Xiong, X.; Liu, Y. M., Chromatographic behavior of 12 polar pteridines in hydrophilic interaction chromatography using five different HILIC columns coupled with tandem mass spectrometry. *Talanta* **2016**, *150*, 493-502.
217. Kim, H. R.; Kim, T. H.; Hong, S. H.; Kim, H. G., Direct detection of tetrahydrobiopterin (BH4) and dopamine in rat brain using liquid chromatography coupled electrospray tandem mass spectrometry. *Biochem Bioph Res Co* **2012**, *419* (4), 632-637.
218. Fismen, L.; Eide, T.; Djurhuus, R.; Svardal, A. M., Simultaneous quantification of tetrahydrobiopterin, dihydrobiopterin, and biopterin by liquid chromatography coupled electrospray tandem mass spectrometry. *Anal Biochem* **2012**, *430* (2), 163-170.
219. Burton, C.; Weng, R.; Yang, L.; Bai, Y.; Liu, H. W.; Ma, Y. F., High-throughput intracellular pteridinic profiling by liquid chromatography-quadrupole time-of-flight mass spectrometry. *Anal Chim Acta* **2015**, *853*, 442-450.
220. Farrants, H.; Hiblot, J.; Griss, R.; Johnsson, K., Rational Design and Applications of Semisynthetic Modular Biosensors: SNIFITs and LUCIDs. *Methods in molecular biology* **2017**, *1596*, 101-117.
221. Brun, M. A.; Tan, K. T.; Nakata, E.; Hinner, M. J.; Johnsson, K., Semisynthetic Fluorescent Sensor Proteins Based on Self-Labeling Protein Tags. *J Am Chem Soc* **2009**, *131* (16), 5873-5884.
222. Brun, M. A.; Tan, K. T.; Griss, R.; Kielkowska, A.; Reymond, L.; Johnsson, K., A Semisynthetic Fluorescent Sensor Protein for Glutamate. *J Am Chem Soc* **2012**, *134* (18), 7676-7678.
223. Griss, R.; Schena, A.; Reymond, L.; Patiny, L.; Werner, D.; Tinberg, C. E.; Baker, D.; Johnsson, K., Bioluminescent sensor proteins for point-of-care therapeutic drug monitoring. *Nature chemical biology* **2014**, *10* (7), 598-603.
224. Blackman, M. L.; Royzen, M.; Fox, J. M., Tetrazine ligation: Fast bioconjugation based on inverse-electron-demand Diels-Alder reactivity. *J Am Chem Soc* **2008**, *130* (41), 13518-+.
225. Lang, K.; Davis, L.; Wallace, S.; Mahesh, M.; Cox, D. J.; Blackman, M. L.; Fox, J. M.; Chin, J. W., Genetic Encoding of Bicyclononynes and trans-Cyclooctenes for Site-Specific Protein Labeling in Vitro and in Live Mammalian Cells via Rapid Fluorogenic Diels-Alder Reactions. *J Am Chem Soc* **2012**, *134* (25), 10317-10320.
226. Roy, R.; Hohng, S.; Ha, T., A practical guide to single-molecule FRET. *Nat Methods* **2008**, *5* (6), 507-516.
227. Krishnamurthy, V. M.; Semetey, V.; Bracher, P. J.; Shen, N.; Whitesides, G. M., Dependence of effective molarity on linker length for an intramolecular protein-ligand system. *J Am Chem Soc* **2007**, *129* (5), 1312-1320.
228. Yuriev, E.; Ramsland, P. A., Latest developments in molecular docking: 2010-2011 in review. *J Mol Recognit* **2013**, *26* (5), 215-239.
229. Trott, O.; Olson, A. J., Software News and Update AutoDock Vina: Improving the Speed and Accuracy of Docking with a New Scoring Function, Efficient Optimization, and Multithreading. *J Comput Chem* **2010**, *31* (2), 455-461.
230. Billeter, S. R.; Webb, S. P.; Agarwal, P. K.; Iordanov, T.; Hammes-Schiffer, S., Hydride transfer in liver alcohol dehydrogenase: Quantum dynamics, kinetic isotope effects, and role of enzyme motion. *J Am Chem Soc* **2001**, *123* (45), 11262-11272.
231. Griss, R., Bioluminescent sensor proteins for point-of-care therapeutic drug monitoring. **2013**.
232. Schuler, B.; Lipman, E. A.; Steinbach, P. J.; Kumke, M.; Eaton, W. A., Polyproline and the "spectroscopic ruler" revisited with single-molecule fluorescence. *P Natl Acad Sci USA* **2005**, *102* (8), 2754-2759.

233. Scarabelli, S.; Tan, K. T.; Griss, R.; Hovius, R.; D'Alessandro, P. L.; Vorherr, T.; Johnsson, K., Evaluating Cellular Drug Uptake with Fluorescent Sensor Proteins. *ACS Sens* **2017**, *2* (8), 1191-1197.
234. Xue, L.; Yu, Q. L. Y.; Griss, R.; Schena, A.; Johnsson, K., Bioluminescent Antibodies for Point-of-Care Diagnostics. *Angew Chem Int Edit* **2017**, *56* (25), 7112-7116.
235. Xue, L.; Prifti, E.; Johnsson, K., A General Strategy for the Semisynthesis of Ratiometric Fluorescent Sensor Proteins with Increased Dynamic Range. *J Am Chem Soc* **2016**, *138* (16), 5258-5261.
236. Plass, T.; Milles, S.; Koehler, C.; Szymanski, J.; Mueller, R.; Wiessler, M.; Schultz, C.; Lemke, E. A., Amino Acids for Diels-Alder Reactions in Living Cells. *Angew Chem Int Edit* **2012**, *51* (17), 4166-4170.
237. Sidhom, M. B.; Velez, M. R., Monitoring the Effect of Triamterene and Hydrochlorothiazide on Dihydrofolate-Reductase Activity Using a New Spectrophotometric Method. *J Pharmaceut Biomed* **1989**, *7* (12), 1551-1557.
238. Chang, J. C.; Hall, T. C., Effect of Triamterene on Nucleic-Acid Synthesis. *Clin Pharmacol Ther* **1972**, *13* (3), 372-&.
239. Perkins, J. P.; Bertino, J. R., Dihydrofolate reductase from the L1210R murine lymphoma. Fluorometric measurements of the interaction of the enzyme with coenzymes, substrates, and inhibitors. *Biochemistry-Us* **1966**, *5* (3), 1005-12.
240. Crabtree, M. J.; Smith, C. L.; Lam, G.; Goligorsky, M. S.; Gross, S. S., Ratio of 5,6,7,8-tetrahydrobiopterin to 7,8-dihydrobiopterin in endothelial cells determines glucose-elicited changes in NO vs. superoxide production by eNOS. *Am J Physiol-Heart C* **2008**, *294* (4), H1530-H1540.
241. Schalhorn, A.; Siebert, W.; Sauer, H. J., Antifolate effect of triamterene on human leucocytes and on a human lymphoma cell line. *European journal of clinical pharmacology* **1981**, *20* (3), 219-24.
242. Crosley, A. P.; Alexander, F.; Strickland, W. H.; Ronquillo, L. M., Triamterene, a New Natrurctic Agent - Preliminary Observations in Man. *Ann Intern Med* **1962**, *56* (2), 241-+.
243. Safayhi, H.; Tiegs, G.; Wendel, A., A Novel Biologically-Active Seleno-Organic Compound .5. Inhibition by Ebselen (Pz-51) of Rat Peritoneal Neutrophil Lipoxygenase. *Biochem Pharmacol* **1985**, *34* (15), 2691-2694.
244. Maiorino, M.; Roveri, A.; Ursini, F., Antioxidant Effect of Ebselen (Pz-51) - Peroxidase Mimetic Activity on Phospholipid and Cholesterol Hydroperoxides Vs Free-Radical Scavenger Activity. *Arch Biochem Biophys* **1992**, *295* (2), 404-409.
245. Sies, H., Ebselen, a Selenoorganic Compound as Glutathione-Peroxidase Mimic. *Free Radical Bio Med* **1993**, *14* (3), 313-323.
246. Masumoto, H.; Sies, H., The reaction of ebselen with peroxynitrite. *Chem Res Toxicol* **1996**, *9* (1), 262-267.
247. Masumoto, K.; Kissner, R.; Koppenol, W. H.; Sies, H., Kinetic study of the reaction of ebselen with peroxynitrite. *Febs Lett* **1996**, *398* (2-3), 179-182.
248. Schewe, T., Molecular Actions of Ebselen - an Antiinflammatory Antioxidant. *Gen Pharmacol* **1995**, *26* (6), 1153-1169.
249. Parnham, M. J.; Graf, E., Seleno-organic compounds and the therapy of hydroperoxide-linked pathological conditions. *Biochem Pharmacol* **1987**, *36* (19), 3095-102.
250. Wagner, G.; Schuch, G.; Akerboom, T. P. M.; Sies, H., Transport of Ebselen in Plasma and Its Transfer to Binding-Sites in the Hepatocyte. *Biochem Pharmacol* **1994**, *48* (6), 1137-1144.
251. Muges, G.; Panda, A.; Singh, H. B.; Punekar, N. S.; Butcher, R. J., Glutathione peroxidase-like antioxidant activity of diaryl diselenides: A mechanistic study. *J Am Chem Soc* **2001**, *123* (5), 839-850.
252. Nogueira, C. W.; Rocha, J. B. T., Toxicology and pharmacology of selenium: emphasis on synthetic organoselenium compounds. *Arch Toxicol* **2011**, *85* (11), 1313-1359.
253. Okumura, M.; Masada, M.; Yoshida, Y.; Shintaku, H.; Hosoi, M.; Okada, N.; Konishi, Y.; Morikawa, T.; Miura, K.; Imanishi, M., Decrease in tetrahydrobiopterin as a possible cause of nephropathy in type II diabetic rats. *Kidney Int* **2006**, *70* (3), 471-6.

254. Chander, P. N.; Gealekman, O.; Brodsky, S. V.; Elitok, S.; Tojo, A.; Crabtree, M.; Gross, S. S.; Goligorsky, M. S., Nephropathy in Zucker diabetic fat rat is associated with oxidative and nitrosative stress: Prevention by chronic therapy with a peroxynitrite scavenger ebselen. *Journal of the American Society of Nephrology* **2004**, *15* (9), 2391-2403.
255. Yamaguchi, T.; Sano, K.; Takakura, K.; Saito, I.; Shinohara, Y.; Asano, T.; Yasuhara, H.; Grp, E. S., Ebselen in acute ischemic stroke - A placebo-controlled, double-blind clinical trial. *Stroke* **1998**, *29* (1), 12-17.
256. Brodsky, S. V.; Gealekman, O.; Chen, J.; Zhang, F.; Togashi, N.; Crabtree, M.; Gross, S. S.; Nasjletti, A.; Goligorsky, M. S., Prevention and reversal of premature endothelial cell senescence and vasculopathy in obesity-induced diabetes by ebselen. *Circ Res* **2004**, *94* (3), 377-384.
257. Nikawa, T.; Schuch, G.; Wagner, G.; Sies, H., Interaction of Albumin-Bound Ebselen with Rat-Liver Glutathione-S-Transferase and Microsomal Proteins. *Biochem Mol Biol Int* **1994**, *32* (2), 291-298.
258. Brooker, L.; Parr, M. K.; Cawley, A.; Flenker, U.; Howe, C.; Kazlauskas, R.; Schanzer, W.; George, A., Development of criteria for the detection of adrenosterone administration by gas chromatography-mass spectrometry and gas chromatography-combustion-isotope ratio mass spectrometry for doping control. *Drug Test Anal* **2009**, *1* (11-12), 587-595.
259. <http://mindandmuscle.net/articles/11-oxo/>, Prohormones: Adrenosterone (11-OXO). accessed **08.2017**.
260. Paul, S. M.; Purdy, R. H., Neuroactive Steroids. *Faseb J* **1992**, *6* (6), 2311-2322.
261. Yang, N. J.; Hinner, M. J., Getting across the cell membrane: an overview for small molecules, peptides, and proteins. *Methods in molecular biology* **2015**, *1266*, 29-53.
262. Mendel, C. M., The Free Hormone Hypothesis - a Physiologically Based Mathematical-Model. *Endocr Rev* **1989**, *10* (3), 232-274.
263. Zhang, J. H.; Chung, T. D. Y.; Oldenburg, K. R., A simple statistical parameter for use in evaluation and validation of high throughput screening assays. *J Biomol Screen* **1999**, *4* (2), 67-73.
264. Heales, S.; Hyland, K., Determination of Quinonoid Dihydrobiopterin by High-Performance Liquid-Chromatography and Electrochemical Detection. *J Chromatogr-Biomed* **1989**, *494*, 77-85.
265. Kasraee, B.; Nikolic, D. S.; Salomon, D.; Carraux, P.; Fontao, L.; Piguet, V.; Omrani, G. R.; Sorg, O.; Saurat, J. H., Ebselen is a new skin depigmenting agent that inhibits melanin biosynthesis and melanosomal transfer. *Exp Dermatol* **2012**, *21* (1), 19-24.
266. Cer, R. Z.; Mudunuri, U.; Stephens, R.; Lebeda, F. J., IC50-to-K-i: a web-based tool for converting IC50 to K-i values for inhibitors of enzyme activity and ligand binding. *Nucleic Acids Res* **2009**, *37*, W441-W445.
267. Arai, N.; Narisawa, K.; Hayakawa, H.; Tada, K., Hyperphenylalaninemia Due to Dihydropteridine Reductase Deficiency - Diagnosis by Enzyme Assays on Dried Blood Spots. *Pediatrics* **1982**, *70* (3), 426-430.







**Violet** : purification tags ( Strep-Tag, His10-Tag); **Green** : SNAP-Tag; **Orange** : Flexible (GGG)n linker, **Red** : hDHPR, **Cyan** : Pro30 spacer, **Grey** : HALO.

#### DHPR(E46X)

**MASWSHPQFEKGADDDDKVPHMAAAAAAGEARRVLVYGGRGALGSRVQAFRRNWWVASVDVVENXEASASIVKMTDSFTEQA  
DQVTAIEVGKLLGEEKVDAILCVAGGWAGGNAKSKSLFKNCDLMWKQSIWTSTISSHLATKHLKEGGLTLGAKAALDGT  
PGMIGYGMAGAVHQLCQSLAGKNSGMPPGAAAIAVLPVTLDTMNRKSMPEADFSSWTPLEFLVETFDWITGKNRPSSGSLIQVVTTEGRTELPAYFGAPGFS  
SISAAAAAAAAAAAA**

**Violet** : purification tags ( Strep-Tag, His10-Tag); **Red** : hDHPR

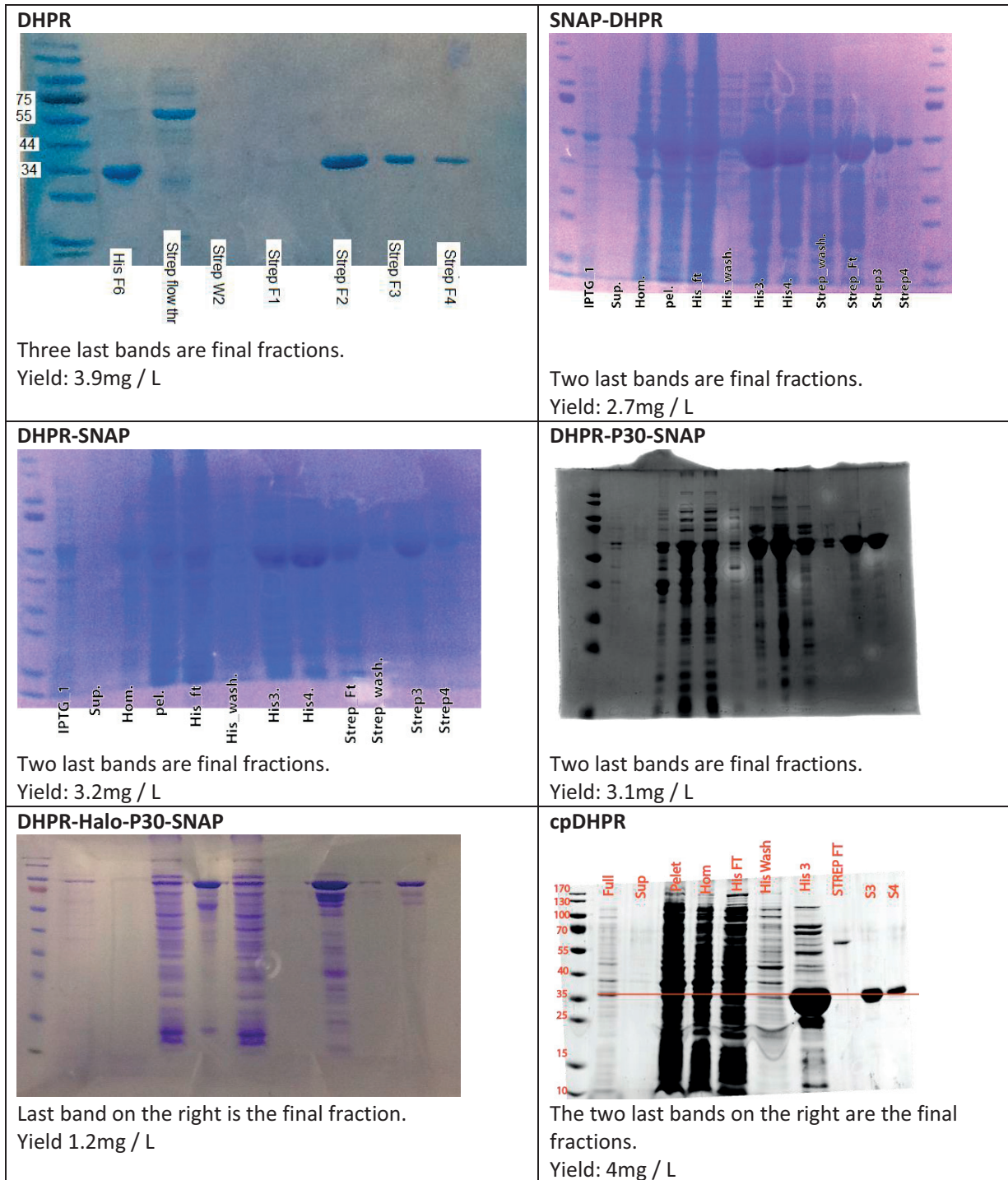
#### cpDHPR

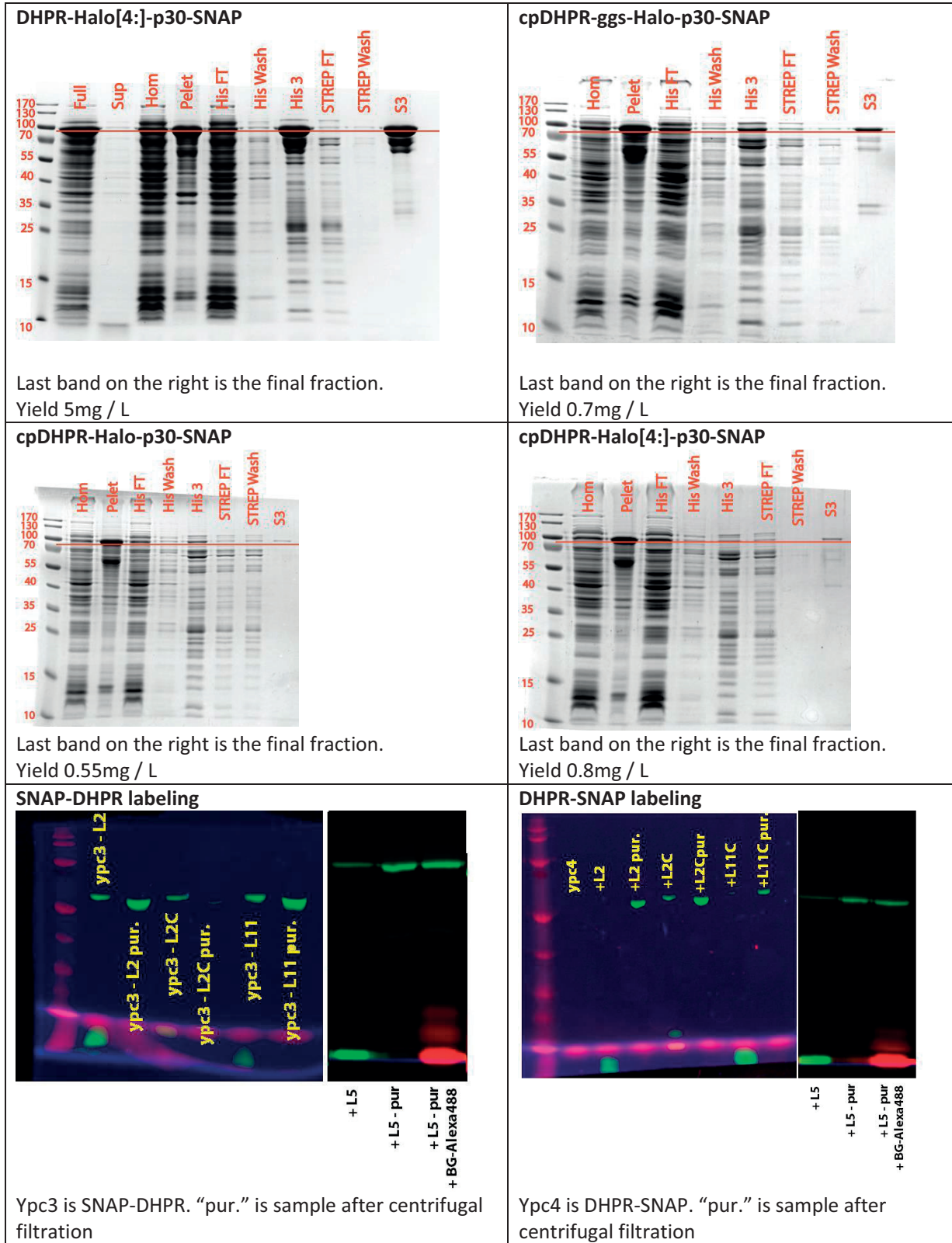
**MASWSHPQFEKGADDDDKVPHMASASIVKMTDSFTEQADQVTAIEVGKLLGEEKVDAILCVAGGWAGGNAKSKSLFKNCDLMWKQSI  
WTSTISSHLATKHLKEGGLTLGAKAALDGT  
PGMIGYGMAGAVHQLCQSLAGKNSGMPPGAAAIAVLPVTLDTMNRKSMPEADFSSWTP  
LEFLVETFDWITGKNRPSSGSLIQVVTTEGRTELPAYFGGSGSGSGSGSMAAAAAAGEARRVLVYGGRGALGSRVQAFRRNWWVASV  
DVVENE**GAPGFSISAAAAAAAAAAAA

**Violet** : purification tags ( Strep-Tag, His10-Tag); **Red** : hDHPR; **Orange** : Flexible (GGG)n linker

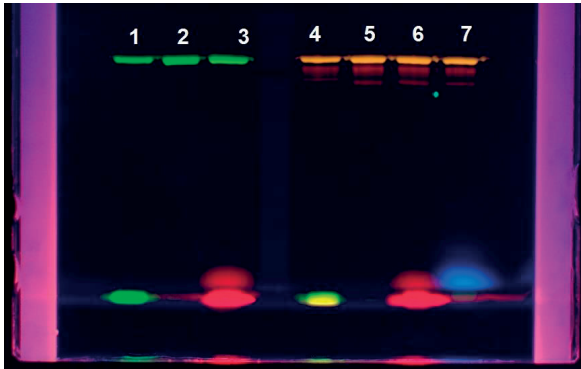
All constructs containing cpDHPR or DHPRE(E46X) had DHPR replaced with the respective sequence

## Appendix: protein gels and yields



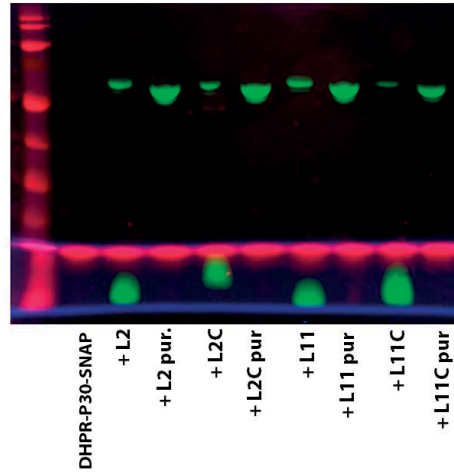


**DHPR-P30-Halo[4:]-SNAP**



Sensor + L11 (1), filtered (2), with BG-Alexa488 (3)  
 Sensor + L11 & Sir-HaloTag(4), filtered (5), with BG-Alexa488 (6), with CPY-HaloTag(7). Was used for screening

**DHPR-P30-SNAP labeling**



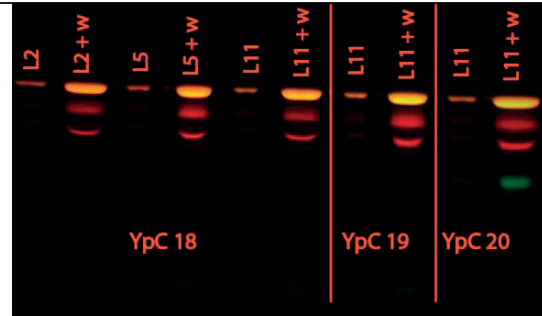
“pur.” is the sample after centrifugal filtration

**YpC 18 is cpDHPR-ggs2-Halo-P30-SNAP**

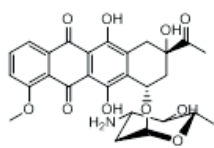
**YpC 19 is cpDHPR-Halo-P30-SNAP**

**YpC 20 is cpDHPR Halo[4:]-P30-SNAP**

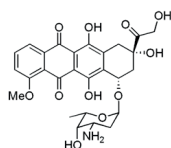
+ w is after centrifugal filtration



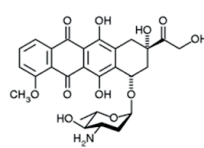
## Appendix: Structures of the Hits



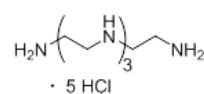
**Daunorubicin**



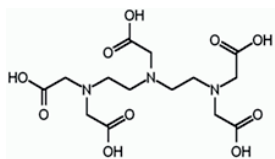
**Doxorubicin**



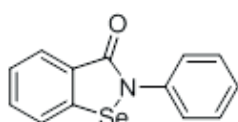
**Epirubicin**



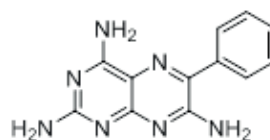
**Tetraethylene-pentamine**



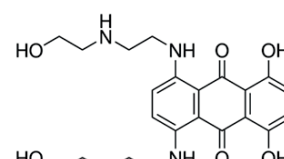
**Pentetic acid**



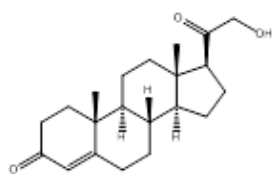
**Ebselen**



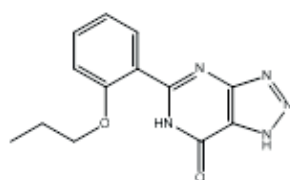
**Triamterene**



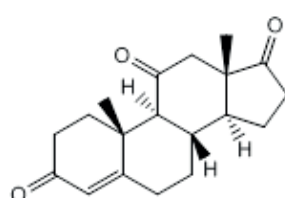
**Mitoxantrone**



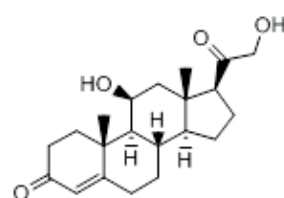
**Deoxycorticosterone**



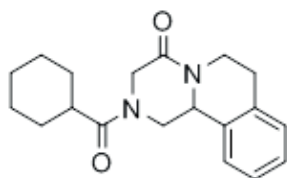
**Zaprinast**



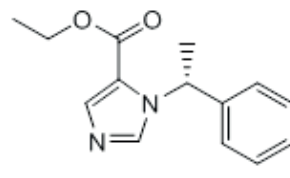
**Adrenosterone**



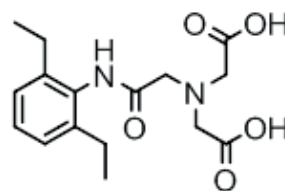
**Corticosterone**



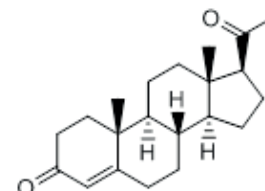
**Praziquantel**



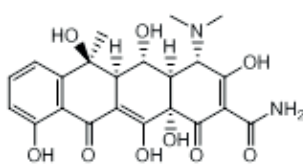
**Etomidate**



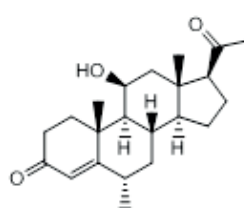
**Etifenin**



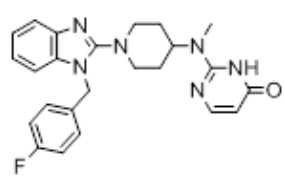
**Progesterone**



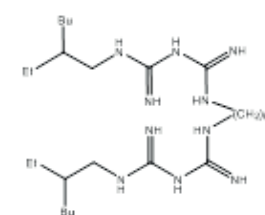
**Oxytetracycline**



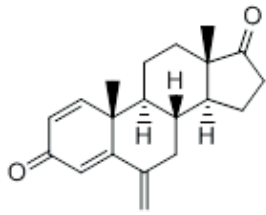
**Medrysone**



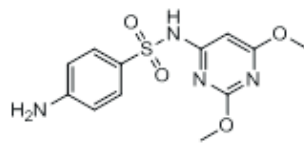
**Mizolastine**



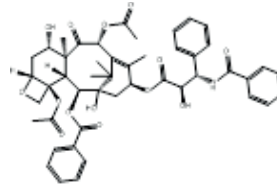
**Alexidine**



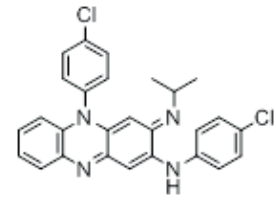
**Exemestane**



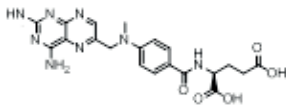
**Sulfadimethoxine**



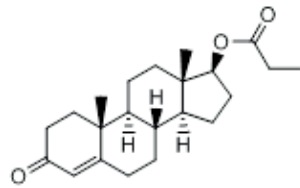
**Paclitaxel**



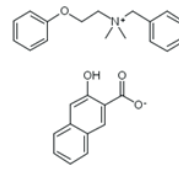
**Clofazimine**



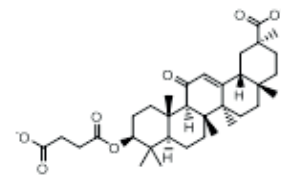
**Methotrexate**



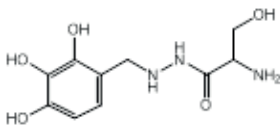
**Testosterone propionate**



**Bephenium hydroxynaphtoate**



**Carbenoxolone**



**Benserazide**

## ***Curriculum Vitae***

Yann Pierson  
Born 11 July 1988, Aigle in Switzerland  
Clos d'Aubonne 19, 1814 La Tour-de-Peilz  
+41774102345  
[Yann.pierson@epfl.ch](mailto:Yann.pierson@epfl.ch)

### **Education**

05.2014 / 10.2017	Ph.D. in Chemical Biology Swiss Federal Institute of Technology (EPFL), Lausanne Supervisor: Prof. Kai Johnsson
09.09.2016	Attestation BSO1 University of Bern Dr. Urs Pauli
09.2013/03.2014	Master Thesis National University of Singapore Supervisors : Dr Ning Yan / Prof. Paul Dyson
09.2012/09.2013	Master in Molecular and Biological Chemistry Swiss Federal Institute of Technology (EPFL), Lausanne
09.2009/09.2012	Bachelor in Chemistry and Chemical Engineering Swiss Federal Institute of Technology (EPFL), Lausanne
09.2008	High school diploma – chemistry and biology Gymnase de Burrier

### **Award**

High school prize of chemistry and biology



## Publications

Yann Pierson, Xi Chen, Felix D. Bobbink, Jianguang Zhang, and Ning Yan  
Acid-Catalyzed Chitin Liquefaction in Ethylene Glycol  
*ACS Sustainable Chem. Eng.*, **2014**, 2 (8), pp 2081–2089

Yann Pierson, Felix Bobbink and Ning Yan\*  
Alcohol Mediated Liquefaction of Lignocellulosic Materials: A Mini Review  
*Chem Eng Process Tech* 1(2): 1014.

Felix D. Bobbink, Jianguang Zhang, Yann Pierson, Xi Chen and Ning Yan  
Conversion of chitin derived N-acetyl-D-glucosamine (NAG) into polyols over transition metal  
catalysts and hydrogen in water  
*Green Chem.*, 2015, 17, 1024-1031

## Employment history

Mass spectrometer R&D technician  
Thermo Fisher Scientific  
02.2013 – 07.2013

Host for the car company Citroën  
Auto Show Geneva  
02.3102 - 03.2013

Fireman in 1<sup>st</sup> emergency response unit  
SDIS, City of Aigle  
01.2009 – 07.2011

Construction and metallic worker  
Pechigaz SA, Colombey  
1 month / year , 2004 - 2008